執筆者の意向により第 5 章はオンラインでは公開していません。

Selective catalytic reduction of N_2O with CH_4 over Fe-zeolite catalysts

~Reaction mechanism and active site structure~

Takeshi Nobukawa

(Doctorial Program in Materials Science)

Submitted to the Graduate School of
Pure and Applied Sciences
in Partial Fulfillment of the Requirements
for the Degree of Doctor of Philosophy in
Engineering

at the
University of Tsukuba

学位論文概要

　本論文は，地球温暖化物質である亜酸化窒素(N_2O)を，過剰酸素共存条件下，メタンを還元剤として選択的に還元除去する為の触媒やその反応機構について述べたものである.

　本論文では，触媒としてイオン交換法により調製した担持量の異なる鉄ゼオライト触媒を使用した. 触媒活性は鉄担持量に大きく依存し，Fe/Alモル比が 0.10 より大きい領域では，Feイオン当たりの活性が急激に増加した. 触媒特性も担持量により大きく変化し，鉄担持量が大きい触媒ほど鉄イオン種はより低温で還元され，触媒表面上の酸素も一部が低温で脱離した. これらの触媒のキャラクタリゼーションや触媒活性の結果から，ダイマー構造を持つ鉄イオン種がN_2O選択還元反応に対して非常に高い活性を示すことを明らかにした. この結果は，EXAFSによる鉄イオンの局所構造解析の結果と良く一致した.

　また，本論文では還元剤としてメタンを用いた. 一般的には，メタンは不活性な還元剤であるが，鉄ゼオライト触媒によるN_2O還元除去反応に対しては非常に高い活性を示した. 特に注目すべき点はその選択性であり，過剰に酸素が共存する条件(10%)でもN_2Oとメタンの反応が選択的に進行した. また，他の還元剤との活性比較では，本研究条件下ではメタンが活性，選択性の点から最も効果的な還元剤であることが明らかとなった.

　鉄ゼオライト触媒によるN_2O+CH_4選択還元反応の反応機構を詳細に検討した. 反応中のFeイオン種上にはメトキシ，フォルメート中間体が形成し，これらの中間体は反応条件下で過剰に存在するO_2よりもN_2Oと優先的に反応することが明らかとなった. また，N_2O解離により，触媒表面上には新たに吸着酸素種が形成されたが，この吸着酸素種はメタンと直接反応しないことが明らかとなった. N_2O選択還元反応では，N_2OとCH_4の共存が必要不可欠であり，低温でメタンを容易に活性化する酸素種として，N_2O解離により生成する発生期酸素(O*(a))が重要であることが示唆された.

Abstract of thesis

This thesis shows the catalytic performance and the reaction mechanism of selective catalytic reduction (SCR) of N_2O with CH_4 under excess oxygen atmosphere over ion-exchanged Fe-zeolite catalysts.

In this thesis, Fe-MFI catalysts with different Fe content were prepared by severely controlled wet ion-exchange method. The performance of Fe-zeolite catalysts for N_2O reduction depended on the Fe content of the catalyst. The turnover frequency was drastically increased in the range of Fe/Al (molar ratio) > 0.10. Fe ion species could be reduced at lower-temperature and a new O_2 desorption peak was observed at low temperature. As a result of characterizations and kinetic studies, it is found that binuclear Fe ion species are active sites for the SCR of N_2O with CH_4. This conclusion is supported by the EXAFS study.

CH_4 was applied as reductant for N_2O removal. Although CH_4 is less active reductant, high activity for N_2O reduction was observed. It should be noted that the reaction between N_2O and CH_4 proceeded selectively even in the presence of excess oxygen atmosphere. Furthermore, it is found that CH_4 is the most efficient reductant in terms of activity and selectivity in this SCR condition compared to other reductants (C_2H_6, C_3H_6, CO, and H_2).

The reaction mechanism of SCR of N_2O with CH_4 over Fe-zeolite catalysts was investigated. The formation of intermediate species such as methoxy and formate species was observed over Fe ion site during the N_2O+CH_4 reaction. These intermediate species were oxidized by N_2O preferentially in the SCR condition.

Although new extra oxygen species were formed over the catalyst surface after N_2O dissociation, the reactivity of the accommodated oxygen species was very poor. It is found that the simultaneous presence of N_2O and CH_4 in the gas phase is essential for the high activity for the SCR reaction, which suggests that nascent oxygen transients formed by N_2O dissociation can activate CH_4 in the SCR of N_2O with CH_4.

Contents

Chapter 1

General introduction

1.1. Background of N_2O emission as one of the greenhouse-effect gases

Nitrous oxide (N_2O) has recently become the subject of intense research and debate, because of its increasing concentrations in the atmosphere, and its known ability to contribute to the greenhouse effect and to deplete the ozone layer. There are both natural and anthropogenic sources for N_2O; however, the man-made sources are increasing at a much higher late than natural ones. The concentration of N_2O in the atmosphere has risen by about 17% as a result of human activity, as shown in Fig. 1-1.
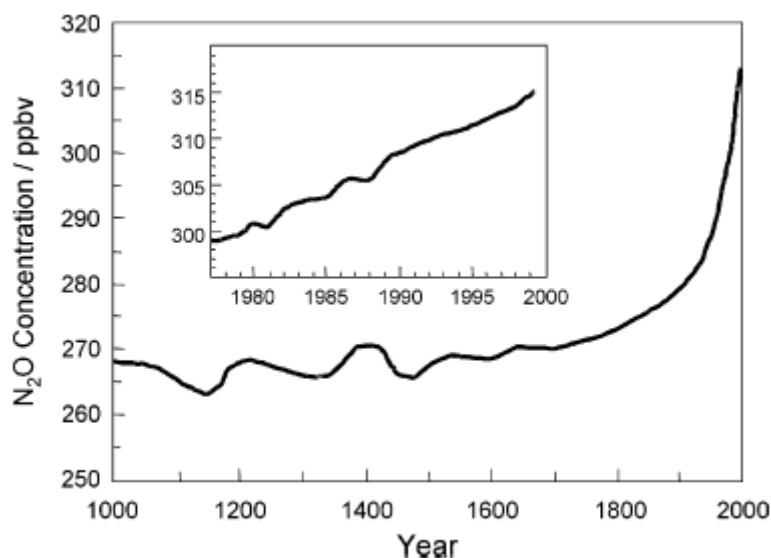
Figure 1-1. Evolution of the atmospheric N_2O concentration [1].

Until recently, strategies for addressing climate change have principally been focused on reducing emission from the main greenhouse gas carbon dioxide, but the importance of other greenhouse gases and opportunities for their abatement have been more and more recognized in the last years. This culminated in an agreement at the Third Conference of the Parties (COP3) to the United Nations Framework Convention on Climate Change (UNFCCC) in Kyoto (Japan) in December 1997 to set legal binding targets for reducing emissions of six greenhouse gases, carbon dioxide (CO_2), methane (CH_4), nitrous oxide (N_2O), hydrofluorocarbons and

perfluorocarbons (HFCs and PFCs), and sulfur hexafluoride (SF_6) [2]. As a result, the Japan agreed to reduce CO_2, CH_4, and N_2O emissions by 6% of 1990 levels in the period 2008-2012 (1995 levels for HFCs, PFCs, and SF_6). Emissions targets for other advanced nations are 8% for EU and Canada and 7% for United States [2]. The Kyoto Protocol, an international and legally binding agreement to reduce greenhouse gases emissions world wide, entered into force on 16 February 2005.

The total amount of green-house gas emissions has already increased about 8.3% from F.Y. 1990/1995 to F.Y. 2003, as shown in Fig. 1-2. After CO_2, N_2O is the second important greenhouse gas in Japan, with emissions of 34.6 million metric tons of carbon dioxide equivalent (MMT CO_2-eq.) in F.Y. 2003 [3]. This represents 2.6% (6.2% in the world [Fig. 1-3]) of total Japan greenhouse-effect gas emissions. N_2O is much less abundant than CO_2 in the atmosphere (0.3 ppm compared to 370 ppm). However, due to its long lifetime of approximately 150 years in the atmosphere, N_2O has 310 and 14.8 times as large as the Global Warming Potential (GWP) of CO_2 and CH_4, respectively [4]. Therefore, N_2O can contribute significantly to global warming and the reduction of N_2O plays an important role in reaching the global 6% target.
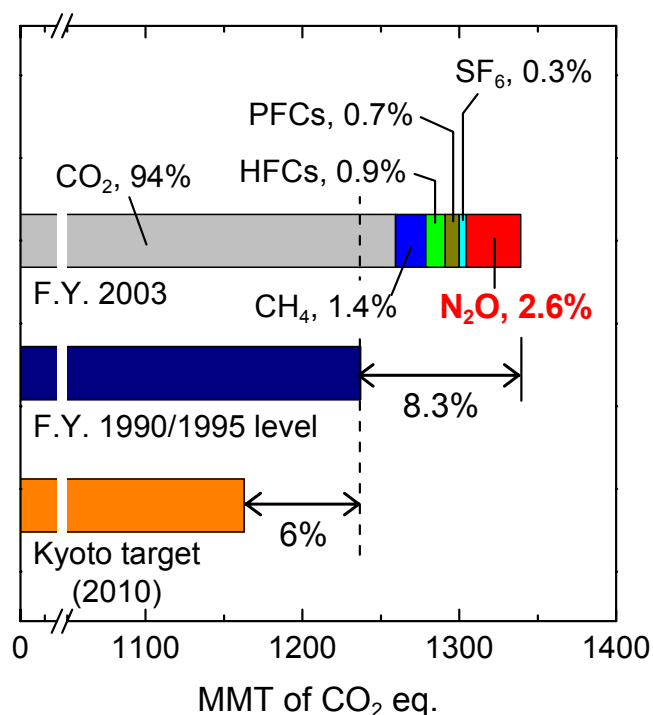
Figure 1-2. Relative importance of the greenhouse gases in the fulfillment of the Kyoto target (Japan). [3]
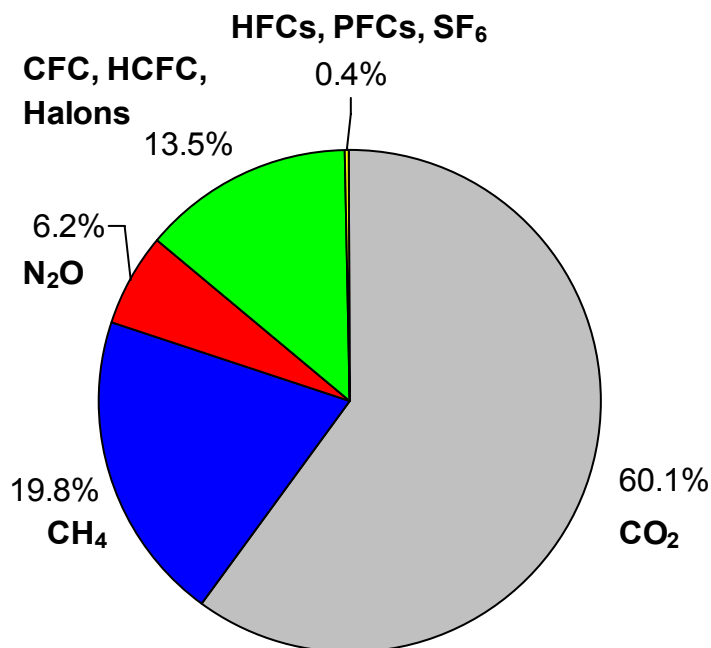
Figure 1-3. Breakdown of contribution of greenhouse effect gases for global warming. [1]

Recently, the catalytic and thermal abatement technologies have been successfully developed for the major source of N_2O in the chemical manufacture (Adipic acid production), due to the high N_2O concentration in the tail gas (25-40 vol. %) [5]. Due to the exothermicity of the decomposition reaction, a large increase in the temperature occurs within the catalyst bed. For instance, the decomposition of 35 vol. % N_2O in air leads to an adiabatic temperature rise of the gas of 920 K. In this temperature window, a large number of catalysts exhibit considerable activity. Therefore, in this case the activity of the catalyst is not a critical factor for the effectiveness of the technology.

Nowadays, the N_2O emission from stationary combustion of fossil fuels, biomass, municipal and industrial waste, and motor vehicles become a major source of N_2O emission (Fig. 1-4). Shimizu has reported that circulating fluidized bed combustion of for instance sewage sludge is a contributor to the N_2O emission with concentrations in flue gasses of about 260 ppm [6]. Individual three-way catalysts of motor vehicles are a relative limited source of N_2O emissions, but the total emission of the transportation sector is quite large. Heavy-duty Diesel engines are also believed to contribute to the N_2O emission of the transportation sector. Although quantification is less accurate, the contribution of N_2O stems from the catalytic converters in

motor vehicles is increasing [5, 7]. In this case, N_2O gas is produced as an unwanted by-product during de-NO_x SCR process. N_2O emissions from aging SCR de-NO_x catalysts increase in time. Arai and co-workers [8] have reported that the maximum concentration of N_2O in the tail gas increases from 6 to 30 ppmv with the increase in the mileage from 15000 to 56000 km. The formation of N_2O is strongly influenced by technical condition of engines and equipped three-way catalytic converters. N_2O emissions from use of fertilizers (soil emissions) is a very diffusive source and therefore hard to abate using end-of-pipe measures.
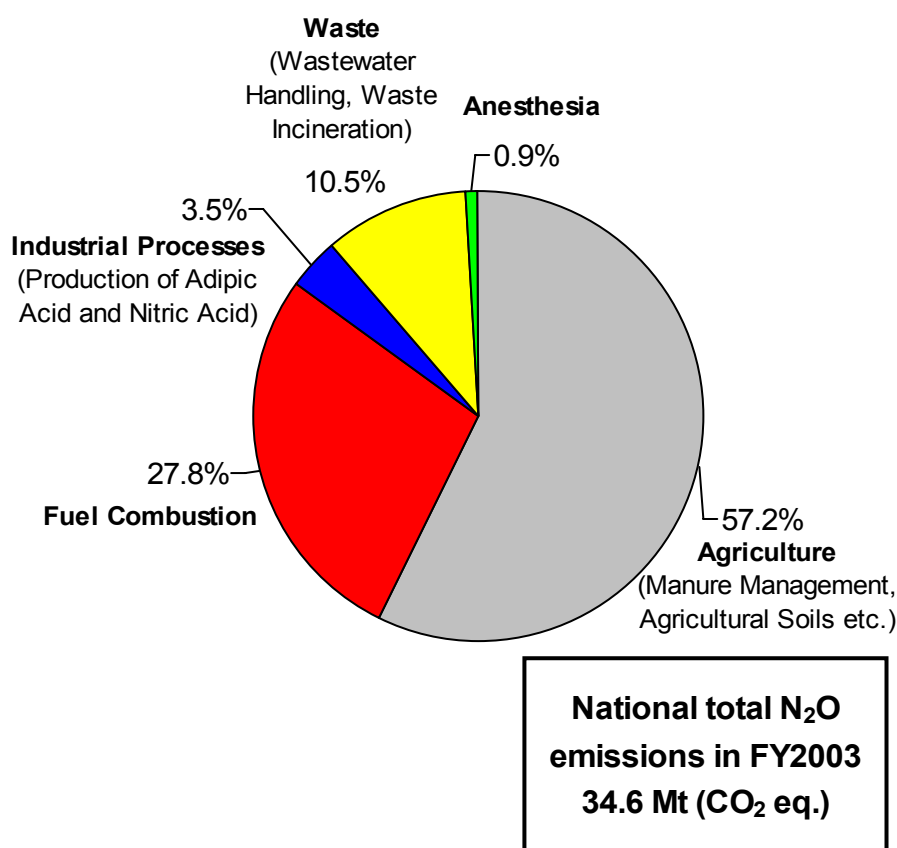
Figure 1-4. National total N_2O emissions in Japan in Fiscal year 2003 [3]

1.2. Catalytic removal of N$_2$O emissions

The catalytic decomposition of N$_2$O (N$_2$O $\rightarrow$ N$_2$ + 1/2O$_2$) and selective catalytic reduction of N$_2$O with hydrocarbons (HC-SCR) and ammonia (NH$_3$-SCR) are two candidate technologies, which can be applied to reduce the N$_2$O emissions.

1.2.1. Catalytic decomposition of N$_2$O

Direct catalytic decomposition of N$_2$O without addition of reducing agents is the simplest method to reduce N$_2$O emissions. Nowadays, the details of the catalytic decomposition of N$_2$O have been described in a number of recent reviews [5, 9-12].

Dann *et al*. examined a Rh/Al$_2$O$_3$ catalyst for decomposition of N$_2$O in the exhausted gas of fluidized bed combustion [13]. Zeng and coworkers [14, 15] studied the N$_2$O decomposition reaction over Ru/Al$_2$O$_3$. They observed that the surface area of Ru/Al$_2$O$_3$ decreased with the increase of the metal loading and that O$_2$ exhibited negligible inhibition effect. Excellent catalytic activity was observed for both dry and wet N$_2$O feeds. Pinna *et al*. examined the N$_2$O decomposition over Ru supported on ZrO$_2$ [16]. They concluded that the oxidized samples exhibited higher conversion than the reduced ones. Li and Armor [17, 18] reported that Rh- and Ru-exchanged ZSM-5 are the most active catalysts for the N$_2$O decomposition. These authors also reported that the activity of the Ru-ZSM-5 catalyst dramatically declined in the presence of oxygen, which was attributed to catalyst deactivation caused by oxygen, presumably due to the formation of Ru oxides. Imamura and co-workers analyzed the excellent performance of Rh/CeO$_2$ catalysts, increasing its thermal stability by incorporation of ZrO$_2$ [19]. Oi *et al*. studied the catalytic N$_2$O decomposition with ZnAlRh hydrotalcite-like compounds. They found that this catalyst exhibited appreciate activity even in the presence of H$_2$O and NO$_2$, which are commonly found in tail-gas from fluidized bed combustors and automobiles, compared to Rh/ZnO catalyst [20, 21]. Yuzaki *et al*. examined the effects of supporting materials, Rh precursors, and Rh dispersion on N$_2$O decompositions over Rh catalysts using 950 or 5000 ppm N$_2$O in He, and demonstrated that Rh/USY, and Rh/Al$_2$O$_3$ catalysts prepared from Rh(NO$_3$)$_3$ had high N$_2$O decomposition activity [22, 23]. They have proposed that the catalytic activity of N$_2$O decomposition was sensitive not only to the Rh dispersion but also to the preparation variables such as the Rh precursors and the supports used. Kunimori and co-workers [24-27] investigated

mechanisms and dynamics of N_2O decomposition using an ^{18}O tracer technique. Over Rh/USY catalyst, N_2O decomposition proceeded via Langmuir-Hinshelwood type desorption (reaction-assisted desorption of O_2) at low temperatures [25, 26]. On the other hand, on Fe-MFI prepared by wet ion-exchange method, Eley-Rideal type desorption has been proposed at a low-temperature region [27]. This result has been supported by Li *et al.* [28]. In the case of Fe-MFI prepared by CVD, a different mechanism has been proposed [29, 30] because of the difference of Fe species on the catalyst [28, 29]. The kinetics of N_2O decomposition over various ion-exchanged Fe-zeolite catalysts was investigated by Hall and co-workers [31-33]. The decomposition of N_2O in operating rooms where halogen-containing organic gases coexist was studied over Rh-Al_2O_3, Pd-Al_2O_3, and Pt-Al_2O_3 catalysts, in order to select the catalysts suitable for decomposition of N_2O in the atmosphere of operating rooms [34]. The effect of alkali metal incorporation in the Rh dispersion was analyzed by Haber and co-workers for Rh/γ-Al_2O_3 system [35]. Muramatsu *et al.* [36] and Satsuma *et al.* [37, 38] clarified effects of CH_4 and O_2 on N_2O decompositions over various metal oxide catalysts (CuO, Co_3O_4, NiO, Fe_2O_3, SnO_2, In_2O_3, Cr_2O_3, TiO_2, Al_2O_3, La_2O_3, MgO, and CaO) experimentally and theoretically.

Current catalysts are not stable and active enough. Therefore, the process cannot be applied economically in practical cases. In particular, using the current catalysts for N_2O decomposition, unfeasible high temperatures are needed for effective catalytic decomposition of N_2O in the presence of inhibiting and deactivating agents which are commonly found in combustion off-gases [5, 17, 39, 40].

1.2.2. Selective catalytic reduction of N_2O

Selective catalytic reduction (SCR) is an alternative to catalytic decomposition with the potential to lower the temperature for effective N_2O removal by addition of a reducing agent, diminishing also the volume of off-gases and the required reactor size, and so reducing cost [40]. In this sense, hydrocarbons are inexpensive and non-corrosive reducing agents and the process presents fewer problems regarding operation, safe, space and cost with respect to conventional NH_3-SCR system [41]. Therefore, the use of widely and easily available hydrocarbons, such as CH_4, C_3H_6 or C_3H_8 is required in order to satisfy the commercial feasibility. The hydrocarbon must be selected by taking into account not only the catalytic activity, but also the selectivity of

the catalyst in order to minimize its consumption as selective reductant. The selected hydrocarbons must be as efficient as possible, that is to say, the addition of low amounts of hydrocarbon should give rise to high conversions for the SCR of N_2O to N_2, CO_2, and H_2O. In most cases, the hydrocarbon added as reducing agent could be consumed in other secondary reactions that compete with the main catalytic reduction reaction, *e.g.* the hydrocarbon combustion and the formation [40, 42, 43] and deposition of carbonaceous species [44, 45].

The groups of Segawa [39, 46-48] and Turek [43, 49] reported that the catalytic activity of Fe-ZSM5 was significantly improved by adding C_3H_6 and C_3H_8 as a reductant under excess O_2 atmosphere. Segawa *et al*. [39, 46-48] studied the selective reduction of N_2O with C_3H_6 and reported high reaction rates over Fe/MFI in the presence of O_2 and H_2O. They assumed that the adsorption and the protonation of C_3H_6 were important steps in the reduction of N_2O with C_3H_6 over Fe/MFI [47]. Turek *et al.* examined that simultaneous catalytic removal of NO and N_2O with C_3H_8 over Fe-MFI catalyst [43, 49]. They reported that the activity for the N_2O removal was strongly inhibited in the presence of NO although the high NO conversions were observed in the presence of N_2O. They demonstrated that high concentrations of reductants (C_3H_6, C_3H_8 etc.) were necessary to achieve 100% conversion in the case of the simultaneous presence of excess oxygen in the reaction gases. On the other hand, we have proposed a new method for treating N_2O with CH_4 in the presence of excess oxygen [50-59]. An ion-exchanged Fe-BEA and Fe-MFI catalysts show good performance in the selective catalytic reduction of N_2O with CH_4 under excess O_2 atmosphere. The reaction of N_2O with CH_4 is proceeded selectively over the ion-exchanged Fe-zeolite catalysts, *i.e.* the addition of only stoichiometric amount of methane needs to reduce N_2O. The formations of intermediate species (methoxy and formate species) [55] and nascent oxygen transients [54, 56, 59] are important for the selective performance. CH_4 (natural gas) is widely available in many parts of the world (more so than the higher hydrocarbons) and is a common fuel used in stationary engines at the power plants which are producing NO_x during the combustion process. However, the reactivity of CH_4 differs fundamentally from that of other hydrocarbons. CH_4 is most difficult to ignite among hydrocarbons. For instance, traditional three-way catalysts, used for controlling emissions from gasoline vehicles, are not able to remove sufficient amounts of CH_4 [60]. The maximum CH_4 emission from a new three-way catalyst converter was 70 ppm, and the CH_4 emission was

increased with increasing vehicle speed and mileage [61]. In the case of vehicles, N_2O emission as well as CH_4 is present in the exhaust gases treated by three-way catalysts. Therefore, we can expect that CH_4 is potentially quite attractive as a viable reductant for N_2O removal.

1.2.3. Selective catalytic reduction of N_2O with ammonia

N$_2$O reduction with ammonia and the simultaneous reduction of NO and N_2O by ammonia has been studied using different Fe-zeolite catalysts (BEA, MFI, FAU, FER etc.) [62-68]. Coq and coworkers reported that BEA zeolite has the most efficient host structure for the reduction of N$_2$O with NH$_3$ [62] because of the presence of the large amount of Fe active sites and widely open porosity of the BEA structure [63]. From the results of kinetics and characterizations (TPD [64, 65], TPR [64, 65], EPR [66], and Mössbauer [67]), they suggested that mononuclear species, binuclear species, and iron-oxides aggregates are present in the ion-exchanged Fe-BEA catalyst with high Fe content. They have proposed that mononuclear iron-oxo species are active sites, and binuclear species and iron-oxides aggregates are less active over the Fe ion-exchanged BEA catalysts [62]. On the other hand, Sugawara *et al.* [69] have revealed that the binuclear Fe site is the most active site based on the results of kinetic study and the elucidation of reaction mechanism. In the real industrial process, however, the use of ammonia as a reductant is limited by the location of the N_2O reduction facility in terms of the problems of NH$_3$ slip and potential hazard of NH$_3$ storage and handling.

1.3. Preparation of Fe-zeolite catalysts

Fe-zeolites are known for the controversies regarding their preparation. Several different methods are described in the literature to prepare Fe-zeolite catalysts. From them, the best known is the following:

(1)   *Wet ion-exchange (WIE):*

WIE is the most common method to prepare metal-exchanged zeolites. A limitation of this technique is that appeared to be impossible to make use of the full ion-exchange capacity of the zeolite, *i.e.* the Fe/Al ratio is limited to about 50% (apart from some reports of Fe/Al = 0.9 obtained with WIE of FeC$_2$O$_4$ by Feng and Hall [70, 71] that

appeared not reproducible [72, 73]) Furthermore, it is reported that when the ion-exchange procedure is carried out in air, Fe_2O_3 (hematite) is formed which is said to have a negative effect on the catalytic activity [74].

(2)   *Solid-state ion-exchange (SSIE):*

An solid iron salt (*e.g.* $FeSO_4$ and $FeCl_3$) is mechanistically mixed with the zeolite powder and subsequently heated carefully in an oven [43, 49, 74].

(3)   *Sublimation (Chemical Vapor Deposition: CVD):*

An iron salt with a low evaporation temperature, *e.g.* $FeCl_3$, is evaporated and reacted with H-form zeolite. This procedure gives a catalyst with a very high exchange rate, *i.e.* every Al-exchange site contains an Fe ion (Fe/Al=1). After CVD, the catalyst has to be washed thoroughly to remove the chlorine and calcined carefully [72, 75-82].

(4)   *Ex-framework:*

This method is based on isomorphous substitution, *i.e.* part of the aluminum in the frame work is replaced by Fe. Using a steamed procedure, the Fe is removed from the framework and becomes available for reaction [83-93].

The most common method of preparing Fe-zeolite catalysts is to introduce Fe by post-synthetic ion exchange in the solid or liquid phase. Calcination of these materials usually leads to the formation of a significant fraction of large iron oxide particles, which are known to be inactive in the different reactions catalyzed by Fe-zeolite catalysts.

Chemical vapor deposition (CVD) of $FeCl_3$ on the zeolite has been suggested as a more reproducible method for preparing over-exchanged Fe-ZSM-5, leading to high iron loadings [72]. However, Pirngruber and Roy reported that Fe-ZSM5 prepared by CVD contains a mixture of small iron oxide clusters whose size may be larger than two iron atoms [81]. Heinrich also observed that Fe-ZSM5 prepared by CVD obviously contains iron in a multitude of species of different aggregation degrees, from isolated ions via dimers, oligomers, and clusters to large aggregates [82].

A distinct approach consists of inserting iron into T positions in the zeolite framework during the hydrothermal synthesis, followed by treatment of the zeolite in air, vacuum, or steam at elevated temperatures [83-93]. In a framework position, iron is not catalytically active [94, 95].

The activation treatments cause the migration of iron to extra-framework positions and their progressive clustering in the form of isolated, dimeric, and polymeric species up to oxidic nanoparticles [85, 89-91]. The extent of iron extraction and aggregation depends on the activation conditions (atmosphere, temperature) and the composition of the MFI framework [89]. The high turnover frequencies in N_2O decomposition [94] and a high stability toward SO_2 [40] have been reported. This method is considered to be a very suitable approach to disperse iron species into the microporous matrix, although typically it does not allow the insertion of iron with high content.

With respect to the catalytic activity and the ease of catalyst manufacture, the wet ion-exchange method to prepare Fe-zeolite is slightly favored over alternative methods. Pirterse and co-workers have suggested that the WIE based Fe-zeolite catalysts show high activities for N_2O decomposition and SCR with good (hydro-thermal) stability [96]. Pirngruber *et al*. have also proposed that WIE samples are more active in NO-assisted N_2O decomposition than the CVD catalysts. They concluded that the main reason for the higher activity of the WIE samples is that the WIE samples contain a higher concentration of Fe^{2+} sites under NO-assisted N_2O decomposition compared to the CVD catalysts [97].

The pH of the suspension of the iron salt and the zeolite during WIE is a key factor in achieving catalysts with high activity in N_2O reduction [98]. The topology of the zeolite is also an important factor for activity as well as stability under realistic practical conditions. Both MFI and BEA zeolite structures exhibit multidirectional channel systems (Fig. 1-5). BEA zeolite is a disordered intergrowth of several hypothetical polymorphs, all characterized by a 3D/12-membered ring channel system, whereas MFI zeolite presents a 3D/10-membered ring channel system. Accordingly, the channel dimensions in BEA (0.66 ✕ 0.67 nm and 0.56 ✕ 0.57 nm) are larger than those in MFI (0.53✕0.56 nm and 0.51✕0.55 nm) [99].

The nature of the iron sites responsible for N_2O decomposition is still under debate. The more controversial point regards their nuclearity. Binuclear Fe species have been considered as an active site for catalytic removal of N_2O over Fe-zeolite catalysts. The presence of Al pairs is necessary for the exchange of bivalent metal cations. Exchange of a "bare" trivalent cation coordinated only to the framework oxygen is not possible in high silica zeolites, because of the lack of sufficient local negative charge. But stabilization of trivalent cations in complexes

bearing negatively charged extra-framework ligands (*e.g.* oxygen atom or OH group) occurs when two Al pairs in different framework six-rings are available [100]. Therefore, exchange capacity of the zeolite and the location and structure of metal ion species, which are accommodated in the zeolite void volume, are controlled by the distribution of aluminum in the zeolite framework. Wichtelová *et al.* estimated spatial distribution of Al atoms in ZSM-5 zeolites by identification of cationic sites containing Al pairs in the zeolite framework [101]. The formation of Al pairs, predominantly with Al–O–Si–O–Si–O–Al sequences, and their distribution in the framework were dramatically affected by the procedure of zeolite synthesis and the Al concentration in the framework [101] as illustrated in Fig. 1-6. Al pairs are preferentially situated at the intersection of the straight and sinusoidal channels of ZSM-5 zeolites. Other local framework structures are occupied by Al pairs at higher content of aluminum in the framework. Such distribution of Al pairs brings high concentration (60–80%) of the α-type metal ions coordinated at the deformed six-member ring at the channel intersection of ZSM-5 zeolite structure.

In this study, the Fe-zeolite catalysts with different Fe content were prepared by severely controlled wet ion-exchange method using Na-form zeolites (Fig. 1-7). Over-exchange (Fe/Al ratio = 1), which can be achieved with the CVD method, but which is also a goal in studies on WIE preparation, is not a key factor in gaining high activity. Wet ion-exchange yields a catalyst with less than 80% of the exchange sites occupied by Fe. In the case of our preparation conditions, at least 2.8 wt% Fe loading (Fe/Al = 0.40) was possible [57].
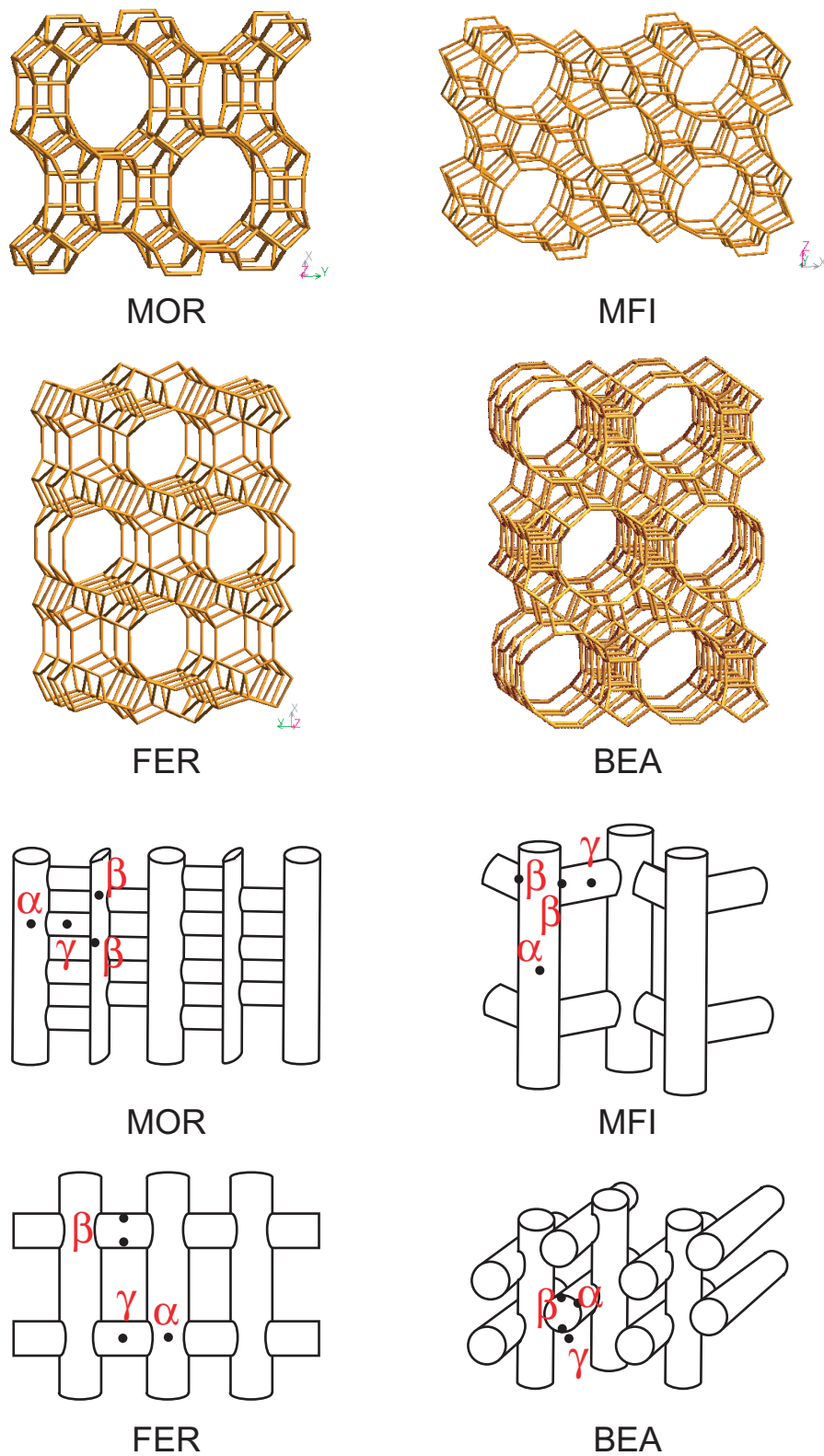
Figure 1-5. Framework structures and connectivity in MOR, FER, MFI and BEA zeolites. The simplified sites of the α-, β- and γ-type Co(II) ions are also shown. The Fe ion distribution found in FER and BEA clearly resembles that found for Co ions. [101]
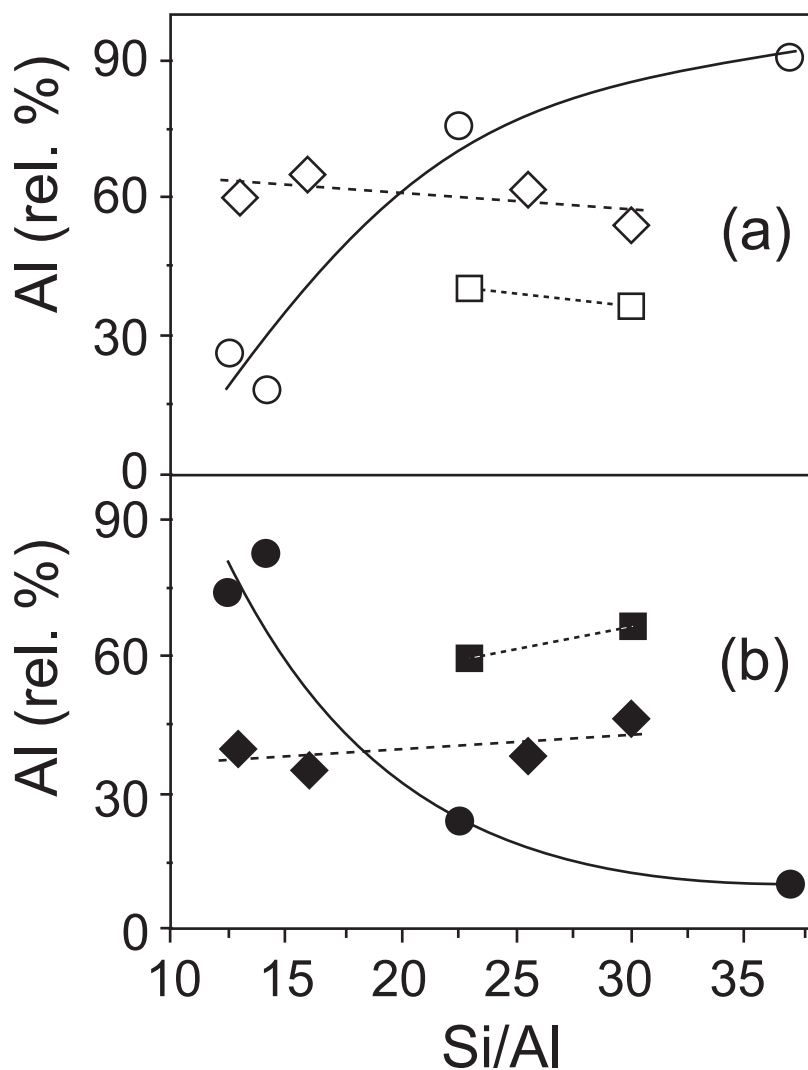
Figure 1-6. Effect of framework Al content and the method of ZSM-5 synthesis on the relative concentration of (a) single Al atoms: (○) commercial samples, (◇) synthesis using Si-Al precursor and (□) synthesis using tetraethyl orthosilicate, and (b) Al in pairs: (●) commercial samples, (◆) synthesis using Si-Al precursor and (■) synthesis using tetraethyl orthosilicate. [100]

H$_2$O 500 ml

N$_2$ bubbling

(100ml/min for 1 hr)

Na-zeolite

(MFI, BEA)

(Si/Al$_2$ = 23.8-25)

Fe source

(FeSO$_4 \cdot$7H$_2$O)

Ion-exchange

N$_2$ bubbling, 323 K, 20 h

pH control
(pH = 4~5)

Calcination

Air, 773 K, 3 h

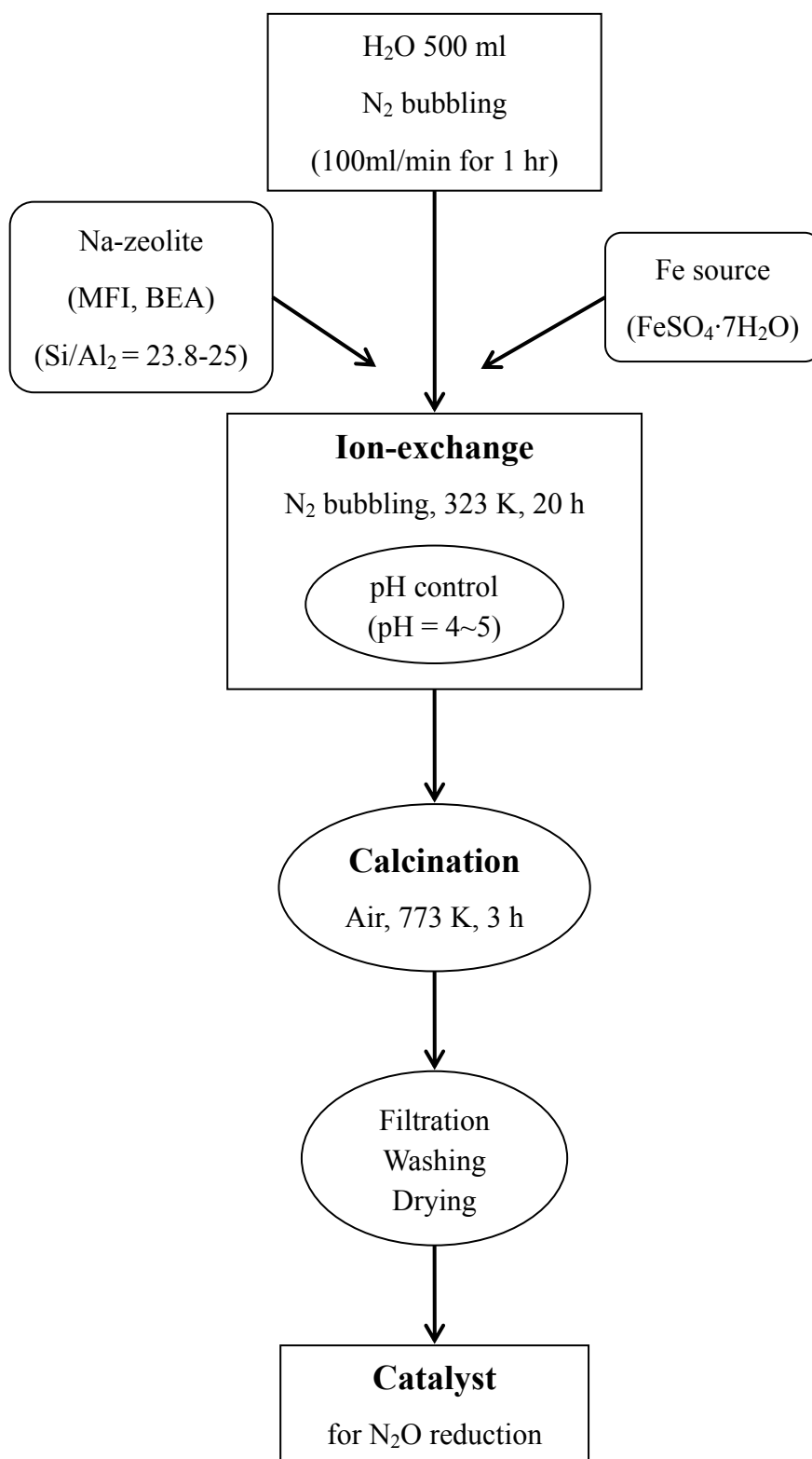Filtration
Washing
Drying

Catalyst

for N$_2$O reduction

Figure 1-7. Preparation procedure of Fe-MFI catalyst

1.4. Purpose of this thesis

The emission control of nitrous oxide as well as NO_x pollutions is one of serious problems in the world. Compared to the research of de-NO_x system, the technical effort to reduce N_2O emissions is not enough. It is well known that catalytic removal of N_2O is the most efficient technique to reduce the N_2O emission in the off-gas from chemical manufacture, anesthesia, and fuel and waste combustions. Recently, Kunimori group found that the selective catalytic reduction of N_2O with CH_4 over ion-exchanged Fe-zeolite catalyst is one of the effective and attractive methods in terms of activity and selectivity. However, the information on active sites and reaction mechanism is not enough to improve the catalysts and develop the catalysis for reducing N_2O emissions. Considered the present situations on catalysis, two main subjects are involved in this thesis.

(A) Elucidation of active site structure over ion-exchanged Fe-zeolite catalysts.

As stated above, we found that ion-exchanged Fe-zeolite catalysts are active for N_2O reduction with CH_4. Recently, Fe-zeolite catalysts have been investigated with great concern, because they are active for NO_x-SCR and N_2O decomposition. The characterization of Fe-zeolite catalysts have also been reported extensively recently. However, the argument on the active sites is not concluded because various kinds of Fe species are present on the catalysts. It can be thought that the formation of un-uniformed Fe species depends on preparation method. Therefore, I prepared the Fe-zeolite catalysts with different Fe content by using severely controlled wet ion-exchange method. Then the effect of Fe loading amount was investigated on features of the catalysts, and the catalytic performance of SCR of N_2O and CH_4 was studied. The active site structure and its role in the SCR of N_2O with CH_4 were discussed from the combination of a number of kinetic studies with characterization results.

(B) Elucidation of reaction mechanism of SCR of N_2O with CH_4.

Selective catalytic reduction of N_2O with CH_4 is a unique and interesting reaction because the reactivity of CH_4 as a reductant is poor in general. However, it is unsolved why N_2O can be reduced by CH_4 at low temperature and why the reaction between N_2O and CH_4 can proceed selectively even in the presence of excess O_2. Therefore, I investigated the reaction mechanism

of the selective catalytic reduction of N_2O with CH_4 in detail. In this study, the observation of intermediate species and the investigation of its reactivity in the SCR condition were carried out. The role of active oxygen species for CH_4 activation and the activation mechanism of CH_4 was investigated and discussed.

1.5. Outline of the thesis

This thesis gives the results of the elucidation of the active site species over Fe-zeolite catalyst and the reaction mechanism of selective catalytic reduction of N_2O with CH_4 under excess O_2 atmosphere. This thesis consists of seven chapters. Each chapter of this thesis is written based on one or two different publications, and can be read independently.

Chapter 1 is general introduction. The background of N_2O emission, the result of recent studies of catalytic N_2O removal, and the features of several preparation methods of Fe-zeolite catalysts are mentioned. The purpose of this thesis is also described.

In chapter 2, the effect of Fe content in Fe-zeolite (MFI) catalysts on the catalyst performance in $N_2O + CH_4$ and $N_2O + CH_4 + O_2$ reactions, and the relation between the activity and the characterization results is discussed. A series of Fe-MFI catalysts are successfully prepared by severely controlled wet ion-exchange technique, and the results of the catalytic activity measurements are given. The features of active Fe species such as reducibility and capacity of oxygen deposition were investigated and discussed by means of reaction kinetics, H_2-TPR, O_2-TPD, and pulse reaction technique.

Chapter 3 describes the effect of reductants (CH_4, C_2H_6, C_3H_6, H_2, and CO) over a series of ion-exchanged Fe-MFI catalysts based on the catalytic performance of N_2O reduction in the presence and absence of excess oxygen atmosphere. From the results of the catalytic activity and selectivity, it is clearly shown that CH_4 is the most efficient reductant for N_2O removal in both the presence and absence of excess oxygen atmosphere. The active site structure has been proposed from the results of kinetic data, various characterizations, and EXAFS spectroscopy.

In chapter 4, the reactions between N_2O and CH_4 over an ion-exchanged Fe-BEA catalyst are studied by using pulse reaction technique, O_2-TPD, and FTIR spectroscopy. The formation of intermediate species is observed over Fe ion sites in the $N_2O + CH_4$ reaction. The reactivity of surface oxygen species adsorbed by N_2O decomposition is investigated. A possible mechanism is

discussed in terms of nascent oxygen transients (O*(a)), which play an important role in the activation/oxidation of CH_4 at initial steps.

In chapter 5, the intermediate species in N_2O + CH_4 reaction over Fe-BEA catalyst are identified by *in-situ* FTIR spectroscopy. The reactivity between intermediates and oxidizing agents (N_2O = 0.01% and O_2 = 10%) is investigated in the similar condition with the activity test experiments. The detailed mechanism of this reaction is proposed.

Chapter 6 focuses on the role of the adsorbed species, which are formed by exposing N_2O to activated Fe-MFI catalyst. The formed adsorbed species gave a distinctive desorption profile compared to the result shown in chapter 2, and these species are known as to active species in the N_2O reduction. The purpose of this study was to measure the activity of the adsorbed oxygen species with CH_4 and to compare the reaction rate in the case of N_2O + CH_4 reaction. In this chapter, the results of the identification of adsorbed oxygen species and the role of these species for activation of CH_4 are shown. On the basis of the comparison of the reaction rates, the CH_4 activation mechanism in the SCR of N_2O with CH_4 is discussed.

In chapter 7, all the results of this thesis are summarized.

References

[1]   J.T. Houghton, *et al*. (Eds.), *Climate Change 2001*, *The Scientific Basis*. C*ontribution of the Working Group I to the Third Assessment Report of the IPCC*, Cambridge (2001).

[2]   UNFCCC, http://unfccc.int/2860.php

[3]   Greenhouse Gas Inventory Office of Japan, http://www-gio.nies.go.jp/index.html

[4]   J.T. Houghton, *et al*. (Eds.), *Climate Change 1995*, *The Science of Climate Change. Contribution of WGI to the second assessment report of the IPCC,* Cambridge (1996).

[5]   F. Kapteijn, J.R. Mirasol, J.A. Moulijn, *Appl. Catal. B* **9** (1996) 25.

[6]   T. Shimizu, *J. Inst. Energy,* **80** (2001) 1021.

[7]   G. Centi, S. Perathoner, F. Vazzana, M. Marella, M. Tomaselli, M. Mantegazza, *Adv. Env. Res.* **4** (2000) 325.

[8]   Z. Zhao, A. Matsunami, K. Kitagawa, N. Arai, *Microchem. J.* **65** (2000) 137.

[9]   C.S. Swamy, J. Christopher, *Catal. Rev. Sci. Eng.* **34** (1992) 409.

[10]   G. Centi, *Appl. Catal. A* **173** (2001) 287.

[11]   T. Turek, *Appl. Catal. B* **9** (1996) 201.

[12]   T. Turek, *Catal. Today* **105** (2005) 275.

[13]   T.W. Dann, K.H. Schulz, M. Mann, M. Collings, *Appl. Catal. B* **6** (1995) 1.

[14]   H.C. Zeng, X.Y. Pang, *Appl. Catal. B* **13** (1997) 113.

[15]   X.F. Wang, H.C. Zeng, *Appl. Catal. B* **17** (1998) 89.

[16]   F. Pinna, M. Scarpa, G. Strukul, E. Guglielminotti, F. Boccuzzi, M. Manzoli. *J. Catal.* **192** (2000) 158.

[17]   Y. Li, J.N. Armor, *Appl. Catal. B* **1** (1992) L21.

[18]   Y. Li, J.N. Armor, *Appl. Catal. B* **3** (1993) 55.

[19]   S. Imamura, R. Hamada, Y. Saito, K. Hashimoto, H. Jindai, *J. Mol. Catal. A* **139** (1999) 55.

[20]   J. Oi, A. Obuchi , G.R. Bamwenda, A. Ogata, H. Yagita, S. Kushiyama, K. Mizuno, *Appl. Catal. B* **12** (1997) 277.

[21]   J. Oi, A. Obuchi , A. Ogata, G.R. Bamwenda, K. Tanaka, T. Hibino, S. Kushiyama, *Appl. Catal. B* **13** (1997) 197.

[22]   K. Yuzaki, T. Yarimizu, K. Aoyagi, S. Ito, K. Kunimori, *Catal. Today* **45** (1998) 129.

[23]   K. Yuzaki, T. Yarimizu, S. Ito, K. Kunimori, *Catal. Lett.* **47** (1997) 173.

[24]   H. Uetsuka, K. Aoyagi, S. Ito, S. Kameoka, K. Kunimori, *Catal. Lett.* **66** (2000) 87.

[25]   S. Tanaka, K. Yuzaki, S. Ito, H. Uetsuka, S. Kameoka, K. Kunimori, *Catal. Today* **63** (2000) 413.

[26]   S. Tanaka, K. Yuzaki, S. Ito, S. Kameoka, K. Kunimori, *J. Catal.* **200** (2001) 203.

[27]   T. Nobukawa, S. Tanaka, S. Ito, K. Tomishige, S. Kameoka, K. Kunimori, *Catal. Lett.* **83** (2002) 5.

[28]   K. Sun, H. Xia, E. Hensen, R. Van Santen, C. Li, *J. Catal.* **238** (2006) 186.

[29]   G.D. Pirngruber, P.K. Roy, *Catal. Lett.* **93** (2004) 75.

[30]   P.K. Roy, G.D. Pirngruber, *J. Catal.* **227** (2004) 164.

[31]   C.M. Fu, V.N. Korchak, W.K. Hall, *J. Catal.* **68** (1981) 166.

[32]   J. Leglise, J.O. Petunchi, W.K. Hall, *J. Catal.* **86** (1984) 392.

[33]   J. Valyon, W.S. Millman, W.K. Hall, *Catal. Lett.* **24** (1994) 215.

[34]   K. Doi, Y.Y. Wu, R. Takeda, A. Matsunami, N. Arai, T. Tagawa, S. Goto, *Appl. Catal. B* **35** (2001) 43.

[35]   J. Haber, T. Machej, J. Janas, M. Nattich, *Catal. Today* **90** (2004) 15.

[36]   H. Muramatsu, K. Tokura, T. Mori, R. Akahori, K. Watanabe, A. Satsuma, T. Hattori, Y. Murakami, *Energy Convers. Manage.* **38** (1997) 1399.

[37]   A. Satsuma, R. Akahori, M. Kato, S. Komai, H. Yoshida, T. Hattori, *J. Mol. Catal. A* **155** (2000) 81.

[38]   A. Satsuma, H. Maeshima, K. Watanabe, K. Suzuki, T. Hattori, *Catal. Today* **63** (2000) 347.

[39]   K. Yamada, S. Kondo, K. Segawa, *Microporous Mesoporous Mater.* **35-36** (2000) 227.

[40]   J. Pérez-Ramírez, F. Kapteijn, G. Mul, J.A. Moulijn, *Appl. Cata. B* **35** (2002) 227.

[41]   G. Centi, F. Vanazza, *Catal. Today* **53** (1999) 683.

[42]   R.W. van den Brink, S. Booneveld, J.R. Pels, D.F. Bakker, M.J.F.M. Verhaak, *Appl. Catal. B* **32** (2001) 73.

[43]   M. Kögel, R. Mönnig, W. Schwieger, A. Tissler, T. Turek, *J. Catal.* **182** (1999) 470.

[44]   S. Kameoka, K. Yuzaki, T. Takeda, S. Tanaka, S. Ito, T. Miyadera, K. Kunimori, *Phys.*

Chem. Chem. Phys. **3** (2001) 256.

[45]   J. Pérez-Ramírez, J.M. Garcia-Cortes, F. Kapteijn, M.J. Illan-Gomez, A. Ribera, C. Salinas-Martínez de Lecea, J. Moulijn. *Appl. Catal. B* **25** (2000) 191.

[46]   C. Pophal, T. Yogo, K. Tanabe, K. Segawa, *Catal. Lett.* **44** (1997) 271.

[47]   C. Pophal, T. Yogo, K. Yamada, K. Segawa, *Appl. Catal. B* **16** (1998) 177.

[48]   K. Yamada, C. Pophal, K. Segawa, *Microporous Mesoporous Mater.* **21** (1998) 549.

[49]   M. Kögel, V.H. Sandoval, W. Schwieger, A. Tissler, T. Turek, *Catal. Lett.* **51** (1998) 23.

[50]   S. Kameoka, T. Suzuki, K. Yuzaki, T. Takeda, S. Tanaka, S. Ito, T. Miyadera, K. Kunimori, *Chem. Commun.* (2000) 745.

[51]   S. Kameoka, K. Kita, T. Takeda, S. Tanaka, S. Ito, K. Yuzaki, T. Miyadera, K. Kunimori, *Catal. Lett.* **69** (2000) 169.

[52]   S. Kameoka, S. Tanaka, K. Kita, T. Nobukawa, S. Ito, T. Miyadera, K. Kunimori, *Stud. Surf. Sci. Catal.* **135** (2001) 321.

[53]   T. Nobukawa, K. Kita, S. Tanaka, S. Ito, T. Miyadera, S. Kameoka, K. Tomishige, K. Kunimori, *Stud. Surf. Sci. Catal.* **142** (2002) 557.

[54]   S. Kameoka, T. Nobukawa, S. Tanaka, S. Ito, K. Tomishige, K. Kunimori, *Phys. Chem. Chem. Phys.* **5** (2003) 3328.

[55]   T. Nobukawa, M. Yoshida, S. Kameoka, S. Ito, K. Tomishige, K. Kunimori, *J. Phys. Chem. B* **108** (2004) 4071.

[56]   T. Nobukawa, M. Yoshida, S. Kameoka, S. Ito, K. Tomishige, K. Kunimori, *Catal. Today* **93-95** (2004) 791.

[57]   M. Yoshida, T. Nobukawa, S. Ito, K. Okumura, K. Tomishige, K. Kunimori, *J. Catal.* **223** (2004) 454.

[58]   T. Nobukawa, M. Yoshida, K. Okumura, K. Tomishige, K. Kunimori, *J. Catal.* **229** (2005) 374.

[59]   T. Nobukawa, K. Sugawara, K. Okumura, K. Tomishige, K. Kunimori, *Appl. Catal. B*, in press.

[60]   S.H. Oh, P.J. Miychell, R.M. Siewert, *J. Catal.* **132** (1991) 287.

[61]   A. Takigawa, A. Matsunami, N. Arai, *Energy* **30** (2005) 461.

[62]   M. Mauvezin, G. Delahay, F. Kißich, B. Coq, S. Kieger, *Catal. Lett.* **62** (1999) 41.

[63]   A. Guzmán-Vargas, G. Delahay, B. Coq, *Appl. Catal. B* **42** (2003) 369.

[64]   B. Coq, M. Mauvezin, G. Delahay, S. Kieger, *J. Catal.* **195** (2000) 298.

[65]   G. Delahay, M. Mauvezin, B. Coq, S. Kieger, *J. Catal.* **202** (2001) 156.

[66]   E.A. Zhilinskaya, G. Delahay, M. Mauvezin, B. Coq, A. Aboukaïs, *Langmuir* **19** (2003) 3596.

[67]   M. Mauvezin, G. Delahay, B. Coq, S. Kieger, J.C. Jumas, J. Olivier-Fourcade, *J. Phys. Chem. B* **105** (2001) 928.

[68]   B. Coq, M. Mauvezin, G. Delahay, J.B. Butet, S. Kieger, *Appl. Catal. B* **27** (2000) 193.

[69]   K. Sugawara, T. Nobukawa, M. Yoshida, Y. Sato, K. Okumura, K. Tomishige, K. Kunimori, *Appl. Catal. B*, submitted.

[70]   X.B. Feng, W.K. Hall, *Catal. Lett.* **41** (1997) 45.

[71]   X.B. Feng, W.K. Hall, *J. Catal.* **166** (1997) 368.

[72]   H.-Y. Chen, W.M.H. Sachtler, *Catal. Today* **42** (1998) 73.

[73]   W.K. Hall, X.B. Feng, J. Dumesic, R. Watwe, *Catal. Lett.* **52** (1998) 13.

[74]   M. Rauser, K. Kesore, R. Monnig, W. Schwieger, A. Tisler, T. Turek, *Appl. Catal. A* **184** (1999) 249.

[75]   A.A. Battiston, J.H. Bitter, D.C. Koningsberger, *Catal. Lett.* **66** (2000) 75.

[76]   H.T. Lee, H.K. Rhee, *Catal. Lett.* **61** (1999) 71.

[77]   A.V. Kucherov, C.N. Montreuil, T.N. Kucherova, M. Shelef, *Catal. Lett.* **56** (1998) 173.

[78]   L.J. Lobree, I.C. Hwang, J.A. Reimer, A.T. Bell, *J. Catal.* **186** (1999) 242.

[79]   P. Marturano, L. Drozdova, G.D. Pirngruber, A. Kogelbauer, R. Prins, *Phys. Chem. Chem. Phys.* **3** (2001) 5585.

[80]   Q. Zhu, E.J.M. Hensen, B.L. Mojet, J.M.H.C. van Wolput, R.A. van Santen, *Chem. Commun.* (2002) 1232.

[81]   G.D. Pirngruber, P.K. Roy, *Catal. Today* **110** (2005) 199.

[82]   F. Heinrich, C. Schmidt, E. Löffler, M. Menzel, W. Grünert, *J. Catal.* **212** (2002)157.

[83]   R.W. van den Brink, S. Booneveld, M.J.F.M. Verhaak, *Catal. Today* **75** (2002) 227.

[84]   P. Fejes, J.B. Nagy, K. Lazar, A. Horvath, J. Halasz, *Appl. Catal. A* **175** (1998) 89.

[85]   J. Pérez-Ramírez, G. Mul, F. Kapteijn, J.A. Moulijn, A.R. Overweg, A. Domenech, A. Ribera, I.W.C.E. Arends, *J. Catal.* **207** (2002) 113.

[86]   L. Kiwi-Minsker, D.A. Bulushev, A. Renken, *J. Catal.* **219** (2003) 273.

[87]   D.A. Bulushev, L. Kiwi-Minsker, A. Renken, *J. Catal.* **222** (2004) 389.

[88]   J. Pérez-Ramírez, F. Kapteijn, J.C. Groen, A. Doménech, G. Mul, J.A. Moulijn, *J. Catal.* **214** (2003) 33.

[89]   J. Pérez-Ramírez, *J. Catal.* **227** (2004) 512.

[90]   S. Bordiga, R. Buzzoni, F. Geobaldo, C. Lamberti, E. Giamello, A. Zecchina, G. Leofanti, G. Petrini, G. Tozzola, G. Vlaic, *J. Catal.* **158** (1996) 486.

[91]   G. Berlier, G. Spoto, S. Bordiga, G. Ricchiardi, P. Fisicaro, A. Zecchina, I. Rossetti, E. Selli, L. Forni, E. Giamello, C. Lamberti, *J. Catal.* **208** (2002) 64.

[92]   A.M. Ferreti, C. Oliva, L. Forni, G. Berlier, A. Zecchina, C. Lamberti, *J. Catal.* **208** (2002) 83.

[93]   K.A. Dubkov, N.S. Ovanesyan, A.A. Shteinman, E.V. Starokon, G.I. Panov, *J. Catal.* **207** (2002) 341.

[94]   J. Perez-Ramirez, F. Kapteijn, G. Mul, J.A.Moulijn, *Chem. Commun.* (2001) 693.

[95]   L.V. Pirutko, O.O. Parenago, E.V. Lunina, A.S. Kharitonov, L.G. Okkel, G.I. Panov, React. Kinet. *Catal. Lett.* **52** (1994) 275.

[96]   J.A.Z. Pieterse, S. Booneveld, R.W. van den Brink, *Appl. Catal. B* **51** (2004) 215.

[97]   G.D. Pirngruber, J.A.Z. Pieterse, *J. Catal.* **237** (2006) 237.

[98]   T. Kagawa, graduate thesis of University of Tsukuba, 2004.

[99]   Database of Zeolite Structures, http://www.iza-structure.org/databases.

[100] B. Wichtelová, Z. Sobalík, J. Dědeček, *Appl. Catal. B* **41** (2003) 97.

[101] J. Dědeček, D. Kaucký, B. Wichterlová, O. Gonsiorová, *Phys. Chem. Chem. Phys.* **4** (2002) 5406.

Chapter 2

Effect of Fe content of ion-exchanged Fe-MFI catalysts in N_2O + CH_4 reaction under an excess O_2 atmosphere

2.1. Introduction

Nitrous oxide (N_2O), which also contributes to catalytic stratospheric ozone destruction, is a strong greenhouse-effects gas with global warming potential (GWP) per molecule of about 300 times that of carbon dioxide (CO_2) [1, 2]. Therefore, from an environmental point of view, the catalytic decomposition of N_2O ($N_2O \rightarrow N_2 + 1/2O_2$) [2-15] and the selective catalytic reduction (SCR) of N_2O with reductant such as various hydrocarbons [16-31] and ammonia [32-34] have been attracting much attention. Various kinds of metal oxides (including mixed oxides) [3,4], supported noble metals (Rh, Ru) [5-8] and transition metal-exchanged zeolites (Cu-MFI, Fe-MFI, etc.) [9-15] have been studied for N_2O decomposition. In the case of the SCR of N_2O over Fe-MFI catalysts, various reductants (except methane) such as propane [16, 17], propene [18-22, 24], ethane [25] and ammonia [32-34] have been utilized.

Kunimori and co-workers have reported that Fe-BEA catalysts prepared by a wet ion-exchange method showed higher activity than Fe-MFI catalyst in the SCR of N_2O with light hydrocarbons [24-30]. Especially, I have been studying the SCR of N_2O by methane (CH_4) over Fe-zeolite. Generally speaking, it is difficult to use CH_4 as the reducing agent since the reactivity of CH_4 is very low. However, CH_4 is efficient reductant in SCR reaction compared with light alkanes [26-30], and that Fe-BEA catalysts are most active for the reduction of N_2O with CH_4 in Fe-zeolite catalysts (MFI, MOR, FAU) [28]. Furthermore, I have proposed that nascent oxygen formed from N_2O dissociation can drastically promote the activation of CH_4 in terms of the reaction mechanism [30, 31].

Recently, studies on the structure and reactivity of Fe-zeolite catalysts, particularly Fe-MFI and Fe-BEA, have been carried out. Sachtler and co-workers have reported that Fe/MFI prepared by a sublimation method has a molar ratio of Fe to Al-centered tetrahedral of 1/1 and that active species over MFI are an oxygen-bridged binuclear iron species [35, 36]. Koningsberger and co-workers have determined the structure of the Fe binuclear complex with Fe-O-Fe bridges on

Fe/ZSM5 catalysts, which were prepared by $FeCl_3$, by EXAFS [37]. Panov and co-workers have indicated that α-oxygen can participate in the direct catalytic oxidation of benzene to phenol by N_2O over Fe-MFI, and the oxygen species are related to the presence of a binuclear Fe complex [38-44].

In addition, it has been pointed out that another kind of structure of iron species appears with increasing amount of Fe loading [32, 33, 45]. Coq and co-workers have proposed that mononuclear iron-oxo cations, which exist mainly on low-exchange-level catalysts, are the most highly reactive sites for the reduction of N_2O by NH_3 over Fe-BEA catalysts, and binuclear iron-oxo species and iron oxides that are formed over high Fe loading catalysts are less active [32-34]. Moreover, when propene was used as reductant in the reduction of N_2O, even low-exchange Fe-ZSM-5 catalysts exhibited high activity [22]. From these comparisons, the active structure of iron species over zeolites is much dependent on the kind of reductant.

Therefore, it is worth elucidating the active sites on Fe-MFI catalysts in the N_2O reduction with CH_4 under an excess oxygen atmosphere. In this chapter, the dependence of the catalytic activity of N_2O reduction with CH_4 on the loading amount of Fe over MFI has been investigated. The catalyst characterization has also been studied by means of H_2-TPR, O_2-TPD, and pulse reactions. From the comparison between the activity and characterization results, the structure of the active sites and the reaction mechanism are considered.

2.2. Experimental

2.2.1. Catalyst preparation

Fe-MFI catalysts were prepared by an ion-exchange method using an aqueous solution of $FeSO_4 \cdot 7H_2O$ (Wako Pure Chemical Industries Ltd., 98%) for 20 h at 323 K under a nitrogen atmosphere to avoid the precipitation of $Fe(OH)_3$. Na-MFI (TOSOH Co., $SiO_2/Al_2O_3 = 23.8$) was used as the catalyst support. The catalyst was separated from the solution by filtration after an ion exchange procedure. It was washed thoroughly with distilled water and dried at 383 K overnight, followed by calcination in air at 773 K for 3 h. The loading amount of the Fe on MFI was determined by subtracting the Fe amount in the solution after the separation, analyzed by ICP analysis, from the total amount. The exchange efficiency of $FeSO_4$, percentage of the iron salt incorporated into the zeolite, was almost 100% in the case of Fe/Al = 0.05 - 0.24. On the

other hand, it was almost 80% in the case of Fe/Al = 0.40. The catalyst is denoted as Fe(X)-MFI, where X stands for molar ratio of Fe/Al. (Table 2-1)

2.2.2. Activity test

Catalytic reduction of N_2O with CH_4 under an excess O_2 atmosphere was carried out in a fixed-bed flow reactor, as shown in Fig. 2-1. Reactant gases were the mixture of N_2O (950 ppm), CH_4 (500 ppm) and O_2 (0-20%) balanced with He. All these research grade gases were purchased from Takachiho Trading Co. Ltd., and they were used without further purification. The catalyst weight was 50 mg, and total pressure was 0.1 MPa, and W/F (W/g = catalyst weight, F/mol h^{-1} = total flow rate) was 0.41 g h mol^{-1}. The catalysts were pretreated at 773 K with O_2 for 1 h in the reactor. As a reference, N_2O decomposition was also carried out. Reactant gases were N_2O (950 ppm) balanced with He. Other reaction conditions were the same as those in N_2O reduction as described above. The products were monitored by an on-line TCD gas chromatograph (Shimadzu GC-8A) equipped with Molecular sieve 5A column for N_2 and O_2, and Porapak Q column for N_2O, and an FID gas chromatograph (Shimadzu GC-14B) equipped with Gaskuropak 54 column and methanator for CO, CO_2 and CH_4. The sampling and analyzing of effluent gas was carried out for 1 h at each reaction temperature. This means that the results of the activity test shown in the Figures were obtained under steady-state conditions.

2.2.3. Catalyst characterization

Temperature-programmed reduction (TPR) with H_2 was performed in a fixed-bed flow reactor. The sample was pretreated in 100% O_2 flow at 773 K for 1 h, and then it was cooled down to room temperature and exposed to helium flow in order to purge the line. The TPR profile of each sample was recorded from room temperature to 973 K under a flow of 5.0% H_2/Ar. The flow rate of 5.0% H_2/Ar was 30 ml/min, and the catalyst weight was 50 mg. The heating rate was 10 K/min and the temperature was maintained at 973 K for 10 min after it reached 973 K. The consumption of H_2 was monitored continuously with a TCD gas chromatograph equipped Molecular Sieve 5A in order to remove H_2O from the effluent gas.

Temperature-programmed desorption of O_2 (O_2-TPD) was carried out in a fixed-bed reactor equipped with a quadrupole mass spectrometer (Balzers QMS 200 F). The catalysts (30

mg) were pretreated with O_2 flow (100% O_2, 773 K, 1 h) or N_2O flow (10% N_2O/He, 773 K, 1 h). After the pretreatment, they were rapidly cooled down to room temperature. Helium gas (flow rate 55 ml/min) was introduced to the reactor, and the sample was heated with heating rate 10 K/min from room temperature to 1273 K. The sample temperature was kept at 1273 K for 30 min just after it reached 1273 K. Desorbed O_2 in He flow (flow rate, 55 ml/min) was analyzed with the quadrupole mass spectrometer.

Pulse reactions of N_2O + CH_4 were carried out in a fixed-bed reactor combined with TCD-GC. For Fe(0.40)-MFI and Fe(0.10)-MFI, three kinds of pretreatment were carried out: H_2 (5% H_2/Ar, 30 ml/min) at 773 K for 1 h, O_2 (100% O_2, 30 ml/min) at 773 K for 1 h, and N_2O (10% N_2O/He, 30 ml/min) at 773 K for 1 h. The catalyst weight was 30 mg for Fe(0.40)-MFI and 120 mg for Fe(0.10)-MFI, where the amount of Fe on the catalyst was just the same (15 μmol). Pulse gas contained 0.82 μmol N_2O and 0.40 μmol CH_4. The gases (N_2O and CH_4) were analyzed by TCD-GC. The pulse was injected 25 times with the 5-min intervals.

2.3. Results and discussion

Selective catalytic reduction of N_2O with CH_4 over ion-exchanged Fe-MFI catalysts was carried out in the N_2O/CH_4/O_2 system in the temperature range between 473 K and 773 K. The gas consisted of 950 ppm N_2O, 500 ppm CH_4 and 10% O_2 diluted with He. Products of this reaction were N_2, CO, CO_2, and H_2O. NO_X was not detected in this reaction. Figs. 2-2(a) and (b) show the temperature dependence of N_2O and CH_4 conversion over Fe-MFI with various kinds of Fe loading, respectively. It is clear that the catalytic activity of N_2O reduction increased with increasing Fe amount. In the case of Fe(0.05)-MFI, the reaction started at about 600 K. On the other hand, the reaction can proceed even under 550 K over Fe(0.40)-MFI. As shown in Fig. 2-2(b), CH_4 conversion increased with the reaction temperature and also with Fe loading. It is interesting that the behavior of N_2O and CH_4 is similar to each other over various Fe-MFI catalysts (Figure 2-2(c)). Furthermore, it should be pointed that there was a plateau in CH_4 conversion at which N_2O conversion reached almost 100%, especially over Fe-MFI (Fe/Al = 0.40) (Figure 2-2(b)). This indicates that the activation of CH_4 requires N_2O, and CH_4 can not be oxidized directly with O_2 even at 773 K. In addition, CO_2 selectivity and (consumed N_2O)/($3CO$ + $4CO_2$) are also shown in Figs. 2-2(d) and (e), respectively. CO_2 selectivity is estimated by

$CO_2/(CO + CO_2)$. Regarding Figure 2-2(e), $3CO + 4CO_2$ represents the total amount of oxidizing agent assuming the equations:

$$CH_4 + 4[O] \rightarrow CO_2 + 2H_2O$$

$$CH_4 + 3[O] \rightarrow CO + 2H_2O$$
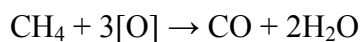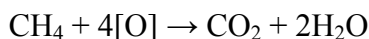
[O] is oxygen atom originated from N_2O and O_2. Therefore, the ratio of the consumption rate of N_2O to the formation rate of $3CO + 4CO_2$ corresponds to the contribution of N_2O in the total amount of the reacted oxidizing agents ($N_2O + O_2$). As shown in Fig. 2-2(d), the selectivity of CO_2 increased with reaction temperature gradually. Fig. 2-2(e) shows the ratio of N_2O to total oxidizing agents (N_2O and O_2) in CH_4 oxidation to CO and CO_2. The ratio was located between 40% and 60%. This indicates that oxygen as well as N_2O is used as an oxidizing agent. Under the presence of excess oxygen, N_2O can be reduced with CH_4 over Fe-MFI. Although the concentration of N_2O (950 ppm) is about 100 times as low as that of O_2 (10%), about half of the oxidizing agents was contributed by N_2O as shown in Fig. 2-2(e). As described above, oxygen can not react with CH_4 directly. Therefore, CH_4 is at first activated with N_2O to give reaction intermediates (i.e., methoxy species etc. [30]), which can react with both N_2O and O_2. The results of our FTIR studies [30, 31] will be commented on later.

N$_2$O reduction with CH_4 in the absence of oxygen over Fe-MFI catalysts was also carried out. Figs. 2-3(a) and (b) show the temperature dependence of N_2O and CH_4 conversion over Fe-MFI with various kinds of Fe loading, respectively. As Fig. 2-3(a) is compared with Fig. 2-2(a), N_2O conversion in the absence of oxygen was a little higher than that under the excess oxygen atmosphere (10%) over each Fe-MFI catalyst. Regarding CH_4 reactivity (Fig. 2-3(b)), the CH_4 conversion curve over each Fe-MFI catalyst showed a plateau at about 60%. This tendency is different from that under an excess oxygen atmosphere, where there was a plateau at about 80%. This is due to the contribution of oxygen in CH_4 oxidation. In terms of CO_2 selectivity, the presence of oxygen increased the CO_2 selectivity. Furthermore, the relation between CH_4 conversion and N_2O conversion shows that N_2O can react with CH_4 selectively in the presence and absence of oxygen (Fig. 2-2(c) and Fig. 2-3(c)).

Figure 2-4 shows profiles of temperature-programmed reduction (TPR) with H_2 over Fe-MFI catalysts after O_2 treatment at 773 K. The TPR profile of Fe_2O_3 is also shown in the figure. It is clear that the TPR profile of Fe-MFI was much different from that of Fe_2O_3. The

peak at 670-680 K can be assigned to the reduction from Fe^{3+} ions to Fe^{2+} ions [32, 34, 35]. The peak at 850 K can be assigned to the reduction of Fe_2O_3 by comparing to TPR profile of Fe_2O_3 reference compound (Fig. 2-4f). This small peak appeared only on Fe(0.40)-MFI catalysts. This is due to the aggregation of Fe ions on the catalyst with high Fe loading. A molar ratio of consumed H_2 to Fe on Fe-MFI can be estimated to be 0.5 on all the Fe-MFI catalysts on the basis of the equation $Fe^{3+} + 1/2H_2 \rightarrow Fe^{2+} + H^+$ (Table 2-2). These results indicate that most of Fe species on Fe-MFI catalysts exist as Fe^{3+} ions after O_2 pretreatment. In addition, it should be noted that the starting temperature of Fe reduction was lower on Fe-MFI with higher Fe loading. For example, the reduction started at *ca.* 600 K on Fe(0.05)-MFI, while it started at 450 K on Fe(0.40)-MFI. This indicates that Fe-MFI catalysts with higher Fe content contain more reducible Fe species. This suggests that the structure of Fe ion species is highly dependent on the Fe loading.

Profiles of temperature-programmed desorption (TPD) of O_2 over the catalysts after O_2 treatment are shown in Fig. 2-5(I). The desorption was observed in the range of 673 K to 1273 K. On Fe(0.05)-MFI and Fe(0.10)-MFI, a single and broad peak is observed. In contrast, on Fe-MFI (Fe/Al $\geq$ 0.15), a sharper peak appeared around 873 K. The results of O_2-TPD also strongly suggest that the structure of Fe ion species is highly dependent on the Fe loading. O_2-TPD profiles on the catalyst after N_2O treatment are also shown in Fig. 2-5(II). It is found that the amount of O_2 desorption of the sample after N_2O treatment is larger than that after O_2 treatment. Especially, this phenomenon is clearly observed on Fe(0.40)-MFI. The O_2-TPD profiles over Fe(0.40)-MFI after N_2O and O_2 treatments and their subtracted profile are shown in Fig. 2-5(III). Although some fluctuation is contained in the subtracted spectrum, it indicates that N_2O-induced desorption is observed mainly at lower-temperatures.

In order to estimate the desorption amount in each peak, the deconvolution of the desorption was carried out on the basis of the following assumptions: (i) O_2 desorption at the higher temperature peak starts at 793 K, at which the desorption on Fe-MFI (Fe/Al = 0.05 and 0.10) started. (ii) The peak top is located at 1043 K, where the peak top on Fe-MFI (Fe/Al = 0.05 and 0.10) was observed. (iii) Each peak has a symmetrical shape. The results of the deconvolution are shown in Fig. 2-6 and they are also listed in Table 2-2. The O_2-TPD profile of Fe(0.05)-MFI and Fe(0.10)-MFI after N_2O treatment was very similar to that of after O_2

treatment. This indicates that the amount of oxygen derived from N$_2$O dissociation (N$_2$O → N$_2$ + O(a)) over O$_2$-treated Fe(0.05)-MFI and Fe(0.10)-MFI is very small. In addition, the catalytic activity of Fe-MFI in N$_2$O decomposition at 773K is listed in Table 2-2. In the terms of the activity of N$_2$O decomposition, both catalysts showed a much lower activity than Fe-MFI with a higher Fe content. This also supports that the activity of N$_2$O dissociation over Fe(0.05)- and Fe(0.10)-MFI was rather low. On the other hand, N$_2$O pretreatment significantly increased the amount of O$_2$ desorption on Fe(0.40)-MFI. Especially, it is found that the amount of O$_2$ desorption at lower temperature mainly increased by N$_2$O treatment. This indicates that N$_2$O can dissociate and oxygen atom is deposited on the catalyst surface on Fe-MFI with higher Fe loading and the oxygen atom (O(a)) is adsorbed on the Fe species which gives O$_2$ desorption at a lower temperature.

Related to this result, Panov and co-workers [38-44] have reported that Fe-MFI catalysts with low Fe loading that were treated at a high temperature are able to abstract an oxygen atom from an impinging N$_2$O molecule at 523 K; *i.e.*, a special form of adsorbed oxygen (O(a)) is formed during N$_2$O treatment at 523 K. These authors observed that this special form of O(a) (so called α-oxygen) showed high reactivity with benzene (or CH$_4$) to form phenol (or CH$_3$OH) even at room temperature [38, 39]. However, the extra O(a) in this study, which gives O$_2$ desorption at the lower temperature, do not seem to be related with the α-oxygen species. The CH$_4$-pulsed experiments revealed that CH$_4$ cannot react with the O(a) species deposited by N$_2$O treatment at 773 K (or at 523 K) even at 600 K [30]. The coexistence of both N$_2$O and CH$_4$ in the gas phase was needed for the CH$_4$ + N$_2$O reaction [30]. Therefore, the nature of the extra O(a) species in this case appears to be quite different from that of the α-oxygen species.

In this work, the ion exchanged Fe catalysts were prepared by calcination in air at 773 K. On the other hand, Panov *et al.* [38] prepared Fe-MFI catalysts by hydrothermal synthesis with the addition of iron as FeCl$_3$ to a starting gel. The Fe-MFI was transferred to the NH$_4$ form by exchange with an ammonia buffer and then calcined in air. Additional calcination in vacuo at 1173 K was performed to increase the concentration of α-oxygen [39, 41]. The calcination at the high temperature seems to be essential for the formation of the active α-sites. Delahay *et al.* [33] observed a sharp O$_2$-desorption peak at around 600 K after a Fe-BEA catalyst was pretreated in H$_2$ at 973 K followed by N$_2$O treatment at 973 K. In fact, I have observed a sharp O$_2$-desorption

peak at 600 K after the Fe-MFI catalyst was treated in H_2 at 873 K or in vacuo at 1073 K followed by N_2O treatment at 523 K (details were shown in Chapter 6). The desorption temperature (600 K) was much lower than the lower peak (873 K) in Fig. 2-5, and the peak (not shown) was much more intense (and sharp), which might be related to a special form of O(a) such as α-oxygen species. Sachtler and co-workers. [46] observed unusual TPR spike at 473 K after an Fe-MFI catalyst was treated in H_2 at 873 K followed by N_2O treatment at 523 K. This unusual TPR peak may also correspond to a special form of O(a). These results show that the states of O(a) species and/or structures of Fe ion species may depend strongly on the conditions of the pretreatment of Fe-zeolite catalysts as well as the Fe loading.

It seems that the behavior of TPD profiles on the Fe loading corresponds to that of H_2-TPR. The catalyst with a higher loading than that of Fe/Al > 0.10 has more reducible iron species in TPR profiles, which can desorb O_2 at lower temperatures in the TPD profiles. In addition I can compare the catalytic activity of N_2O reduction with CH_4 under the excess O_2 atmosphere and the characterization results. At first, it is possible to calculate the turnover frequency (TOF) of N_2O reduction activity: the N_2O conversion rate was divided by the total amount of Fe on the catalyst. The reaction rates of N_2O in the catalytic reaction in the presence of excess oxygen at 598 K on the basis of Figure 2-2(a) and that in the absence of oxygen at 550 K on the basis of Figure 2-3(a) are applied to the estimation of TOF, respectively. Since the conversion level over all the catalysts was lower than 40%, the reaction temperature 598 K in the presence of oxygen (10%) and the temperature 550 K in the absence of oxygen are applied to the estimation of TOF. Figure 2-7 shows the dependence of TOF on the molar ratio of Fe to Al (Fe/Al) on Fe-MFI. In the range of Fe/Al ≤ 0.10, the TOF was constant; however, it increased drastically with Fe loading (Fe/Al ≥ 0.15). On the other hand, the relation between the desorption amount of oxygen atom derived from O_2 in the lower temperature peak per Fe content (O_{low}/Fe) and the Fe loading of Fe-MFI is also shown in Figure 2-7. The O_{low}/Fe was very low level in the range of Fe/Al ≤ 0.10; however, it increased at Fe/Al ≥ 0.15. It is clear that the behavior of TOF is similar to that of O_{low}/Fe. This suggests that Fe species with low-temperature O_2 desorption give much higher TOF of the N_2O reduction. The activity of N_2O decomposition is also related to the lower temperature O_2 desorption. As listed in Table 2-2, the activity of N_2O decomposition at 773 K over Fe(0.05)- and Fe (0.10)-MFI was rather low, and much higher activity was observed on

Fe-MFI (Fe/Al $\geq$ 0.15). This behavior agrees with the previous report by Pirngruber [47].

Figure 2-8 shows the effects of O_2 partial pressure on the catalytic activity and selectivity over Fe(0.40)-MFI. The activity of N_2O reduction decreased with increasing O_2 concentration as shown in Figure 2-8(a). In the case of CH_4 + N_2O reaction without O_2, CH_4 conversion was constant at about 60% when N_2O conversion reached 100% (Fig. 2-8(b)), while the selectivity of CO_2 was lower than that under other conditions (Fig. 2-8(d)). When 2–20% oxygen was added to the reactant gas, a similar behavior regarding CO_2 selectivity and the contribution ratio of N_2O in all the oxidizing agents was observed, as shown in Figs. 2-8(d) and (e). This indicates that O_2 addition to the reaction gases decreased the conversion level of N_2O and CH_4 a little, and the effect on the selectivity is not so significant. In contrast, the difference between CH_4 + N_2O and CH_4 + N_2O + O_2 reactions was larger. As a result, O_2 addition decreased N_2O conversion and increased CH_4 conversion. This indicates that CH_4 is oxidized with both N_2O and O_2 in CH_4 + N_2O + O_2 reactions. However, CH_4 conversion reached a plateau when N_2O conversion reached 100% even though a large amount of O_2 is present. These results also indicate that CH_4 cannot react with O_2 directly. This strongly suggests again that N_2O is essential for the activation of CH_4. From these results, it is suggested that N_2O dissociates to N_2 and adsorbed oxygen atoms, at first, and then the adsorbed oxygen atoms activate CH_4 molecules.

According to our previous reports on Fe-BEA by means of FTIR studies, methoxy CH_3O-) and formate ($HCOO-$) species on Fe ion sites have been observed [30, 31], and kinetic parameters in the oxidation of methoxy and formate species with N_2O and O_2 were determined. It is concluded that the oxidation rate of methoxy species with N_2O is much higher than that with O_2; in contrast, the oxidation rate of formate species with N_2O was comparable to that with O_2 under the condition of N_2O 1000 ppm and O_2 10% at temperatures where N_2O + CH_4 + O_2 reactions can proceed. This indicates that methane can be totally oxidized with both N_2O and O_2. These results also suggest the formation of methoxy species over Fe-MFI, which can be oxidized with N_2O and O_2 in CH_4 + N_2O + O_2 reactions. Furthermore, this indicates that the dissociative adsorption of N_2O can influence the catalytic activity of N_2O + CH_4 + O_2. According to the results of O_2-TPD, the increase in the amount of desorbed O_2 by N_2O treatment was more significant over Fe-MFI with higher Fe loadings. This suggests that more sites for N_2O dissociation are present over the catalysts with higher Fe loading. In addition, the result that N_2O

conversion decreased with higher O_2 pressure (Figure 2-8(a)) means the inhibition of N_2O dissociation by the presence of oxygen. In addition, it has been reported that O_2 molecules can be activated by surface oxygen species derived from N_2O under the coexistence of N_2O and O_2 [48]. Therefore, there may be the reaction path of methane activation by O_2; however, the contribution is thought to be very small. This is because methane conversion in $CH_4 + N_2O$ reaction was higher than other contributions in $CH_4 + N_2O + O_2$ reactions.

In order to investigate the effect of oxygen partial pressure in detail, the pulse reactions of $CH_4 + N_2O$ were carried out over Fe-MFI after the pretreatments in H_2, O_2 or N_2O. According to the results of H_2-TPR, Fe species are present as Fe^{3+} over the catalyst after O_2 treatment at 773 K, and the Fe species are reduced to Fe^{2+} after H_2 treatment at 773 K. Furthermore, it can be assumed that Fe species are oxidized to $Fe^{(3+\delta)+}$ after N_2O treatment at 773 K, especially on Fe-MFI (Fe/Al = 0.40). These kinds of pretreatment can control the chemical state of Fe species over Fe-MFI. The pulse gas consisted of CH_4 (0.40 μmol) and N_2O (0.82 μmol) balanced with He, and the ratio of N_2O molecules to Fe atoms in the catalyst was 1/19. Figure 2-9(a) shows the results of $CH_4 + N_2O$ pulse reaction over Fe(0.40)-MFI after the pretreatments. When $CH_4 + N_2O$ pulse was introduced to Fe(0.40)-MFI after H_2 treatment, both CH_4 and N_2O conversions were very high. A part of N_2O oxidized Fe(0.40)-MFI; however, most of N_2O reacted with CH_4. Conversions of N_2O and CH_4 decreased with increasing pulse number. This is because of the gradual oxidation of the reduced Fe(0.40)-MFI with increasing pulse number. It should be noted that CH_4 conversion was higher at the initial stage. This indicates that the reaction does not proceed with the stoichiometry of catalytic $N_2O + CH_4$ reaction. In the catalytic $CH_4 + N_2O$ reaction, N_2O conversion was always higher than methane conversion as shown in Figure 2-3. The results in the pulse experiments can be explained by methoxy and formate formation over the catalyst. In the pulse experiments, the introduced amount of N_2O and CH_4 was much smaller than the Fe amount. Therefore, oxygen species from N_2O dissociation is not enough for the oxidation of CH_4 to CO and CO_2. This phenomenon is observed by FTIR measurement [31]:

$$OH^-(a) + N_2O + CH_4 \rightarrow CH_3O^-(a) + N_2 + H_2O \qquad (1)$$
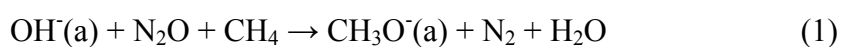
High methane conversion can be interpreted by reaction (1). As shown in Fig. 2-9(a), the activity of $CH_4 + N_2O$ pulse over Fe(0.40)-MFI after O_2 treatment was much lower than that

over the catalyst after H_2 treatment. This indicates that the activity over Fe^{2+} is higher than that over Fe^{3+}. In addition, it is very interesting that the activity of the O_2-treated catalyst increased with increasing pulse number. From comparison between H_2 and O_2 treatments, the increase of the activity can be explained by the reduction of the catalyst after O_2 treatment during each pulse reaction. Furthermore, it should be noted that the pulse activity over the O_2-treated catalyst reached the constant level (N_2O conversion = 35%) and it was almost the same level of the constant activity over the H_2-treated catalyst. These results suggest that the oxidation and the reduction of the catalyst with $CH_4 + N_2O$ pulse are balanced at this conversion level. In addition, no pulse activity was observed on the N_2O-treated catalyst. Figure 2-9(b) shows the result over Fe(0.10)-MFI. High activity was observed over H_2-treated Fe(0.10)-MFI; however, almost no activity was observed over O_2-treated and N_2O-treated catalysts.

In the results of Fe(0.40)-MFI and Fe(0.10)-MFI, a different behavior was observed over the O_2-treated catalysts. This difference is thought to be related to the results of O_2-TPD over O_2- and N_2O-treated catalysts. On Fe(0.40)-MFI, N_2O treatment enhanced the amount of O_2 desorption; in contrast, it did not increase that over Fe(0.10)-MFI. This indicates that Fe(0.10)-MFI after O_2 treatment does not have the ability to dissociate N_2O. The activity of the pulse reaction is closely related to the probability of N_2O dissociation. This is also supported by no activity on the N_2O-treated catalysts and high activity on the H_2-treated catalysts. On the basis of the above results, I discuss what determines the catalytic performance. On Fe(0.40)-MFI, the oxidation and the reduction with $CH_4 + N_2O$ pulse were balanced and its activity level was very high. This indicates that $CH_4 + N_2O$ reaction proceeds by redox mechanism of Fe^{2+} and Fe^{3+}. The important point is that Fe^{3+} can be reduced to Fe^{2+} during the reaction over Fe(0.40)-MFI. In contrast, since Fe^{3+} cannot be reduced to Fe^{2+} over Fe(0.10)-MFI, the oxidation and the reduction were not balanced on Fe(0.10)-MFI. Therefore, the steady-state activity under the presence of excess oxygen is expected to be the activity over O_2-treated catalyst. These are related to the catalytic activities of Fe(0.40)-MFI and Fe(0.10)-MFI (Figures 2-2, 2-3 and 2-8). This can be caused by Fe species with higher reducibility in H_2-TPR and the ability to desorb oxygen at lower temperatures in O_2-TPD. In this study, the elucidation of the structure of this kind of Fe species is not enough. However, several studies about the structure of Fe species over Fe-MFI have been reported [35-38, 40, 49]. These reports suggest that this kind of Fe species is binuclear

one. In contrast, it is interpreted that mononuclear Fe is present on Fe(0.10)-MFI. This indicates that the activity of N_2O reduction with CH_4 over Fe binuclear is much higher than that over mononuclear Fe. Considering the effect of oxygen partial pressure, the catalytic activity decreased with increasing oxygen partial pressure. As discussed above, in the case that this reaction proceeds via a redox mechanism between Fe^{2+} and Fe^{3+}, the ratio of Fe^{2+} to total Fe species can decrease under a higher pressure of oxygen. The activity of N_2O dissociation over Fe^{2+} is much higher than that over Fe^{3+} of Fe(0.40)-MFI. Therefore, the decrease of Fe^{2+} ratio causes the decrease of the activity.

2.4. Conclusions

(1) The activity of N_2O reduction with CH_4 under an excess O_2 atmosphere over Fe-MFI catalysts increased with higher Fe loading on Fe-MFI catalysts.

(2) The turnover frequency of the reaction drastically increased in the range of Fe/Al ≥ 0.15.

(3) From the characterization by means of H_2-TPR, more reducible Fe ion species were formed over Fe-MFI with higher Fe loading.

(4) In the profiles of O_2-TPD, two kinds of desorption peak were observed. The catalysts with low Fe loading (Fe/Al = 0.05, 0.10) had only a high-temperature peak, and in contrast, the catalysts with higher Fe loading (Fe/Al = 0.15, 0.24, and 0.40) also gave a lower temperature peak. This peak intensity increased with N_2O treatment.

(5) The dependence of turnover frequencies on the Fe loading is similar to that of the amount of oxygen desorption in the lower temperature peak.

(6) From the catalytic activity and characterization results, it is suggested that the active sites are Fe species which are more reducible and give a lower temperature O_2 desorption peak.

(7) The pulse reaction of $CH_4 + N_2O$ over Fe(0.40)-MFI indicates that the reaction proceeds via a redox mechanism between Fe^{2+} and Fe^{3+}. On the other hand, the reaction did not proceed over Fe^{3+} in Fe(0.10)-MFI. It is found that the more reducible Fe^{3+} over Fe(0.40)-MFI plays an important role in high catalytic activity.

(8) In a comparison between the previous reports and the result in this work, the active species are thought to be binuclear Fe.

References

[1]   H. Rodhe, *Science* **298** (1990) 1217.

[2]   F. Kapteijn, J. Rodrigues-Mirasol, J.A. Moulijn, *Appl. Catal. B* **9** (1996) 25.

[3]   M. Nakamura, H. Mitsuhashi, N. Takezawa, *J. Catal.* **138** (1992) 686.

[4]   T. Yamashita, A. Vannice, *J. Catal.* **161** (1996) 254.

[5]   K. Yuzaki, T. Yarimizu, K. Aoyagi, S. Ito, K. Kunimori, *Catal. Today* **45** (1998) 129.

[6]   S. Tanaka, K. Yuzaki, S. Ito, S. Kameoka, K. Kunimori, *J. Catal.* **200** (2001) 203.

[7]   X.F. Wang, H.C. Zeng, *Appl. Catal. B* **17** (1998) 89.

[8]   G. Centi, L. Dall'Olio, S. Perathoner, *J. Catal.* **192** (2000) 224.

[9]   Y. Li, J.N. Armor, *Appl. Catal. B* **1** (1992) L21.

[10] T. Turek, *Appl. Catal. B* **9** (1996) 201.

[11] B.I. Palella, M. Cadoni, A. Frache, H.O. Pastore, R. Pirone, G. Russo, S. Coluccia, L. Marchese, *J. Catal.* **217** (2003) 100.

[12] J. Leglise, J.O. Petunchi., W.K. Hall, *J. Catal.* **86** (1984) 392.

[13] T. Nobukawa, S. Tanaka, S. Ito, K. Tomishige, S. Kameoka, K. Kunimori, *Catal. Lett.* **83** (2002) 5.

[14] Q. Zhu, B.L. Mojet, R.A. J. Jassen, E.J.M. Hensen, J. van Grondelle, P.C.M.M. Magusin, R.A. van Santen, *Catal. Lett.* **81** (2002) 205.

[15] J. Pérez-Ramírez, F. Kapteijn, G. Mul, J.A. Moulijin, *J. Catal.* **208** (2002) 211.

[16] M. Kögel, V.H. Sandoval, W. Schwieger, A. Tissler, T. Turek, *Catal. Lett.* **51** (1998) 23.

[17] G. Centi, F. Vazzana, *Catal. Today* **53** (1999) 683.

[18] R.W. van den Brink, S. Booneveld, J.R. pels, D.F. Bakker, M.J.F.M. Verhaak, *Appl. Catal. B* **32** (2001) 73.

[19] C. Pophal, T. Yogo, K. Tanabe, K. Segawa, *Catal. Lett.* **44** (1997) 271.

[20] C. Pophal, T. Yogo, K. Yamada, K. Segawa, *Appl. Catal. B* **16** (1998) 177.

[21] K. Yamada, C. Pophal, K. Segawa, *Microporous Mesoporous Mater.* **21** (1998) 549.

[22] K. Yamada, S. Kondo, K. Segawa, *Microporous Mesoporous Mater.* **35-36** (2000) 227.

[23] A. Satsuma, H. Maeshima, K. Watanabe, K. Suzuki, T. Hattori, *Catal. Today* **63** (2000) 347.

[24] S. Kameoka, K. Yuzaki, T. Takeda., S. Tanaka, S. Ito, T. Miyadera, K. Kunimori, *Phys. Chem. Chem. Phys.* **3** (2001) 256.

[25] S. Kameoka, K. Kita, S. Tanaka, T. Nobukawa, S. Ito, K. Tomishige, T. Miyadera, K. Kunimori, *Catal. Lett.* **79** (2002) 63.

[26] S. Kameoka, T. Suzuki, K. Yuzaki, T. Takeda, S. Tanaka, S. Ito, T. Miyadera, K. Kunimori, *Chem. Commun.* (2000) 745.

[27] S. Kameoka, K. Kita, T. Takeda, S. Tanaka, S. Ito, K. Yuzaki, T. Miyadera, K. Kunimori, *Catal. Lett.* **69** (2000) 169.

[28] S. Kameoka, S. Tanaka, K. Kita, T. Nobukawa, S. Ito, T. Miyadera, K. Kunimori, *Stud. Surf. Sci. Catal.* **135** (2001) 321.

[29] T. Nobukawa, K. Kita, S. Tanaka, S. Ito, T. Miyadera, S. Kameoka, K. Tomishige, K. Kunimori, *Stud. Surf. Sci. Catal.* **142** (2002) 557.

[30] S. Kameoka, T. Nobukawa, S. Tanaka, S. Ito, K. Tomishige, K. Kunimori, *Phys. Chem. Chem. Phys.* **5** (2003) 3328.

[31] T. Nobukawa, M. Yoshida, S. Kameoka, S. Ito, K. Tomishige, K. Kunimori, *J. Phys. Chem. B* **108** (2004) 4071.

[32] M. Mauvezin, G. Delahay, B. Coq, S. Kieger, J.C. Jumas, J. Olivier-Fourcade, *J. Phys. Chem. B* **105** (2001) 928.

[33] G. Delahay, M. Mauvezin, B. Coq, S. Kieger, *J. Catal.* **202** (2001) 156.

[34] G. Delahay, M. Mauvezin, A. Guzmán-Vargas, B. Coq, *Catal. Commun.* **3** (2002) 385.

[35] H.Y. Chen, W.M.H. Sachtler, *Catal. Today* **42** (1998) 73.

[36] El-M. El-Malki, R.A. van Santen, W.M.H. Sachtler, *J. Catal.* **196** (2000) 212.

[37] A.A. Battiston, J.H. Bitter, F.M.F. de Groot, A.R. Overweg, O. Stephan, J.A. van Bokhoven, P.J. Kooyan, C. van der Spek, G. Vankó, D.C. Koningsberger, *J. Catal.* **213** (2003) 251.

[38] G. I. Panov, A. K. Uriarte, M. A. Rodkin, V. I. Sobolev, *Catal. Today* **41** (1998) 365.

[39] K.A. Dubkov, V.I. Sobolev, G.I. Panov, *Kinet. Katal.* **39** (1998) 72.

[40] K.A. Dubkov, N.S. Ovanesyan, A.A. Shteinman, E.V. Starokon, G.I. Panov, *J. Catal.* **207** (2002) 341.

[41] E.V. Starokon, K.A. Dubkov, L.V. Pirutko, G.I. Panov, *Top. Catal.* **23** (2003) 137.

[42] M.A. Rodkin, V.I. Sobolev, K.A. Dubkov, N.H. Watkins, G.I. Panov, *Stud. Surf. Sci. Catal.* **130** (2000) 875.

[43] V.I. Sobolev, G.I. Panov, A.S. Kharitonov, V.N. Romannikov, A.M. Volodin, K.G. Ione, *J. Catal.* **139** (1993) 435.

[44] G.I. Panov, V.I. Sobolev, A.S. Kharitonov, *J. Mol. Catal.* **61** (1990) 85-97

[45] L.J. Lobee, I-C. Hwang, J.A. Reimer, A.T. Bell, *J. Catal.* **186** (1999) 242.

[46] J.F. Jia, Q. Sun, B. Wen, L.X. Chen, W.M.H. Sachtler, *Catal. Lett.* **82** (2002) 7

[47] G.D. Pirngruber, *J. Catal.* **219** (2003) 456.

[48] J. Nováková, Z. Sobalík, *Catal. Lett.* **89** (2003) 243.

[49] A.L. Yakovlev, G.M. Zhidomirov, R.A. van Santen, *J. Phys. Chem. B* **105** (2001) 12297.

Table 2-1
Ion-exchanged Fe-MFI catalysts at different loadings.

Catalyst	Fe/Al	Fe content /wt%	Fe amount /mol g-cat.$^{-1}$	Exchange degree /%
Fe(0.40)-MFI	0.40	2.81	5.03×10^{-4}	80
Fe(0.24)-MFI	0.24	1.74	3.12×10^{-4}	48
Fe(0.15)-MFI	0.15	1.05	1.88×10^{-4}	30
Fe(0.10)-MFI	0.10	0.70	1.25×10^{-4}	20
Fe(0.05)-MFI	0.05	0.35	6.27×10^{-4}	10

Table 2-2

Results of (a) O_2-TPD over Fe-MFI after O_2 and N_2O treatments, (b) N_2O decomposition, and (c) H_2-TPR.

Catalyst	Treatment	(a) O_2-TPD				(b) N_2O decomposition[a]	(c) H_2-TPR
		Total, O_2 amount		Lower-temperature peak, O_2 amount		N_2O conversion (%)	H_2/Fe
		/ mol	O/Fe	/ mol	O/Fe		
Fe(0.40)-MFI	O_2	1.8	0.23	0.54	0.072	84	0.5
	N_2O	2.4	0.32	0.96	0.13		
Fe(0.24)-MFI	O_2	1.3	0.28	0.33	0.071	43	0.5
	N_2O	1.4	0.31	0.43	0.092		
Fe(0.15)-MFI	O_2	0.88	0.31	0.18	0.064	13	0.5
	N_2O	0.87	0.31	0.18	0.064		
Fe(0.10)-MFI	O_2	0.59	0.32	0.0	0.00	5	0.5
	N_2O	0.62	0.33	0.0	0.00		
Fe(0.05)-MFI	O_2	0.36	0.38	0.0	0.00	3	0.5
	N_2O	0.36	0.36	0.0	0.00		

[a] N_2O conversion was measured at 773 K.

Reaction conditions: N_2O (950 ppm) balanced with He, $W/F = 0.41$ g h/mol, catalysts were pretreated in O_2 at 773 K for 1 h.
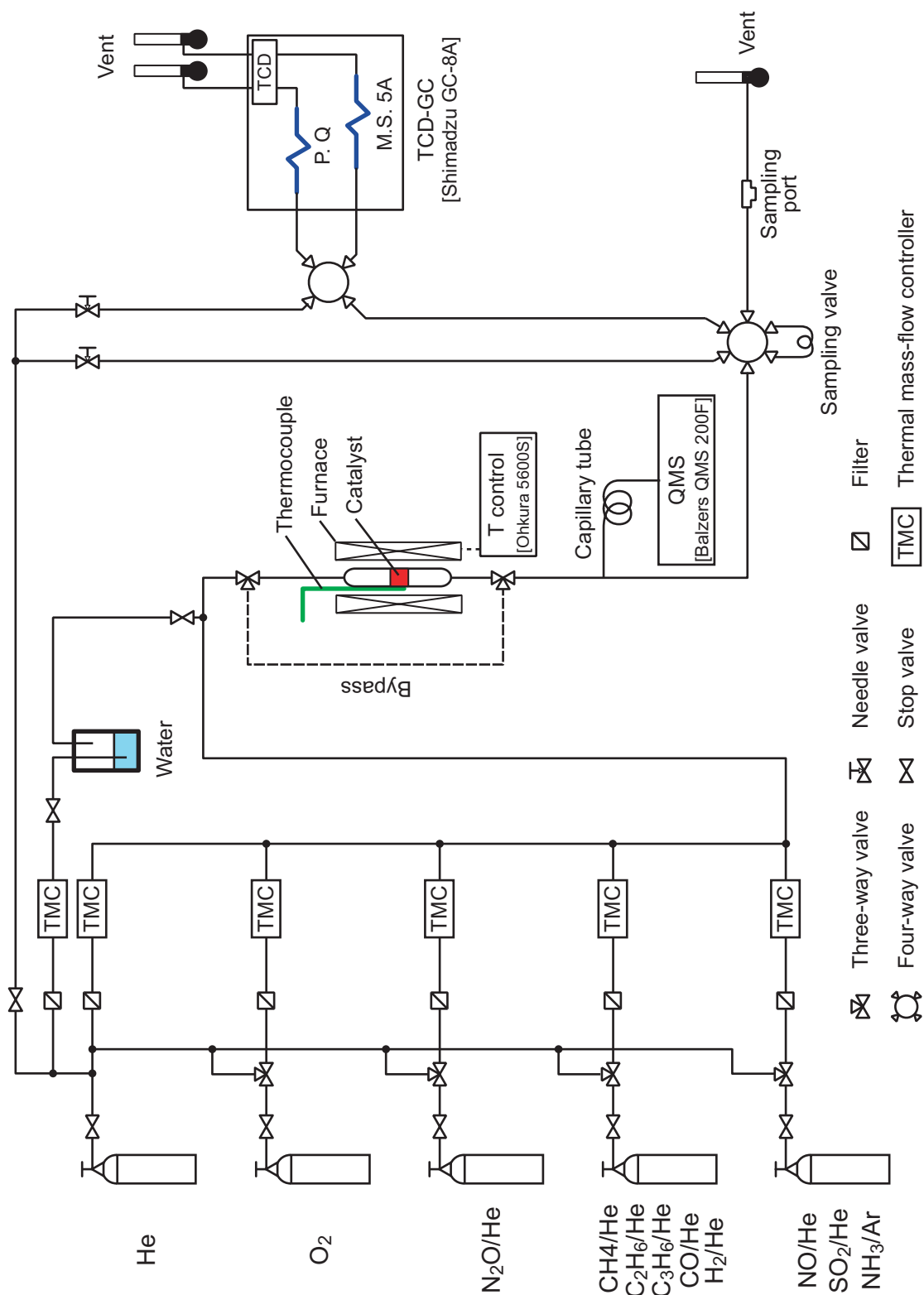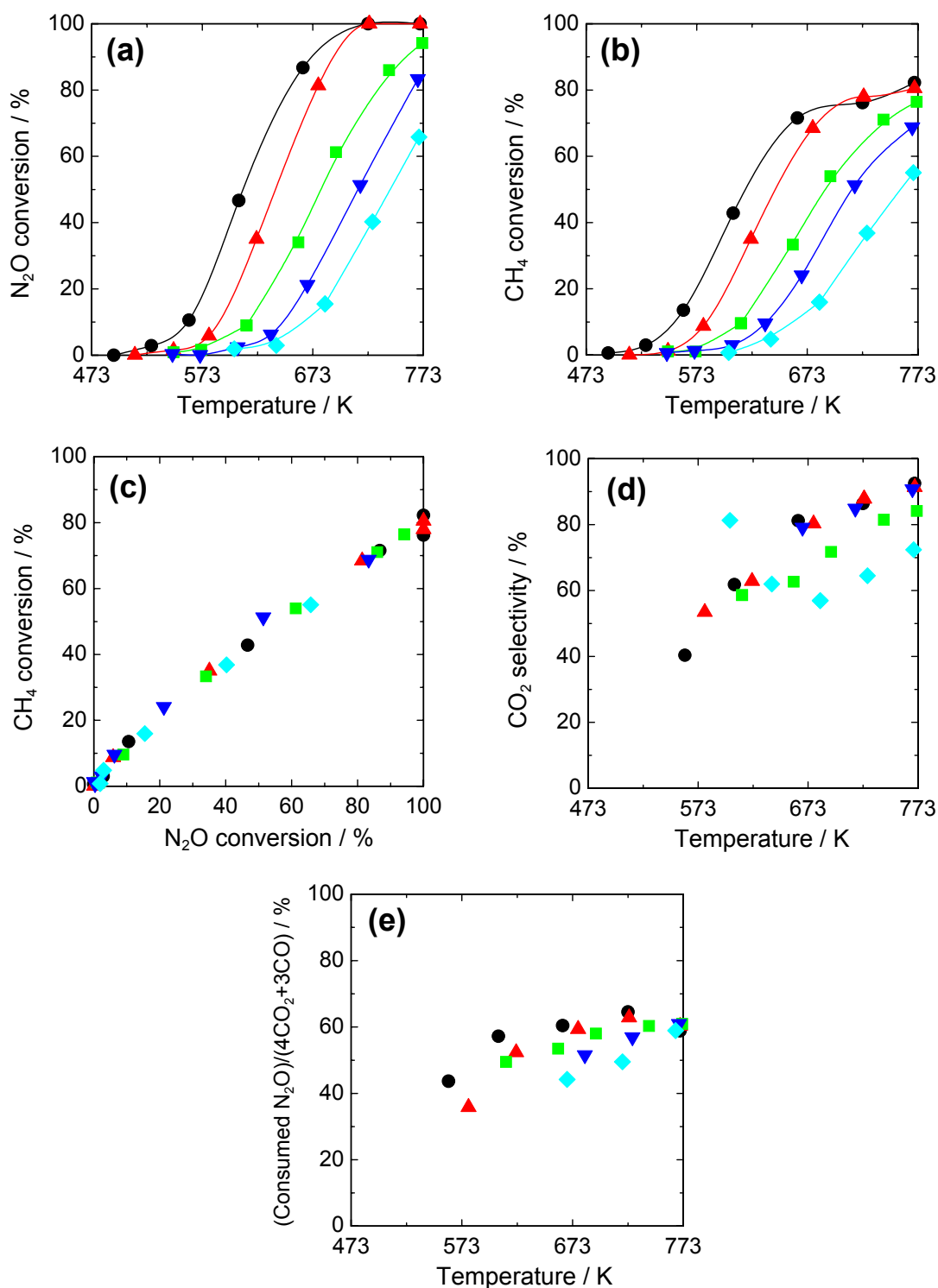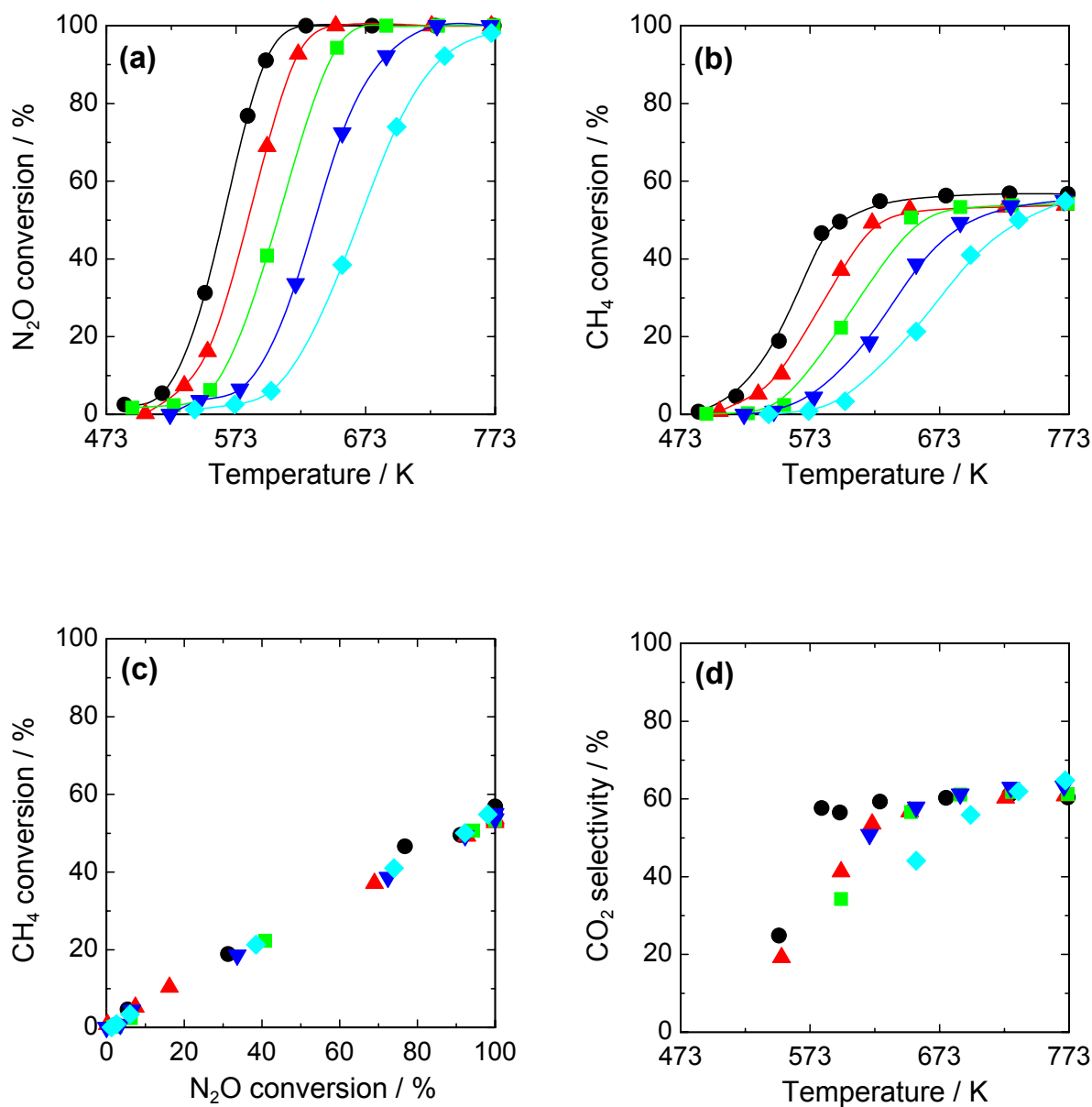
**Figure 2-1.** Schematic diagram of conventional fixed-bed flow reactor.

Figure 2-2. Reaction temperature dependence of catalyst performance of Fe-MFI catalysts in N_2O reduction with CH_4 under an excess O_2 atmosphere. (a) N_2O conversion, (b) CH_4 conversion, (c) CH_4 conversion as function of N_2O conversion, (d) CO_2 selectivity ($CO_2/(CO + CO_2)$), (e) (consumed $N_2O)/(4CO_2 + 3CO$). (●) Fe(0.40)-MFI, (▲) Fe(0.24)-MFI, (■) Fe(0.15)-MFI, (▼) Fe(0.10)-MFI, and (◆) Fe(0.05)-MFI. Reaction conditions: 950 ppm N_2O, 500 ppm CH_4, 10% O_2 (He balance). (Consumed $N_2O)/(4CO_2 + 3CO$) corresponds to the contribution of N_2O in total oxidizing agents.

Figure 2-3. Reaction temperature dependence of catalyst performance of Fe-MFI catalysts in N_2O reduction with CH_4 in the absence of O_2. (a) N_2O conversion, (b) CH_4 conversion, (c) CH_4 conversion as function of N_2O conversion, (d) CO_2 selectivity ($CO_2/(CO + CO_2)$). (●) Fe(0.40)-MFI, (▲) Fe(0.24)-MFI, (■) Fe(0.15)-MFI, (▼) Fe(0.10)-MFI, and (◆) Fe(0.05)-MFI. Reaction conditions: 950 ppm N_2O, 500 ppm CH_4 (He balance).
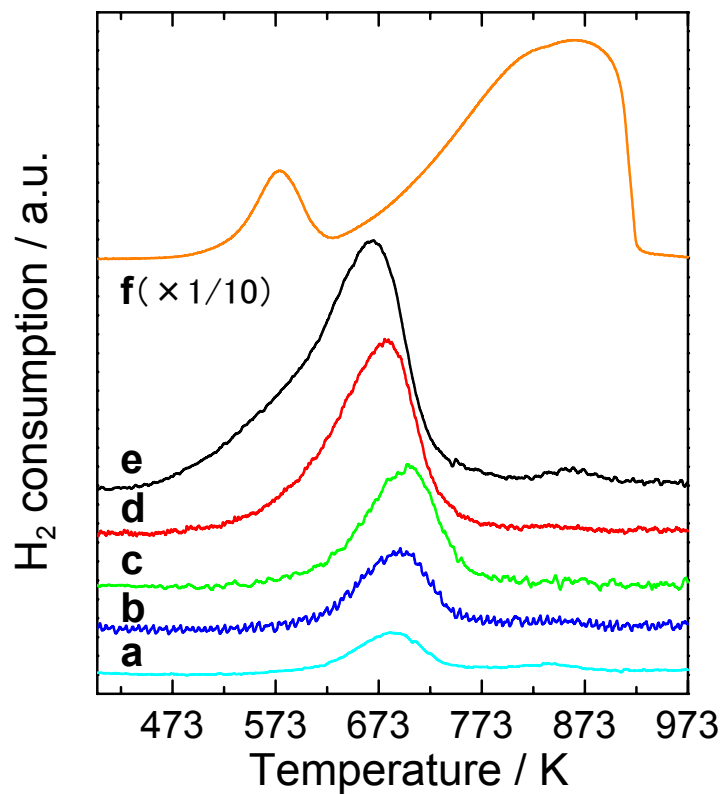
Figure 2-4. Temperature-programmed reduction in hydrogen over Fe-MFI catalysts. (a) Fe(0.05)-MFI, (b) Fe(0.10)-MFI, (c) Fe(0.15)-MFI, (d) Fe(0.24)-MFI, (e) Fe(0.40)-MFI, and (f) Fe_2O_3 (10 mg).
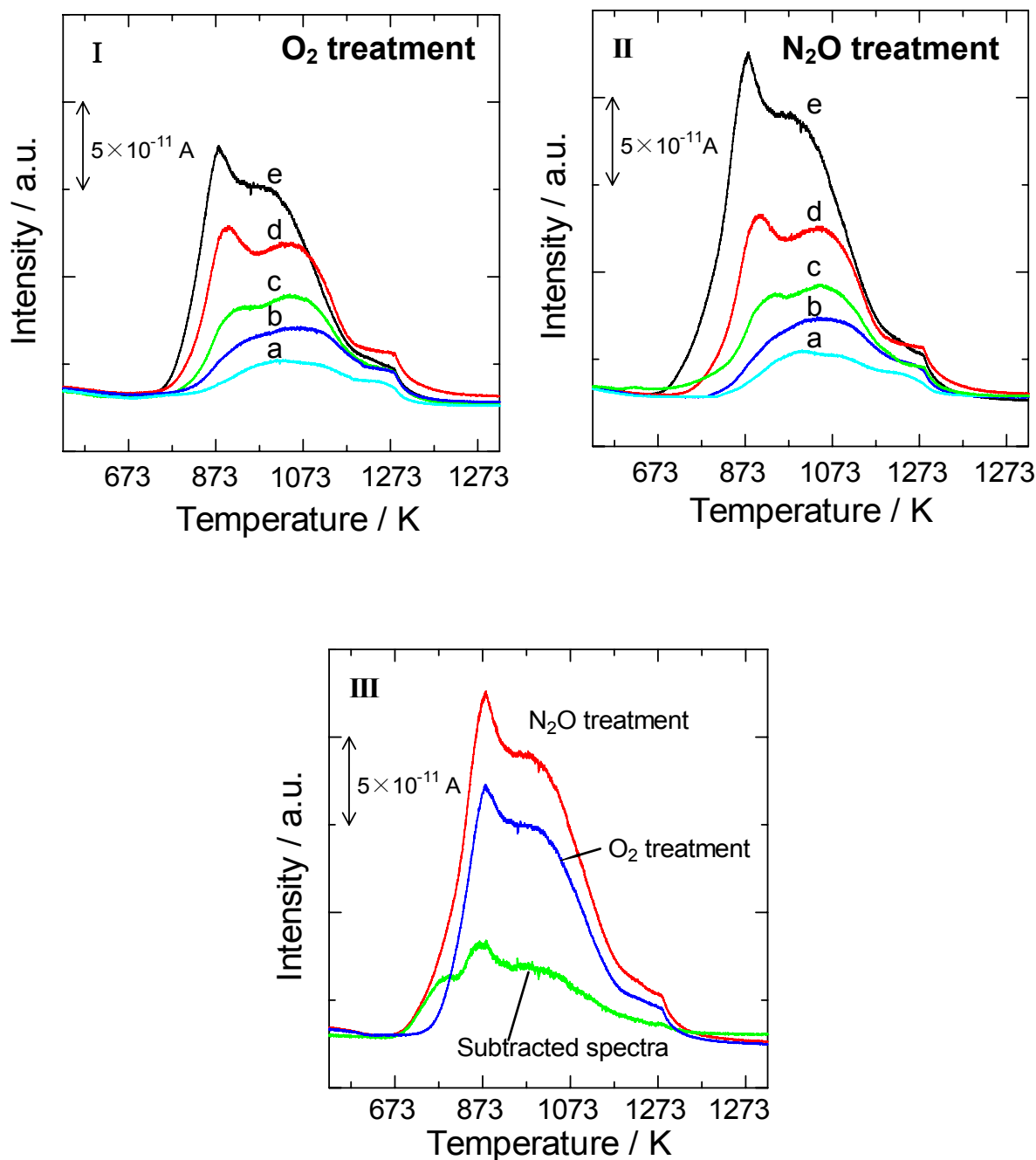
Figure 2-5. Temperature-programmed desorption of oxygen (I) after O_2 treatment, (II) after N_2O treatment, and (III) subtracted spectra: (II-e) − (I-e). (a) Fe(0.05)-MFI, (b) Fe(0.10)-MFI, (c) Fe(0.15)-MFI, (d) Fe(0.24)-MFI, and (e) Fe(0.40)-MFI.
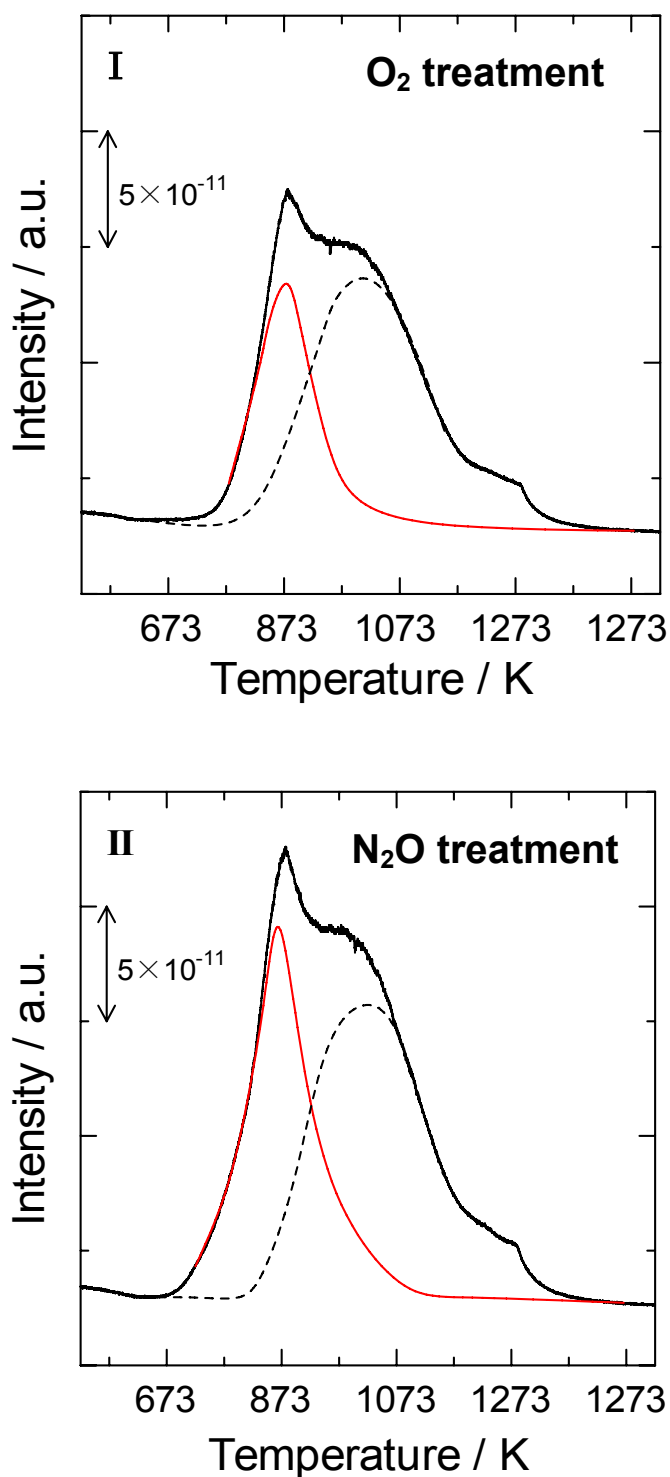
**Figure 2-6.** The results of the deconvolution of O_2 desorption peak over Fe(0.40)-MFI after (I) O_2 treatment and (II) N_2O treatment. (Solid line) lower temperature peak, (broken line) higher temperature peak.
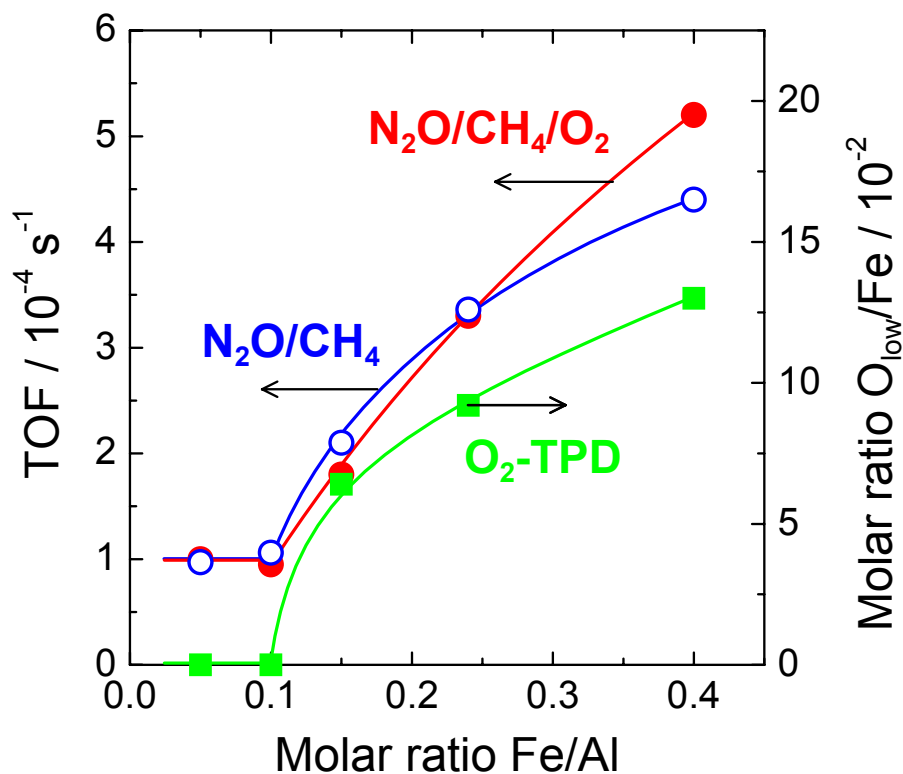
Figure 2-7. Dependence of TOF (●: in the presence of 10% oxygen, ○: in the absence of oxygen) in N_2O reduction with methane and molar ratio O_{low}/Fe (■) obtained from TPD profile on the molar ratio Fe/Al in Fe-MFI catalyst. TOFs are estimated from the reaction rate of N_2O in the activity test at 598 K in the presence of 10% oxygen and total Fe amount on the basis of Fig. 2-2(a), and that at 550 K in the absence of oxygen on the basis of Fig. 2-3(a), respectively. Molar ratio O_{low}/Fe is determined by the desorption amount of oxygen atom derived from O_2 in lower temperature peak after N_2O treatment and total Fe amount (see Fig. 2-5 and Table 2-2).
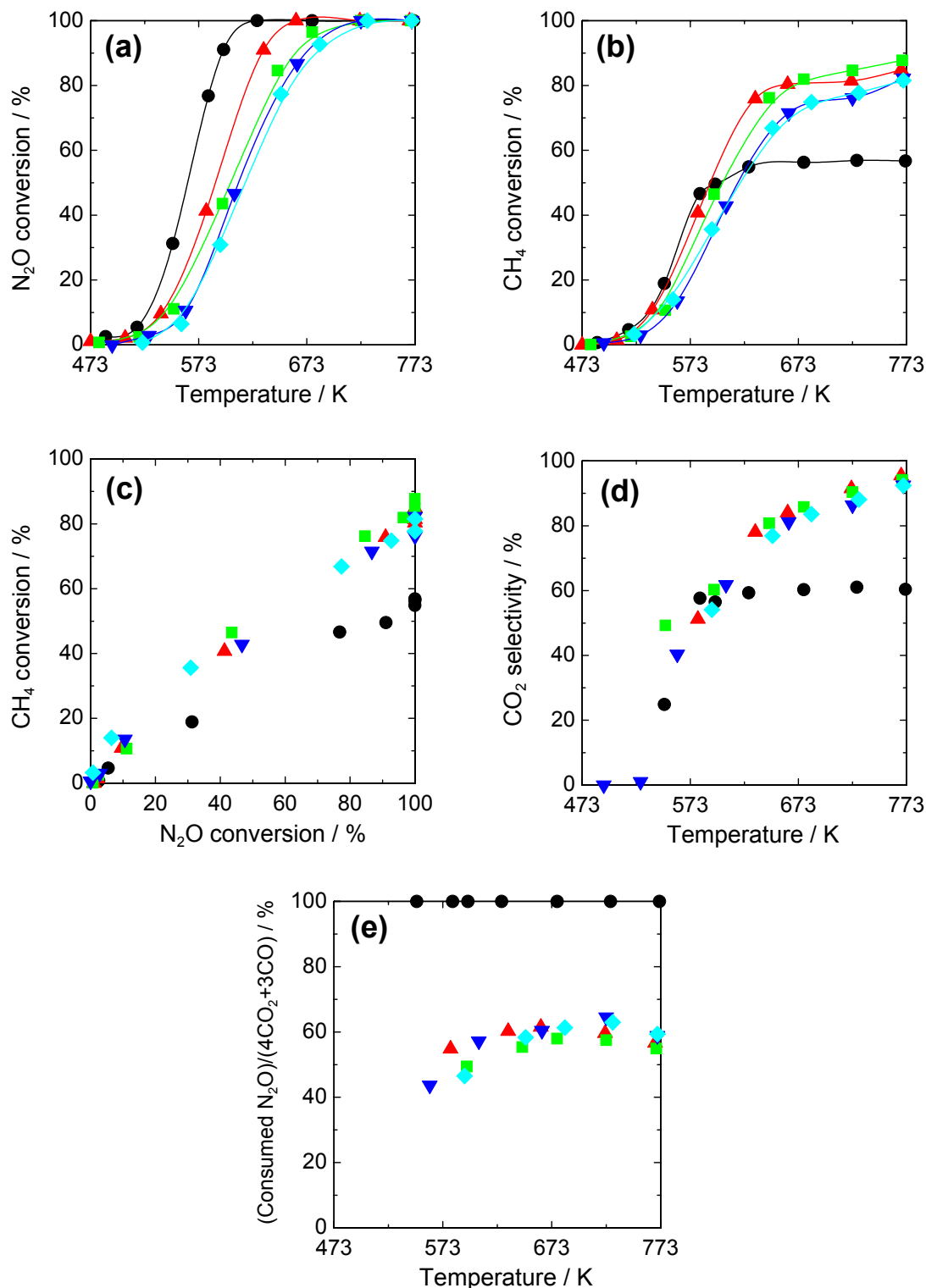
Figure 2-8. Reaction temperature dependence of catalytic performance of Fe(0.40)-MFI catalyst in N_2O reduction with CH_4: the effect of partial pressure of O_2. (a) N_2O conversion, (b) CH_4 conversion, (c) CH_4 conversion as function of N_2O conversion, (d) CO_2 selectivity ($CO_2/(CO + CO_2)$), (e) (consumed $N_2O)/(4CO_2 + 3CO)$. (●) 0%, (▲) 2%, (■) 5%, (▼) 10%, and (◆) 20%. Reaction conditions: 950 ppm N_2O, 500 ppm CH_4, 0-20% O_2 (He balance). (Consumed $N_2O)/(4CO_2 + 3CO)$ corresponds to the contribution of N_2O in total oxidizing agents.
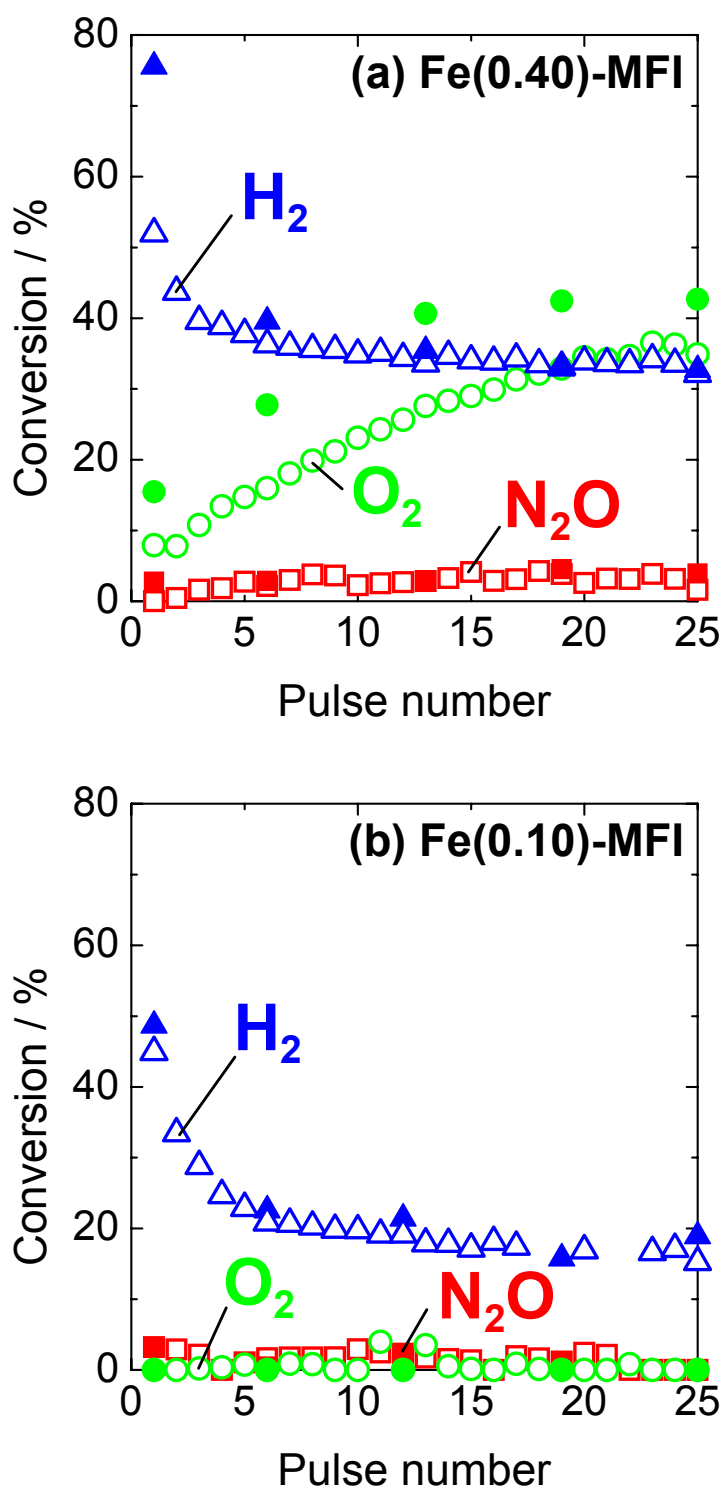
Figure 2-9. Results of $CH_4 + N_2O$ pulse reaction over Fe-MFI catalysts after the pretreatments. Conversion: N_2O (open symbol), CH_4 (closed symbol). Pretreatment: H_2 treatment (▲, △), O_2 treatment(●, ○), and N_2O treatment (■, □). Pulse gas composition: 0.82 μmol N_2O and 0.40 μmol CH_4 (He balance). Reaction temperature: 523 K.

Chapter 3

Effect of reductants in N_2O reduction and analysis of active site structure over Fe-MFI catalysts

3.1. Introduction

Nitrous oxide (N_2O) has been long considered as a relatively harmless gas and has suffered from a lack of interest from environmental scientists and engineers. However, during the last decade, a growing concern can be noticed since N_2O is a harmful gas in our environment, contributing to the greenhouse effect and the ozone layer depletion. Therefore, catalytic decomposition of N_2O [1-10] and selective catalytic reduction (SCR) of N_2O with reductants such as hydrocarbons [11-20] and ammonia [21-23] have been proposed as an effective method of N_2O abatement.

Recently, a number of researches have reported that binuclear Fe species are active sites for NO_x SCR and N_2O decomposition on the basis of characterization by means of H_2-TPR, CO-TPR, FTIR, EPR, EXAFS, and Mössbauer spectroscopies [24-32]. Koningsberger *et al.* [24-26] have reported evidence for binuclear iron-oxo complex on the basis of EXAFS study of fully exchanged Fe-MFI (Fe/Al = 1). They have also proposed that the evolution and reactivity of the binuclear iron-oxo species in the thermal pretreatment on the fully exchanged Fe-MFI prepared by sublimation. Prins *et al.* [27, 28] have reported that the diiron structure resembles the core unit in methane monooxygenase (MMO), in terms of an Fe-Fe distance of approximately 0.3 nm. Joyner and Stockenhuber [33] have shown that the nature of the Fe species in Fe-MFI depends markedly on the ion-exchange method used for the preparation as well as the type of pretreatment. On the basis of EXAFS results, these authors reported that in Fe/ZSM-5 zeolites prepared using different ion-exchange methods Fe was stabilized in different forms ranging from isolated metal ions to large oxide clusters, and concluded that ion-oxo nanoclusters are most active in NO_x SCR reaction [33]. On the other hand, mononuclear iron-oxo species, which exist mainly on Fe-MFI with low exchange level, have been proposed as active species for the reduction of N_2O [13, 22]. Delahay *et al.* [22] have reported that the most active species in the reduction by NH_3 on Fe-BEA in an oxygen-rich atmosphere are in higher

proportion at low exchange level. Furthermore, Segawa *et al.* [13] have also reported that even low-exchanged Fe-ZSM-5 catalysts exhibited high activity when C_3H_6 was used as a reductant.

In chapter 2, the catalytic activity in N_2O reduction with CH_4 on the Fe-MFI was dependent on the exchange level of Fe ion [19]. From the results of activity test and catalyst characterization, it is concluded that the active sites are Fe species which are more reducible and give lower-temperature O_2 desorption peak [19]. From these comparisons, it is expected that the active structure of iron species over zeolites can be influenced by the kinds of the reductant. In this chapter, the relation between exchange level of iron and the activity of N_2O reduction with various reductants (such as CH_4, C_2H_6, C_3H_6, H_2, and CO) is investigated. Furthermore, the structure of Fe species on the Fe-MFI catalysts is also characterized by means of temperature-programmed desorption of O_2 (O_2-TPD), temperature-programmed reduction with H_2 (H_2-TPR), and extended X-ray absorption fine structure (EXAFS). The nature of the active sites of N_2O reduction on the basis of the relation between catalyst structure and performance is discussed.

3.2. Experimental

3.2.1. Catalyst preparation

Fe-MFI catalysts were prepared by an ion-exchange method using an aqueous solution of $FeSO_4 \cdot 7H_2O$ (Wako Pure Chemical Industries Ltd., 98%) for 20 h at 323 K under nitrogen atmosphere to avoid the precipitation of $Fe(OH)_3$ [34]. Na-MFI (TOSOH Co., SiO_2/Al_2O_3 = 23.8) was used as the catalyst support. The catalyst was separated from the solution by the filtration after ion exchange procedure. And it was washed thoroughly with distilled water and dried at 383 K overnight, followed by the calcination in air at 773 K for 3 h. The loading amount of Fe on MFI was determined by subtracting the Fe amount in the solution after the separation, analyzed by ICP analysis, from the total amount. The exchange-efficiency of $FeSO_4$, percentage of the iron salt incorporated into the zeolite, was almost 100% in the case of Fe/Al = 0.05 ~ 0.24. On the other hand, it was almost 80% in the case of Fe/Al = 0.40. The catalyst is denoted as Fe(X)-MFI, where X stands for molar ratio of Fe/Al.

3.2.2. Activity tests

Catalytic reduction of N_2O with various reductants under the presence of excess O_2 or in the absence of O_2 was carried out in a fixed-bed flow reactor. Composition of reactant gases is listed in Table 3-1. All these research grade gases were purchased from Takachiho Trading Co. Ltd., and they were used without further purification. The catalyst weight was 50 or 100 mg, and total pressure was 0.1 MPa, and W/F (W/g = catalyst weight, F/mol h^{-1} = total flow rate) was 0.41 g h/mol. The catalysts were pretreated at 773 K with O_2 for 1 h in the reactor. The products were monitored by an on-line TCD gas chromatograph (Shimadzu GC-8A) equipped with Molecular sieve 5A column for N_2 and O_2, and Porapak Q column for N_2O, FID gas chromatograph (Shimadzu GC-14B) equipped with Gaskuropak 54 column and methanator for CO, CO_2 and CH_4, and the other gas chromatograph equipped with VZ-10 column for C_2H_6 and C_3H_6. The sampling and analyzing of effluent gas was carried out for 1 h at each reaction temperature. The results of the activity tests shown in the figures were obtained under steady-state conditions.

3.2.3. Catalyst characterization

Temperature-programmed reduction (TPR) with H_2 was performed in a fixed-bed flow reactor. The sample was pretreated in 100% O_2 flow at 773 K for 1 h, and then it was cooled down to room temperature and exposed to helium flow in order to purge the line. The TPR profile of each sample was recorded from room temperature to 973 K under flowing of 5.0% H_2 diluted with Ar. The flow rate of H_2/Ar was 30 ml/min, and the catalyst weight was 50 mg. The heating rate was 10 K/min and the temperature was maintained at 973 K for 10 min after it reached 973 K. The consumption of H_2 was monitored continuously with a TCD gas chromatograph equipped Molecular Sieve 5A in order to remove H_2O from the effluent gas.

Temperature-programmed desorption of O_2 (O_2-TPD) was carried out in a fixed-bed reactor equipped with a quadrupole mass spectrometer (Balzers QMS 200 F). The catalysts (30 mg) were pretreated with O_2 flow (100% O_2, 773 K, 1 h) or N_2O flow (10% N_2O/He, 773 K, 1 h). After the pretreatment, they were cooled down to room temperature. Helium gas (flow rate 55 ml/min) was introduced to the reactor, and the sample was heated with heating rate 10 K/min from room temperature to 1273 K. The sample temperature was kept at 1273 K for 30 min just

after it reached 1273 K. Desorbed O_2 in He flow (flow rate, 55 ml/min) was analyzed with the quadrupole mass spectrometer.

3.2.4. EXAFS measurement and analysis

The sample for EXAFS measurements was prepared by pressing catalyst powder of 60 mg. The thickness of the samples was chosen to be 0.6-0.7 mm (10 mmϕ) to give edge jump of 0.2 - 0.7. The sample was pretreated at 773 K with 11 kPa O_2, H_2, or N_2O for 0.5 h in a closed circulating reactor, respectively. After these kinds of pretreatment, the samples were transferred to the measurement cell without exposing the sample disk to air using a glove box filled with nitrogen.

Fe *K*-edge XAFS was measured at the BL-12C station of the Photon Factory at the High Energy Accelerator Research Organization in Tsukuba, Japan (Figure 3-1). The storage ring was operated at 2.5 GeV with ring current of 300 - 450 mA. A Si(111) single crystal was used to obtain monochromatic X-ray beam. The monochromator was detuned to 60 % of the maximum intensity to avoid higher harmonics in the X-ray beam. Two ion chambers filled with N_2 and 15% Ar diluted with N_2 were used as detectors of I_0 and I, respectively. EXAFS data were collected in a transmission mode at liquid nitrogen temperature (Figure 3-2). For EXAFS analysis, the oscillation was first extracted from the EXAFS data by a spline smoothing method [35]. The oscillation was normalized by the edge height around 50 eV. The Fourier transformation of the k^3-weighted EXAFS oscillation from k space to r space was performed over the range 23-120 nm^{-1} to obtain a radial distribution function. The inversely Fourier filtered data were analyzed by a usual curve fitting method [36, 37]. For the curve fitting analysis, the empirical phase shift and amplitude functions for Fe-O were extracted from the data for Ferric acetylacetonate. The phase shift and backscattering amplitude of Fe-Si and Fe-Fe bonds were calculated using the software FEFF8.2 [38]. The program ATOMS [39] was employed to calculate coordination numbers and interatomic distances from reported XRD data of reference compounds. The theoretical Fe-Fe reference was calibrated on EXAFS data obtained from Fe_2O_3 (hematite) at liquid nitrogen temperature, by fitting in R space. The analysis of EXAFS data was performed using the "REX2000" program (RIGAKU Co. Version: 2.3.3).

3.3. Results and discussion

3.3.1. N₂O reduction with hydrocarbons over Fe-MFI under excess oxygen atmosphere

Figure 3-3 shows the temperature dependence of the catalyst performance of Fe-MFI in N_2O reduction with C_3H_6 under excess oxygen atmosphere. In this experiment, the activity test was carried out from high temperature (773 K) to low temperature (at most 473 K) in order to avoid the influence of carbon deposition, which was observed at lower temperature described by open marks as shown in Fig. 3-3(a). In this temperature region, the color of catalyst became black during the reaction and the disagreement in the carbon mass balance was observed. The introduced carbon amount did not agree with the carbon amount in the effluent gas at the lower temperature described by open marks. This behavior due to carbon deposition has also been shown in the previous report [40]. In addition, the carbon deposition was confirmed on the catalyst after reaction by thermo gravimetry analysis (TGA). In TGA, the weight loss due to coke combustion was observed during the heating under air atmosphere. On the other hand, for the data described by closed marks, the mass balance was good. N_2O conversion increased with the loading amount of Fe. According to Figure 3-3(b), C_3H_6 conversion increased with reaction temperature over Fe-MFI with low loading of Fe (Fe/Al = 0.05 and 0.10). In contrast, C_3H_6 conversion reached almost 100% in rather low temperature range over Fe-MFI (Fe/Al = 0.15 and 0.24). CO_2 and CO were observed as the carbon-containing products, and CO_2 selectivity is represented in Figure 3-3(c). Figure 3-3(d) shows the relation between N_2O conversion and C_3H_6 conversion. It is clearly shown that C_3H_6 conversion reached 100% even under low level of N_2O conversion. Furthermore, C_3H_6 conversion reached some level even when N_2O conversion was zero, and this means that C_3H_6 reacted with oxygen, not with N_2O.

Figure 3-4 shows the temperature dependence of the catalyst performance of Fe-MFI in N_2O reduction with C_2H_6 under excess oxygen atmosphere. N_2O and C_2H_6 conversions increased with reaction temperature and the loading amount of Fe (Figs. 3-4(a) and (b)). In the relation between N_2O and the reductant conversion, the behavior in N_2O reduction with C_2H_6 was much different from that in N_2O reduction with C_3H_6. As shown in Figure 3-4(d), C_2H_6 conversion increases proportionally with N_2O conversion in the range of N_2O conversion 0 - 50%. This means that C_2H_6 conversion is almost zero when N_2O conversion is zero. This suggests N_2O is necessary for the activation of C_2H_6. The similar behavior has also been observed on Fe-BEA

catalyst in the previous report [17]. In addition, the carbon amount in the effluent gas was balanced with that introduced in the case of C_2H_6 in all the temperature range, unlike the case of C_3H_6.

Figure 3-5 shows the temperature dependence of catalyst performance in N_2O reduction with CH_4 under excess oxygen atmosphere. Conversions of N_2O and CH_4 increased with Fe amount (Figs. 3-5(a) and (b)). It is known that CH_4 is less reactive than C_2H_6 and C_3H_6. However, N_2O reduction with CH_4 started at almost the same temperature as that with C_2H_6 and C_3H_6. For example, the reduction of N_2O started at almost the same temperature (about 523 K) over Fe(0.40)-MFI in the case of CH_4 and C_2H_6. It is characteristic that N_2O conversion in Fig. 3-5(a) reached 100% at about 700 K over Fe(0.40)-MFI in the case of N_2O reduction with CH_4. In contrast, in the case of N_2O reduction with C_2H_6 and C_3H_6, N_2O conversion did not reach about 100% below *ca.* 760 K (Figs. 3-3(a) and 3-4(a)). In addition, it should be pointed out that there was a plateau in CH_4 conversion at which N_2O conversion reached 100% in Figure 3-5(b), especially over Fe-MFI (Fe/Al = 0.40). This indicates that CH_4 cannot react directly with O_2 even at 700 K. These results indicate that CH_4 is most efficient reductant for the SCR of N_2O. Since the feeding ratio of hydrocarbons to N_2O is higher than the stoichiometry of N_2O reduction with hydrocarbons, as listed in Table 3-1, N_2O conversion can reach 100% before the conversion of hydrocarbons when the reaction proceeds stoichiometrically. However, this is not the case when hydrocarbons react with oxygen, and this tendency is related to the reactivity between hydrocarbons and oxygen. Therefore in order to evaluate the contribution of N_2O in total oxidizing agent, the results are shown in Figure 3-6. In the case of N_2O reduction with CH_4, the contribution of N_2O can be calculated by (consumed N_2O)/($4CO_2$ + $3CO$) on the basis of the equations below.

$$CH_4 + 4[O] \rightarrow CO_2 + 2H_2O$$

$$CH_4 + 3[O] \rightarrow CO + 2H_2O$$
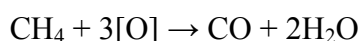
$$[O]: \text{oxygen atom originated from } N_2O \text{ and } O_2$$

The details of C_2H_6 and C_3H_6 are referred to the caption in Figure 3-6. On both Fe-MFI catalysts, N_2O contribution in $N_2O/CH_4/O_2$ system is higher than that in the case of $N_2O/C_2H_6/O_2$ and $N_2O/C_3H_6/O_2$ systems. This indicates that CH_4 reacted with N_2O more efficiently than C_2H_6 and

C_3H_6. In other words, a higher concentration of reductants must be supplied for higher N_2O conversion and removal in the case of C_2H_6 and C_3H_6, compared to CH_4. From these viewpoints, CH_4 is a more suitable reductant when N_2O is removed from containing air. In terms of the practical aspect, the suitability of hydrocarbons as N_2O reductant can be estimated as follows: $CH_4 > C_2H_6 > C_3H_6$ on the basis of the order of N_2O contribution. In addition, N_2O conversion was almost proportional to CH_4 conversion as shown in Figure 3-5(d), and the line goes through the origin. This also suggests that N_2O is necessary for the activation of CH_4. On the other hand, C_3H_6 can be activated without N_2O on the basis of the result in Figure 3-3(d). In the three reactions, Fe-MFI with higher Fe loading amount exhibited higher activity. The relation between the activity and Fe loading is discussed in detail in the next section. From these results, it can be concluded that CH_4 is superior to C_2H_6 and C_3H_6 in N_2O reduction with hydrocarbons under excess oxygen atmosphere.

3.3.2. Reaction of N_2O with various reductants over Fe-MFI catalysts

In the previous section, the activity test was carried out under the presence of excess oxygen atmosphere. This is because N_2O should be removed from the gas containing air in the practical process. In contract, in this section, I carried out the activity test in the absence of oxygen. This is because it is possible to exclude the reaction of the reductant with oxygen in order to investigate the effect of reductant in N_2O reduction. Reaction temperature dependence in N_2O decomposition over Fe-MFI catalysts is shown in Figure 3-7. These results are also based on the activity under steady-state conditions. Therefore, the product N_2/O_2 ratio was 2/1, which means that the reaction proceeded stoichiometrically. N_2O conversion was dependent on the Fe loading amount. Furthermore, the starting temperature was also influenced by the Fe loading amount. This behavior can be related to O_2 desorption temperature in O_2-TPD profiles. The starting temperature of oxygen desorption in O_2-TPD profiles became lower over Fe-MFI with higher Fe loading. As shown in Figure 3-8, the starting temperature of O_2 desorption can be estimated to be 670 K and 790 K over Fe(0.40)- and Fe(0.10)-MFI, respectively. The temperature, at which N_2O decomposition starts to proceed, corresponds well to the temperatures in O_2-TPD of N_2O-treated catalysts. This suggests that the rate-limiting step of N_2O decomposition is oxygen desorption from the catalyst surface. This is also supported by the

previous reports [10, 41, 42]. Figure 3-7(b) shows turnover frequency (TOF) of N_2O decomposition as a function of the molar ratio of Fe/Al in Fe-MFI. It is found that TOF of N_2O decomposition at 673 K was almost zero in the range of Fe/Al $\leq$ 0.10, however, the TOF drastically increased with Fe loading (Fe/Al > 0.10). The profile of O_2-TPD over Fe(0.10)-MFI gave only one peak. In contrast, another sharp peak at lower desorption temperature (~873 K) appeared over Fe(0.40)-MFI (Fig. 3-8(a)). This kind of Fe species can contribute to the high catalytic activity over Fe(0.40)-MFI. The behavior of TOF can be explained by the Fe species which gave the lower-temperature peak. As shown in Fig. 3-8(a), the amount of O_2 desorption after N_2O treatment was larger than that after O_2 treatment, the origin of which has been discussed extensively in chapter 2 and the previous report [19].

Figure 3-9(a) shows the temperature dependence of N_2O conversion in N_2O reduction with H_2. N_2O conversion in the N_2O + H_2 reaction was much higher than that in N_2O decomposition. Catalytic activity as well as the temperature at which the N_2O + H_2 reaction started was also dependent on the loading amount of Fe. Figure 3-10 shows the profiles of temperature programmed reduction (TPR) of Fe-MFI after O_2 treatment. Fe-MFI (Fe/Al = 0.05 and 0.1) started to be reduced in H_2 at about 600 K. In contrast, Fe-MFI (Fe/Al = 0.15-0.40) started to be reduced at lower temperature than Fe-MFI (Fe/Al = 0.05 and 0.10). For example, the reduction started at 450 K on Fe(0.40)-MFI. This suggests that Fe-MFI catalysts with higher Fe loading contain more reducible Fe species. The tendency in H_2-TPR is similar to that in the N_2O + H_2 reaction. Although the difference of starting temperatures between H_2-TPR and the N_2O + H_2 reaction was clearly observed, it is thought to be explained by the pressure difference. Figure 3-9(b) shows the result of N_2O reduction with CO. Although N_2O conversion in the N_2O + CO reaction was higher than that of the N_2O + H_2 reaction, the tendency of N_2O + CO reaction was similar to that of the N_2O + H_2 reaction. The relations between the TOF value and the Fe/Al ratio are shown Figure 3-9(c). TOFs of the N_2O + H_2 and N_2O + CO reactions increased with increasing Fe/Al, which can be interpreted on the basis of TPR profiles. More reducible Fe species can work as the active site at lower reaction temperatures. The amount of more reducible Fe species increased with increasing Fe loading amount, and this can explain the relations between TOFs and Fe/Al.

Figure 3-11 shows the temperature dependence in N_2O reduction with CH_4 in the absence

of oxygen. The carbon amount in the effluent was balanced with that introduced in this reaction. This means that the results correspond to the steady state activity and coke was not deposited. Although the details are not shown here, large amount of coke was deposited in $N_2O + C_2H_6$ and $N_2O + C_3H_6$ reactions in the absence of excess oxygen. From this viewpoint, the data in the case of C_2H_6 and C_3H_6 were not able to be available under this type of conditions. CH_4 conversion had the plateau since N_2O conversion reached almost 100%. These profiles are also observed in N_2O reduction with CH_4 in the presence of excess oxygen. The temperature, at which the $N_2O +$ CH_4 reaction started, was also dependent on Fe loading, and the tendency is also observed in the $N_2O + H_2$ and $N_2O + CO$ reactions. Figure 3-11(d) shows the relation between TOF of the $N_2O +$ CH_4 reaction and Fe/Al. The TOF value jumped at Fe/Al = 0.15, and increased with increasing Fe/Al. This TOF behavior is similar to that in the $N_2O + H_2$ and $N_2O + CO$ reactions. It is suggested that more reducible Fe species can also contribute to the enhancement of TOF in the case of the $N_2O + CH_4$ reaction.

Figure 3-12 shows the comparison of N_2O conversion in various reactions over Fe(0.40)-MFI and Fe(0.05)-MFI. The order of N_2O conversion over Fe(0.40)-MFI and Fe(0.05)-MFI was $CH_4 > CO > H_2$ in all the temperature range. It should be noted that the $N_2O +$ CH_4 reaction gave the highest N_2O conversion over all the catalysts and in all the temperature range. Considering that the reactivity of methane is generally much lower than H_2 and CO, it is very interesting that methane has higher reactivity than H_2 and CO for N_2O reduction. According to the results of TOF in various reactions, the structure of the active sites is almost the same on Fe-MFI (Fe/Al = 0.05 and 0.10) catalysts, and another active sites appear on Fe-MFI (Fe/Al = 0.15-0.40), which are more reducible iron species.

3.3.3. Fe K-edge EXAFS analysis after different treatment

I carried out the structure analysis of the Fe(0.10)- and Fe(0.40)-MFI catalysts with some treatments on the basis of the results from O_2-TPD by means of EXAFS. Figures 3-11(a) and (b) show the Fe *K*-edge EXAFS oscillations for Fe(0.10)-MFI measured after treatment with O_2 or N_2O. It seems that the oscillation on Fe(0.10)-MFI treated with O_2 is similar to that with N_2O. As shown in Fig. 3-8(b), only one O_2 desorption peak was observed on Fe(0.10)-MFI, and the desorption profile of the sample after O_2 treatment was almost the same that after N_2O treatment.

This means that the additional oxygen deposition by N_2O treatment did not occur on Fe(0.10)-MFI. This can explain the similarity of the spectra. The Fourier transforms (FT) of k^3-weighted EXAFS oscillations for Fe(0.10)-MFI were shown in Figure 3-13(c), and their fitting results are shown in Figures 3-13(d) and (e). The details of the curve fitting parameters are listed in Table 3-2. Two major peaks were observed in the regions of 0.1 - 0.2 nm, and 0.2 - 0.3 nm in FT spectra. One peak with shorter bond length of 0.1 - 0.2 nm can be assigned to Fe-O bond, which have already been reported by EXAFS studies [25, 27, 43]. And the other peak with longer bond length of 0.2 – 0.3 nm can be assigned to Fe-Si bond, as shown later. In O_2-TPD profile of Fe(0.10)-MFI, the amount of O_2 desorption from O_2- and N_2O-treated samples is estimated to be $O_2/Fe = 0.16$ and 0.17, respectively. These values are less than $O_2/Fe = 0.25$, which is based on the equation.

$$4Fe^{3+} + 2O^{2-} \rightarrow 4Fe^{2+} + O_2$$
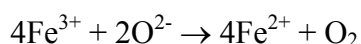
This suggests that a part of Fe can give oxygen desorption, and the other can not give it. Therefore, regarding the Fe-O bond, it is expected that there are two kinds of Fe-O bond on the basis of the amount of O_2 desorption. This suggestion makes us use two kinds of Fe-O bond in the curve fitting analysis (Table 3-2).

The Fe-O band with shorter distance of 0.187 nm can be ascribed to O atoms of the OH species coordinated with Fe ion species. In the previous reports, Koningsberger *et al*. [25, 26] have assigned the Fe-O distance of 0.188 nm to a terminal OH group and the Fe-O distance of 0.193 nm to the bridging Fe-O-Fe oxygen atom. The Fe-O band with longer distance of 0.204 nm is ascribed to O atoms in the zeolite lattice, by which the Fe atoms are stabilized to the zeolite lattice like Fe-O-Si and Fe-O-Al, and it is expected that the oxygen species are difficult to be desorbed. This assignment is supported by the previous reports [25, 28].

From the fitting results of EXAFS data, I could fit the spectra with Fe-Si shell. Joyner *et al*. [33] have reported that the distance of Fe-Si shell is about 0.32 nm, which is almost the same value compared to this results. On the other hand, Choi *et al*. [43] have reported EXAFS analysis of Fe-ZSM-5 prepared by solid ion-exchanged, and they have assigned the peak between 0.25 and 0.30 nm to Fe-Al bond. Generally speaking, it is difficult to distinguish between Al and Si as a backscattering atom because the difference of atomic number is very small. However, this

tendency can be explained by the local structure of Fe on MFI. It has been proposed that an Fe ion over the acid site is neighboring one Al and two or more Si atoms through the lattice oxygen atoms. This suggests that the Si atoms have more contribution than Al atom. The possibility of Fe-Fe bond over Fe(0.10)-MFI can be unacceptable because this catalyst contains almost exclusively Fe ions with lower reducibility from H_2-TPR and O_2-TPD results (Figs. 3-8(b) and 3-10). In addition, the Fe loading amount of Fe(0.10)-MFI catalyst is low, and because the catalyst was prepared by severely controlled wet ion-exchange method, it is expected that the Fe species over Fe(0.10)-MFI catalyst can be isolated. In fact, it is difficult to fit the FT peak with one wave of Fe-Fe. From these comparisons, for the Fe(0.10)-MFI after O_2 treatment, three-shell fitting (Fe-O_1, Fe-O_2, Fe-Si) gave the appropriate result. The comparison of the results between O_2 and N_2O treatments shows that the coordination number and the distance were almost the same values. This also shows that N_2O treatment did not make the structure change of Fe species.

Figures 3-14(a) - (c) show EXAFS oscillations for Fe(0.40)-MFI after the treatments with O_2, N_2O, and H_2. It is found that the oscillation of Fe(0.40)-MFI after N_2O treatment is different from that after O_2 treatment, especially in higher k region. In addition, it is also found that the oscillations of Fe(0.40)-MFI are similar to that of Fe(0.10)-MFI in the case of O_2 treatment. The FT spectra of k^3-weighted EXAFS oscillations for Fe(0.40)-MFI with different treatments are shown in Figure 3-14(d). Their fitting results are shown in Figures 3-15(a) - (c), and listed in Table 3-3. Regarding Fe(0.40)-MFI after O_2 treatment, the curve fitting was carried out on the basis of the results of Fe(0.10)-MFI because of the similarities in EXAFS oscillations. Curve fitting results on these two samples were also similar. In addition, a different point is the bond length of the short Fe-O_1 bond. It seems that the length of Fe-O_1 bond in Fe(0.40)-MFI is a little longer than that in Fe(0.10)-MFI. Koningsberger *et al*. [26] have reported that Fe-O distance of Fe-O-Fe bridged oxygen (0.193 nm) is longer than that of terminal OH species (0.188 nm). In this case, although the difference of the bond distance is not so large, the contribution of the bridged oxygen species can be added to the bond of Fe-O_1 on Fe(0.40)-MFI. This interpretation can be supported by the O_2-TPD profiles (Fig. 3-8). In the case of Fe(0.40)-MFI after O_2 treatment, the desorption peak at lower temperature was observed, and this was not observed over Fe(0.10)-MFI. This indicates that Fe(0.40)-MFI has different oxygen species from

Fe(0.10)-MFI, which can be desorbed more easily. In the case of Fe(0.40)-MFI, N_2O treatment can make the Fe structure change, and this is not the case of Fe(0.10)-MFI. The difference was clearly observed in the FT spectra. N_2O treatment decreased the peak intensity at $0.1 - 0.2$ nm and in contrast, it increased the peak intensity at $0.2 - 0.3$ nm. N_2O treatment increased O_2 desorption amount from the TPD profiles, however, the peak intensity due to Fe-O band decreased. According to the curve fitting analysis, the increase of the contribution of the Fe-O_1 can explain this behavior. On the other hand, in the FT peak at larger region, the Fe-Fe bond was added, because of the oscillation difference at higher k region. Four-shell fitting of Fe(0.40)-MFI after N_2O treatment requires 16 parameters, and this can not be allowed on the basis of the limitation of the independent parameters (N_I) [44]. Here, N_I can be calculated to be 15.3 using Δk = 91 nm^{-1}, ΔR = 0.23 nm. For the profile of Fe(0.40)-MFI after O_2 treatment, the best fitting result was obtained by a three-shell fitting. However, I could not obtain good fitting results for Fe(0.40)-MFI after N_2O treatment by the three-shell fitting. As a result, the curve fitting was carried out using two Fe-O, one Fe-Si, one Fe-Fe shells. The results are listed in Table 3-3. Considering also other characterization results from H_2-TPR and O_2-TPD, it is strongly suggested that binuclear Fe species are formed on Fe(0.40)-MFI (Fig. 3-16).

From the results of EXAFS studies, many research groups have reported the various structures of Fe species prepared by different methods [24-33]. Sachtler *et al.* [30-32] have reported that Fe/MFI prepared by sublimation method has a molar ratio of Fe to Al-centered tetrahedral of 1/1 and that active species over MFI are oxygen bridged binuclear iron species. Koningsberger *et al.* [24-26] have determined the structure of the Fe binuclear complex with Fe-O-Fe bridges on Fe/ZSM5 catalyst, which was prepared by $FeCl_3$ by EXAFS. Prins *et al.* [27, 28] have reported that the diiron structure resembles the core unit in methane monooxygenase (MMO). In addition, Panov *et al.* [29] have indicated that α-oxygen can participate in the direct catalytic oxidation of benzene to phenol by N_2O over Fe-MFI, and the oxygen species are related to the presence of binuclear Fe complex. These reports suggest that the Fe species with the coordination of $0.25 - 0.30$ nm are binuclear. On the other hand, Joyner *et al.* [33] have reported that the presence of very small iron-oxygen clusters of unusual structure such as Fe_4O_4 with a short iron-iron distance of *ca.* 0.25 nm. However, I could not observe the short Fe-Fe bond in EXAFS spectra. This can be interpreted that there are no iron-oxo nanoclusters such as Fe_4O_4 on

the Fe-MFI catalysts, and this is also supported by H_2-TPR, in which no H_2 consumption due to Fe oxide was observed (see Fig. 3-10). In the previous H_2-TPR study, H_2 consumption with the peak at 850 K was observed on Fe_2O_3 [19]. Although the presence of oligonuclear Fe species can be possible (binuclear, trinuclear etc.), highly aggregated oligonuclear Fe species can be ruled out, because the Fe-Fe coordination number is determined to be 0.6 after N_2O treatment, which is clearly less than unity (Table 3-3). This also indicates that binuclear Fe species as well as isolated Fe ions are present. This interpretation is also supported by O_2-TPD and H_2-TPR: binuclear iron species are more reducible, and they give lower-temperature O_2 desorption. In addition, the coordination number of Fe-O_1 shell became larger after N_2O treatment than that after O_2 treatment. This behavior can be explained by oxygen deposition on the Fe species by N_2O treatment (see Fig. 3-8).

The sum of Fe-O coordination is 5.0, which indicates Fe ion species are octahedrally coordinated with zeolite lattice oxygen, bridged oxygen and OH ligands. In a previous report [25], it is shown that binuclear Fe species have an octahedral environment. These results also support that binuclear Fe species are present on the Fe(0.40)-MFI catalyst. However, I could not observe the Fe-Fe bond in Fe(0.40)-MFI after O_2 treatment. It seems that some of the bridged oxygen on binuclear Fe species are not present on Fe(0.40)-MFI after O_2 treatment. In contrast, Fe-Fe bond is formed by N_2O treatment, and this is due to bridging two Fe ions induced by deposited oxygen during the N_2O treatment. From the H_2-TPR profile, it is found that all the iron species can be reduced from Fe^{3+} to FeP^{2+} with H_2 reduction at 773 K. After H_2 treatment (Fig. 3-15(c)), the coordination number of Fe-O_1 decreased due to oxygen removal during H_2 treatment (see Table 3-3). This behavior is observed more significantly in Fe-O_1. On the other hand, the coordination number of the Fe-O_2 shell, which can be assigned to the bond between Fe and lattice oxygen, was almost constant. This can be interpreted by the presence of the oxygen species, which are hardly removed even after H_2 treatment.

3.3.4. Relation between catalyst structure and performance in N_2O reduction

From the results of EXAFS analysis combined with other characterization, it is found that Fe(0.40)-MFI contains binuclear and mononuclear Fe species, and Fe(0.10)-MFI contains only mononuclear one. In the case of N_2O reduction with H_2, CO and CH_4, TOF increased with

increasing Fe loading, and this can be due to the formation of binuclear Fe species. From the comparison with H_2-TPR and O_2-TPD, more reducible Fe species are also assigned to binuclear Fe species.

The effect of reductants on N_2O reduction activity over Fe(0.40)-MFI is interesting in terms of the effectiveness of methane. Generally speaking, the reactivity of methane is very low compared to H_2 and CO. However, methane can play an important role for the reductant at almost same temperature range as H_2 and CO. Pérez-Ramírez *et al*. [45] have proposed that the N_2O + CO reaction proceeds with a different mechanism on different Fe ion species. Mononuclear Fe^{3+} species participate in this reaction via coordinated CO species on Fe^{3+} ions and their oxidation state is not changed during the reaction. The reaction over oligonuclear Fe_xO_y clusters proceeds via redox Fe^{3+}/Fe^{2+} process via the formation of O^- species as a reaction intermediate. Here, the Fe^{3+} in oligonuclear Fe_xO_y clusters can be easily reduced by CO. Therefore, they have concluded that active sites of the N_2O + CO reaction are oligonuclear Fe_xO_y clusters [45]. In this work, no formation of oligonuclear Fe_xO_y clusters was observed on the basis of H_2-TPR. The structure sensitivity of the N_2O + CO reaction in this study can be explained by the reducibility of binuclear Fe species.

I can also conclude that the N_2O + H_2 reaction is also structure-sensitive and the behavior is similar to that of the N_2O + CO reaction. In the case of the N_2O + H_2 reaction, the structure sensitivity can be related to the results from H_2-TPR (Fig. 3-10), which indicates that the reducibility of Fe species increased with increasing Fe loading amount and the formation of binuclear Fe species. The structure sensitivity can also be expected by more reducible binuclear Fe species, which give higher TOF (Fig. 3-16).

In this work, I have shown that CH_4 is the most effective reductant in the presence and absence of excess oxygen. From the result of *in-situ* FTIR study [20], the formation of methoxy species was observed during the N_2O + CH_4 reaction on a Fe-BEA catalyst (shown in chapters 4 and 5). From the result of pulse reactions, I have proposed that the formation of methoxy species promotes the reduction of Fe ion species on the active sites, which are suggested to be binuclear Fe species [19]. In addition, higher TOF was observed in the N_2O + CH_4 reaction (Fig. 3-11(d)) over Fe-MFI with higher Fe loading. These results indicate that the structure sensitivity of the N_2O + CH_4 reaction can be related to the formation of methoxy species from methane activated

with oxygen supplied from N_2O dissociation over binuclear Fe species [19].

3.4. Conclusions

(1) In the selective catalytic reduction (SCR) of N_2O with hydrocarbons in the presence of excess O_2, CH_4 and C_2H_6 were not activated by O_2 but by N_2O, although C_3H_6 could react with oxygen. The order of N_2O contribution in the SCR under excess oxygen is as follows: $CH_4 > C_2H_6 > C_3H_6$. This means that CH_4 is a more efficient reductant for the SCR of N_2O.

(2) The TOFs of N_2O reduction by H_2, CO and CH_4 and N_2O decomposition in the absence of oxygen increased with increasing molar ratio of Fe/Al, when Fe/Al is above 0.15, while TOFs were lower and constant in the range of Fe/Al $\leq$ 0.10.

(3) From H_2-TPR, more reducible Fe species were formed over Fe-MFI with higher Fe loading. In O_2-TPD, Fe(0.40)-MFI had oxygen species which can be desorbed at lower temperatures than Fe(0.10)-MFI.

(4) From the result of EXAFS analysis, only mononuclear Fe species were observed over Fe(0.10)-MFI after treatment with O_2 or N_2O. On the other hand, binuclear Fe species as well as mononuclear Fe species were observed over Fe(0.40)-MFI after treatment with N_2O or H_2. More reducible Fe species, which gave lower-temperature O_2 desorption, can be due to binuclear Fe species over Fe(0.40)-MFI.

(5) Although the reactivity of methane is usually very low, CH_4 can be oxidized by N_2O more easily than H_2 and CO. Formation of methoxy species on the Fe ion species promotes the reduction of Fe ion sites even in excess oxygen, and this can promote the redox cycle of binuclear Fe species.

References

[1]   F. Kapteijn, J. Rodrigues-Mirasol, J.A. Moulijn, *Appl. Catal. B* **9** (1996) 25.

[2]   M. Nakamura, H. Mitsuhashi, N. Takezawa, *J. Catal.* **138** (1992) 686.

[3]   S. Tanaka, K. Yuzaki, S. Ito, S. Kameoka, K. Kunimori, *J. Catal.* **200** (2001) 203.

[4]   X.F. Wang, H.C. Zeng, *Appl. Catal.* B **17** (1998) 89.

[5]   G. Centi, L. Dall'Olio, S. Perathoner, *J. Catal.* **192** (2000) 224.

[6]   Y. Li, J.N. Armor, *Appl. Catal.* B **1** (1992) L21.

[7]   T. Turek, *Appl. Catal.* B **9** (1996) 201.

[8]   J. Leglise, J.O. Petunchi., W.K. Hall, *J. Catal.* **86** (1984) 392.

[9]   T. Nobukawa, S. Tanaka, S. Ito, K. Tomishige, S. Kameoka, K. Kunimori, *Catal. Lett.* **83** (2002) 5.

[10]   J. Pérez-Ramírez, F. Kapteijn, G. Mul, J.A. Moulijin, *J. Catal.* **208** (2002) 211.

[11]   G. Centi, F. Vazzana, *Catal. Today* **53** (1999) 683.

[12]   R.W. van den Brink, S. Booneveld, J.R. Pels, D.F. Bakker, M.J.F.M. Verhaak, *Appl. Catal. B* **32** (2001) 73.

[13]   K. Yamada, S. Kondo, K. Segawa, *Mocroporous Mesoporous Mater.* **35-36** (2000) 227.

[14]   A. Satsuma, H. Maeshima, K. Watanabe, K. Suzuki, T. Hattori, *Catal. Today* **63** (2000) 347.

[15]   S. Kameoka, T. Suzuki, K. Yuzaki, T. Takeda, S. Tanaka, S. Ito, T. Miyadera, K. Kunimori, *Chem. Commun.* (2000) 745.

[16]   S. Kameoka, K. Yuzaki, T. Takeda., S. Tanaka, S. Ito, T. Miyadera, K. Kunimori, *Phys. Chem. Chem. Phys.* **3** (2001) 256.

[17]   S. Kameoka, K. Kita, S. Tanaka, T. Nobukawa, S. Ito, K. Tomishige, T. Miyadera, K. Kunimori, *Catal. Lett.* **79** (2002) 63.

[18]   S. Kameoka, T. Nobukawa, S. Tanaka, S. Ito, K. Tomishige, K. Kunimori, *Phys. Chem. Chem. Phys.* **5** (2003) 3328.

[19]   M. Yoshida, T. Nobukawa, S. Ito, K. Tomishige, K. Kunimori, *J. Catal.* **223** (2004) 454.

[20]   T. Nobukawa, M. Yoshida, S. Kameoka, S. Ito, K. Tomishige, K. Kunimori, *J. Phys. Chem. B* **108** (2004) 4071.

[21]   B. Coq, M. Mauvezin, G. Delahay, S. Kieger, *J. Catal.* **195** (2000) 298.

[22] G. Delahay, M. Mauvezin, B. Coq, S. Kieger, *J. Catal.* **202** (2001) 156.

[23] G. Delahay, M. Mauvezin, A. Guzmán-Vargas, B. Coq, *Catal. Commun.* **3** (2002) 385.

[24] A.A. Battiston, J.H. Bitter, F.M.F. de Groot, A.R. Overweg, O. Stephan, J.A. van Bokhoven, P.J. Kooyan, C. van der Spek, G. Vankó, D.C. Koningsberger, *J. Catal.* **213** (2003) 251.

[25] A.A. Battiston, J.H. Bitter, W.M. Heijboer, F.M.F. de Groot, D.C. Koningsberger, *J. Catal.* **215** (2003) 279.

[26] A.A. Battiston, J.H. Bitter, D.C. Koningsberger, *J. Catal.* **218** (2003) 163.

[27] P. Marturano, L. Drozdová, A. Kogelbauer, R. Prins, *J. Catal.* **192** (2000) 236.

[28] P. Marturano, L. Drozdová, G.D. Pirngruber, A. Kogelbauer, R. Prins, *Phys. Chem. Chem. Phys.* **3** (2001) 5585.

[29] K.A. Dubkov, N.S. Ovanesyan, A.A. Shteinman, E.V. Starokon, G.I. Panov, *J. Catal.* **207** (2002) 341.

[30] H.-Y. Chen, W.M.H. Sachtler, *Catal. Today* **42** (1998) 73.

[31] H.-Y. Chen, El-M. El-Malki, X. Wang, R.A. van Santen, W.M.H. Sachtler, *J. Mol. Catal. A* **162** (2000) 159.

[32] El-M. El-Malki, R.A. van Santen, and W.M.H. Sachtler, *J. Catal.* **196** (2000) 212.

[33] R. Joyner, M. Stockenhuber, *J. Phys. Chem. B* **103** (1999) 5963.

[34] W.N. Delgass, R.L. Garten, M. Boudart, *J. Chem. Phys.* **50** (1969) 4603.

[35] J.W. Cook, D.E. Sayers, *J. Appl. Phys.* **52** (1981) 5024.

[36] K. Okumura, J. Amano, N. Yasunobu, M. Niwa, *J. Phys. Chem. B* **104** (2000) 1050.

[37] K. Okumura, S. Matsumoto, N. Nishiaki, M. Niwa, *Appl. Catal. B* **40** (2003) 151.

[38] L. Ankudinov, B. Ravel, J.J. Rehr, S.D. Conradson, *Phys. Rev. B* (1998) 7565.

[39] B. Ravel, version 3.0beta8 4 March, The university of Washington, 2003.

[40] S. Kameoka, K. Yuzaki, T. Takeda, S. Tanaka, S. Ito, T. Miyadera, K. Kunimori, *Phys. Chem. Chem. Phys.* **3** (2001) 256.

[41] D.A. Bulushev, L. Kiwi-Minsker, A. Renken, *J. Catal.* **222** (2004) 389.

[42] G.D. Pirngruber, *J. Catal.* **219** (2003) 456.

[43] S.H. Choi, B.R. Wood, J.A. Ryder, A.T. Bell, *J. Phys. Chem. B* **107** (2003) 11843.

[44] E.A. Stern, *Phys. Rev. B* **48** (1993) 9825.

[45] J. Pérez-Ramírez, M.S. Kumar, A. Brückner, *J. Catal.* **223** (2004) 13.

Table 3-1

Reaction conditions in N_2O reduction*

Reductant	Gas composition			Catalyst weight	*W/F*
	N_2O / ppm	Reductant / ppm	O_2 / %	/ mg	/ g h mol^{-1}
CH_4	950	500	10	50	0.41
C_2H_6	1000	250	10	100	0.41
C_3H_6	1000	250	20	100	0.41
CH_4	950	500	0	50	0.41
H_2	1000	1000	0	100	0.41
CO	1000	1000	0	100	0.41
None	950	0	0	50	0.41

*All gases were balanced with He.

Table 3-2

Fe *K*-edge EXAFS fitting results for Fe(0.10)-MFI catalyst pretreated under different conditions.

Shells	CN^a	R / 10^{-1} nm ^{b}	σ / 10^{-1} nm ^{c}	ΔE_0 / eV ^{d}	R_f / % ^{e}
Fitting results of Fe(0.10)-MFI after O$_2$ treatment^f					
Fe-O$_1$	1.7 ± 0.1	1.87 ± 0.01	0.041 ± 0.012	-0.1 ± 0.8	0.69
Fe-O$_2$	1.7 ± 0.1	2.04 ± 0.01	0.045 ± 0.015	3.8 ± 0.9	
Fe-Si	1.9 ± 0.2	3.17 ± 0.01	0.058 ± 0.018	-5.6 ± 1.0	
Fitting results of Fe(0.10)-MFI after N$_2$O treatment^g					
Fe-O$_1$	1.6 ± 0.1	1.88 ± 0.01	0.064 ± 0.011	-5.8 ± 1.0	1.09
Fe-O$_2$	2.0 ± 0.1	2.04 ± 0.01	0.070 ± 0.011	3.1 ± 0.9	
Fe-Si	1.9 ± 0.2	3.19 ± 0.01	0.066 ± 0.018	-4.7 ± 1.1	

^{a} Coordination number. ^{b} Distance. ^{c} Debye-Waller factor. ^{d} Difference in the origin of photoelectron energy between the reference and the sample. ^{e} Residual factor. ^{f} Fourier filtering range: 0.083–0.304 nm. ^{g} Fourier filtering range: 0.077–0.304 nm.

Table 3-3

Fe *K*-edge EXAFS fitting results for Fe(0.40)-MFI catalyst pretreated under different conditions.

Shells	CN^a	R / 10^{-1} nm^b	σ / 10^{-1} nm^c	ΔE_0 / eV^d	R_f / %^{e}
Fe(0.40)-MFI after O$_2$ treatment^f					
Fe-O$_1$	1.4 ± 0.1	1.90 ± 0.01	0.063 ± 0.013	-4.3 ± 1.1	0.54
Fe-O$_2$	2.5 ± 0.2	2.05 ± 0.01	0.078 ± 0.010	4.7 ± 0.8	
Fe-Si	1.5 ± 0.2	3.19 ± 0.01	0.060 ± 0.023	-5.3 ± 1.4	
Fe(0.40)-MFI after N$_2$O treatment^g					
Fe-O$_1$	2.7 ± 0.1	1.89 ± 0.01	0.077 ± 0.007	5.5 ± 0.7	0.44
Fe-O$_2$	2.3 ± 0.1	2.05 ± 0.01	0.066 ± 0.010	0.6 ± 0.8	
Fe-Si	1.5 ± 0.2	3.19 ± 0.01	0.057 ± 0.022	-9.8 ± 1.3	
Fe-Fe	0.6 ± 0.1	2.95 ± 0.01	0.059 ± 0.021	3.0 ± 1.7	
Fe(0.40)-MFI after H$_2$ treatment^h					
Fe-O$_1$	0.9 ± 0.1	1.89 ± 0.01	0.077 ± 0.023	4.6 ± 2.1	0.90
Fe-O$_2$	2.3 ± 0.2	2.06 ± 0.01	0.074 ± 0.010	0.6 ± 0.8	
Fe-Si	0.9 ± 0.2	3.22 ± 0.02	0.064 ± 0.039	-2.9 ± 2.3	
Fe-Fe	0.4 ± 0.1	2.91 ± 0.02	0.060 ± 0.031	-13.7 ± 2.6	

^{a} Coordination number. ^{b} Distance. ^{c} Debye-Waller factor. ^{d} Difference in the origin of photoelectron energy between the reference and the sample. ^{e} Residual factor. ^{f} Fourier filtering range: 0.077–0.298 nm. ^{g} Fourier filtering range: 0.083–0.304 nm. ^{h} Fourier filtering range: 0.080–0.304 nm.
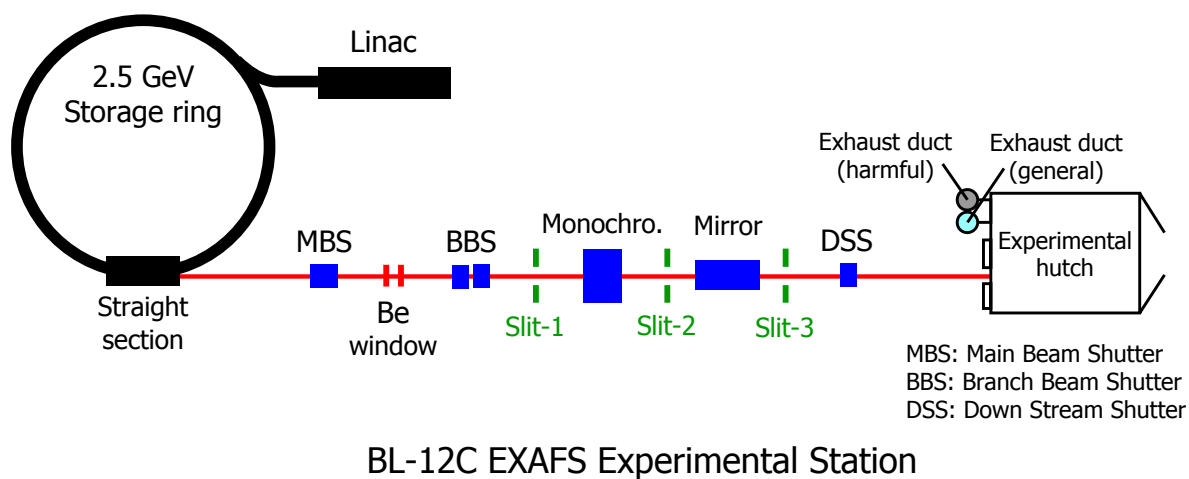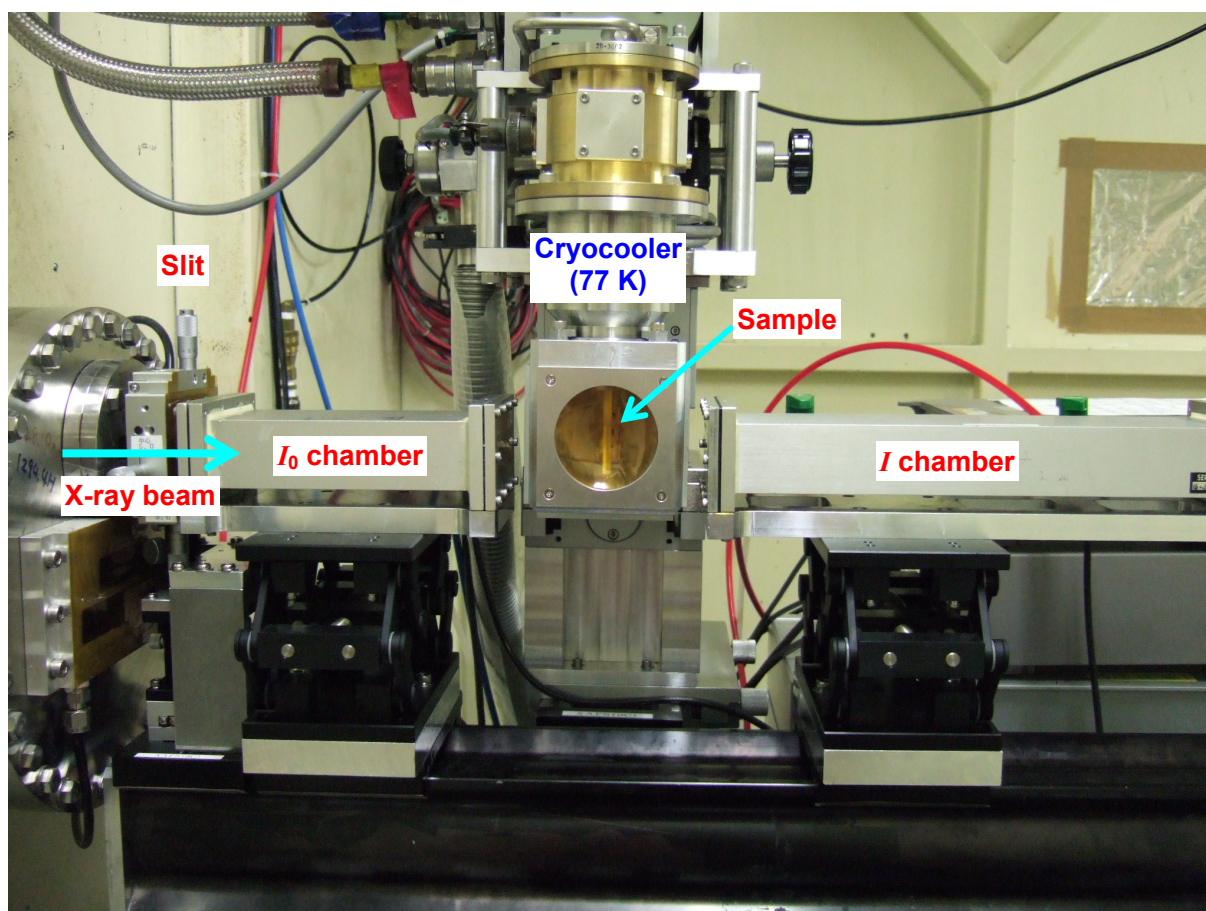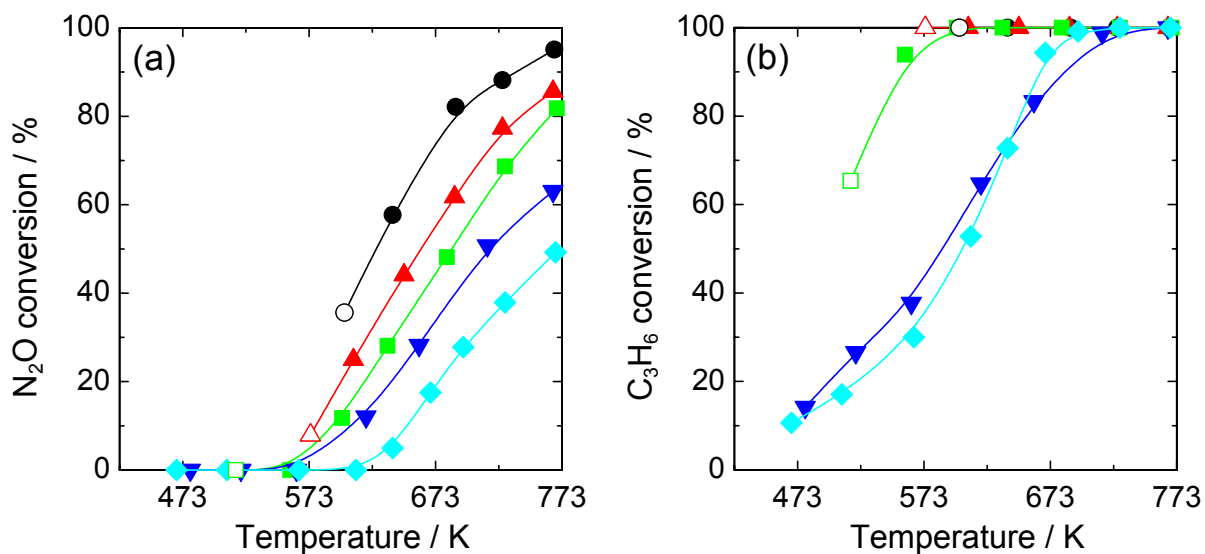
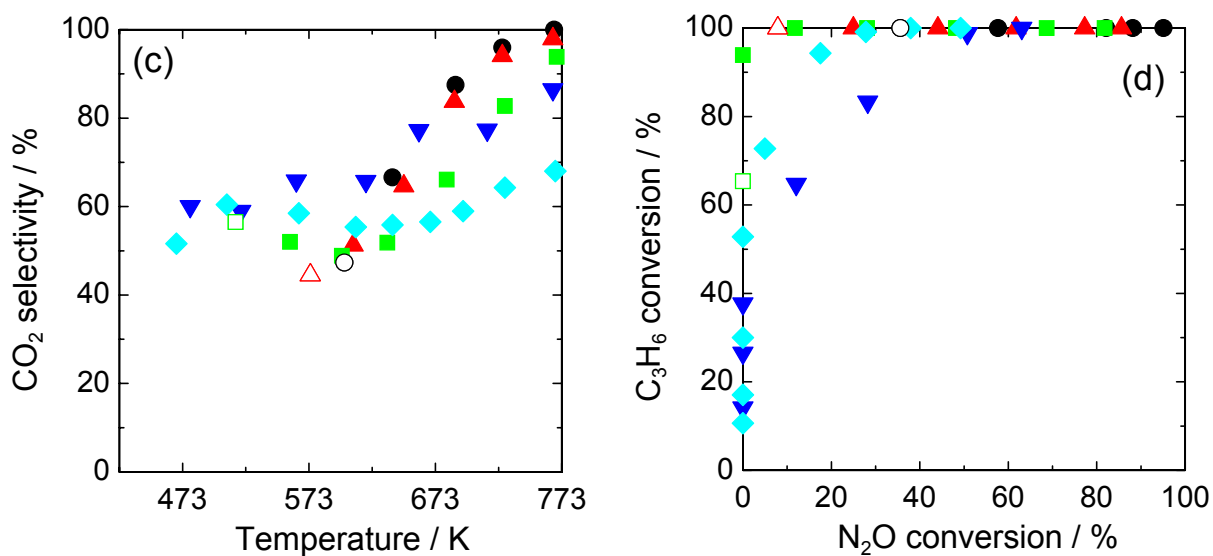**Figure 3-1.** Illustration of BL-12C station
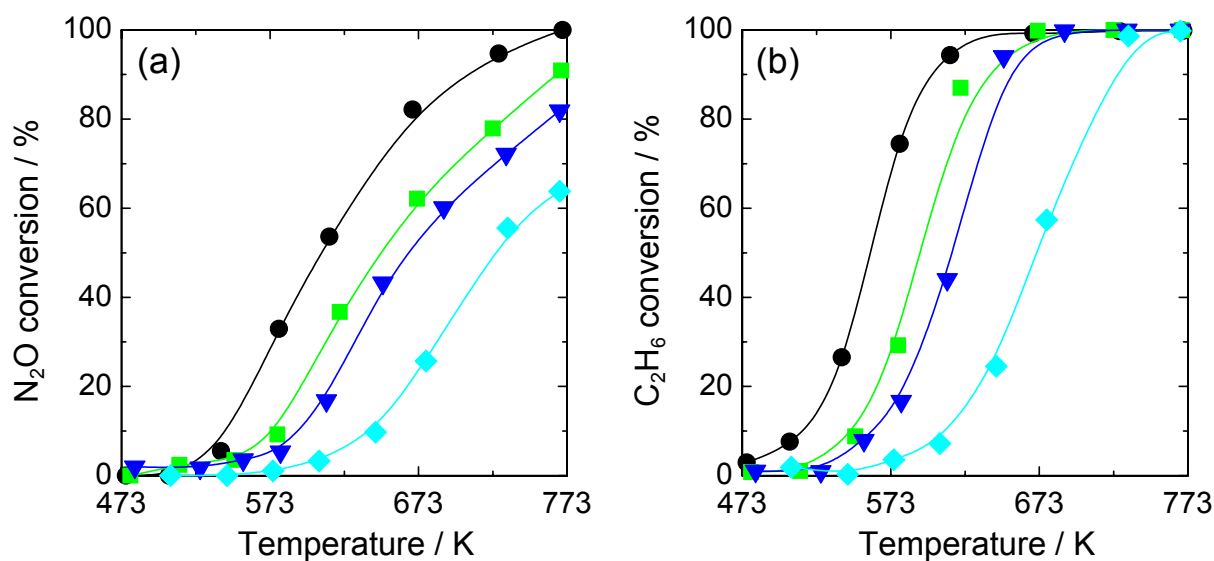

Figure 3-2. Photograph of the transmission setup.

(a) N₂O conversion

(b) C₃H₆ conversion

(c) CO₂ selectivity (CO₂/(CO + CO₂))

(d) C₃H₆ conversion as function of N₂O conversion

Figure 3-3. Reaction temperature dependence of catalyst performance of Fe-MFI catalyst in N_2O reduction with C_3H_6 under excess O_2 atmosphere.

● : Fe(0.40)-MFI, ▲ : Fe(0.24)-MFI, ■ : Fe(0.15)-MFI, ▼ : Fe(0.10)-MFI and ◆ : Fe(0.05)-MFI.

Gas composition: 1000 ppm N_2O, 250 ppm C_3H_6, 20% O_2 (He balance).

Open marks represent the data at which carbon deposition was observed.

(a) N₂O conversion

(b) C₂H₆ conversion
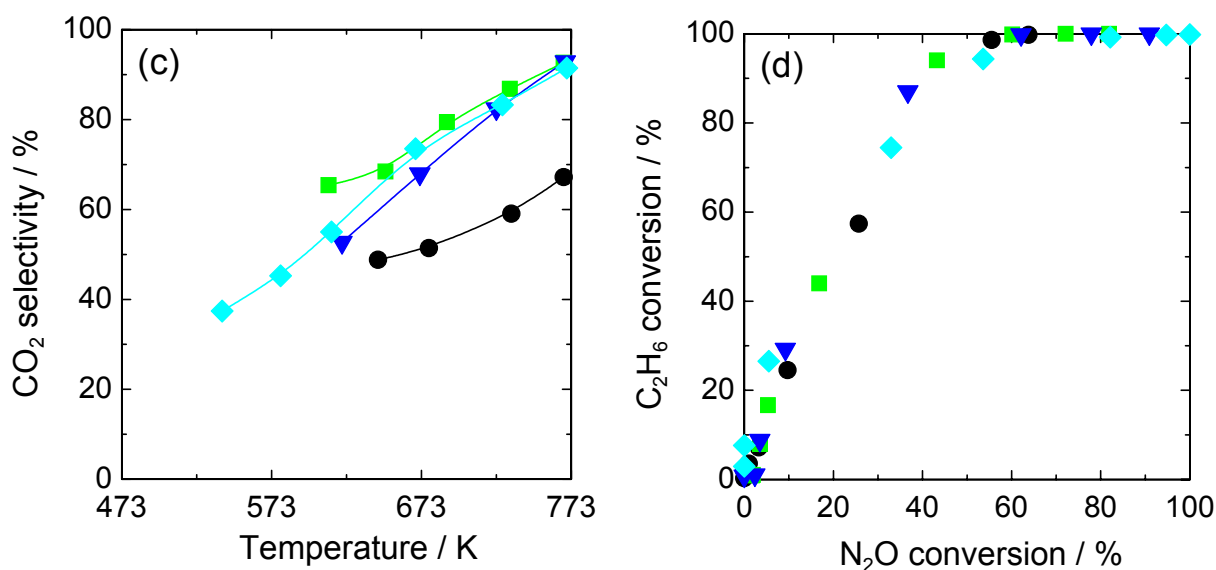
(c) CO₂ selectivity (CO₂/(CO + CO₂))

(d) C₂H₆ conversion as function of N₂O conversion

Figure 3-4. Reaction temperature dependence of catalyst performance of Fe-MFI catalyst in N_2O reduction with C_2H_6 under excess O_2 atmosphere.

●: Fe(0.40)-MFI, ■: Fe(0.15)-MFI, ▼: Fe(0.10)-MFI and ◆: Fe(0.05)-MFI.

Gas composition: 1000 ppm N_2O, 250 ppm C_2H_6, 10% O_2 (He balance).

(a) N₂O conversion

(b) CH₄ conversion

(c) CO₂ selectivity (CO₂/(CO + CO₂))

(d) CH₄ conversion as function of N₂O conversion
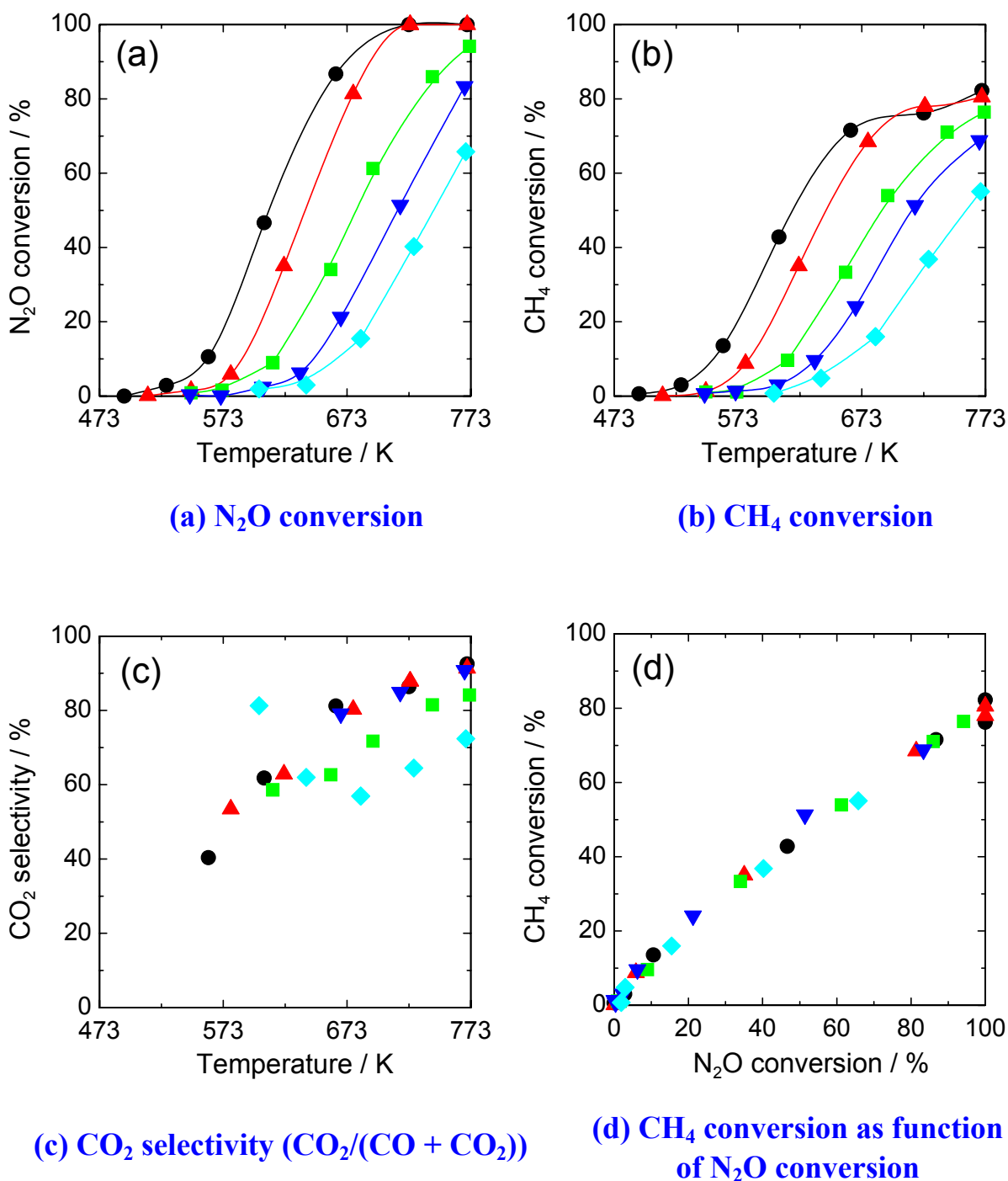
Figure 3-5. Reaction temperature dependence of catalyst performance of Fe-MFI catalyst in N_2O reduction with CH_4 under excess O_2 atmosphere.

● : Fe(0.40)-MFI, ▲ : Fe(0.24)-MFI, ■ : Fe(0.15)-MFI, ▼ : Fe(0.10)-MFI and ◆ : Fe(0.05)-MFI.

Gas composition: 950 ppm N_2O, 500 ppm CH_4, 10% O_2 (He balance).
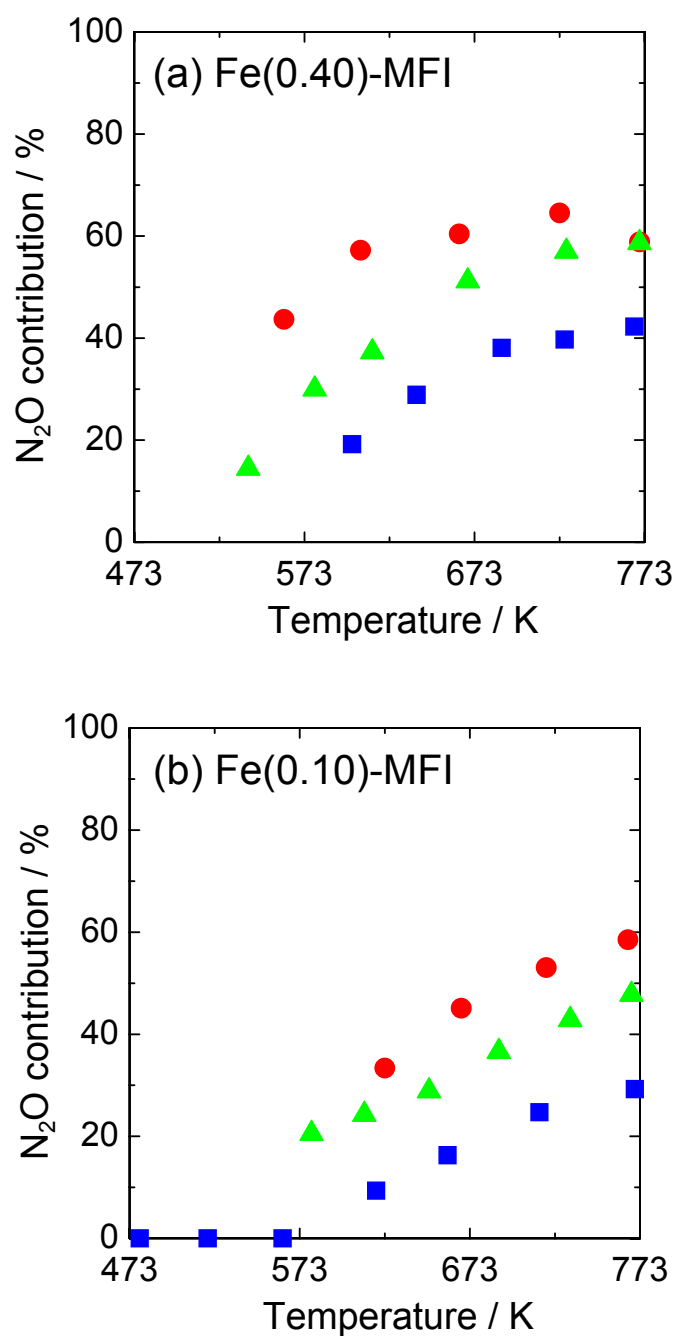
Figure 3-6. N_2O contribution in total oxidizing agents during N_2O reduction with various hydrocarbons under excess oxygen atmosphere. ●: CH_4, ▲: C_2H_6, ■: C_3H_6.
The reaction of CO and CO_2 formation is assumed below.

$$C_mH_n + (m + n/2)[O] \rightarrow mCO + n/2\ H_2O$$
$$C_mH_n + (2m + n/2)[O] \rightarrow mCO_2 + n/2\ H_2O$$

On the basis of the assumptions, N_2O contribution is calculated below.

$$N_2O\ contribution = (consumed\ N_2O)/((1+n/2m)CO + (2 + n/2m)CO_2)$$
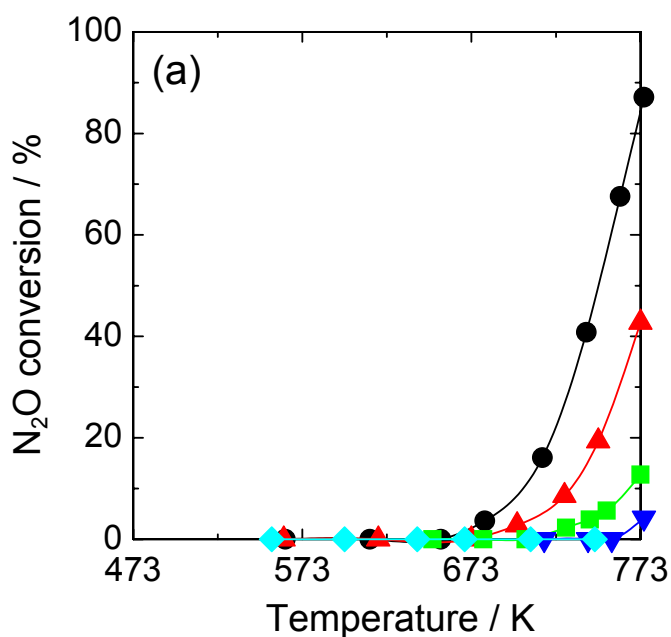
(a) N₂O conversion
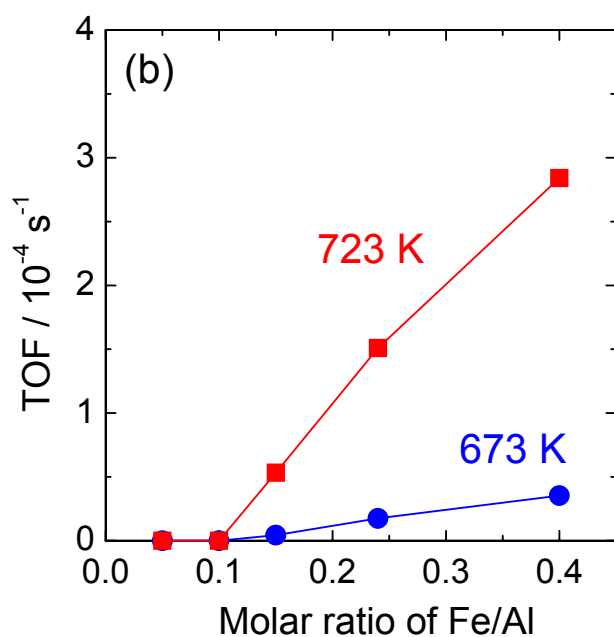
(b) TOF as a function of molar ratio of Fe/Al

Figure 3-7. Reaction temperature dependence of catalyst performance of Fe-MFI catalyst in N$_2$O decomposition in the absence of O$_2$. ●: Fe(0.40)-MFI, ▲: Fe(0.24)-MFI, ■: Fe(0.15)-MFI, ▼: Fe(0.10)-MFI and ◆: Fe(0.05)-MFI.
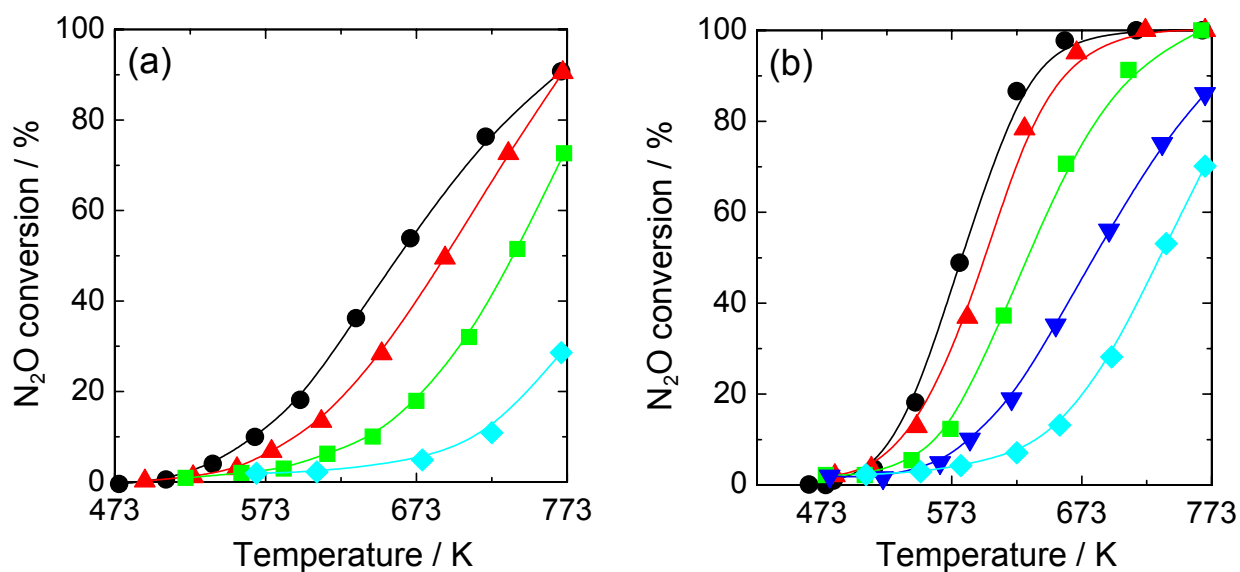Gas composition: 950ppm N$_2$O (He balance).
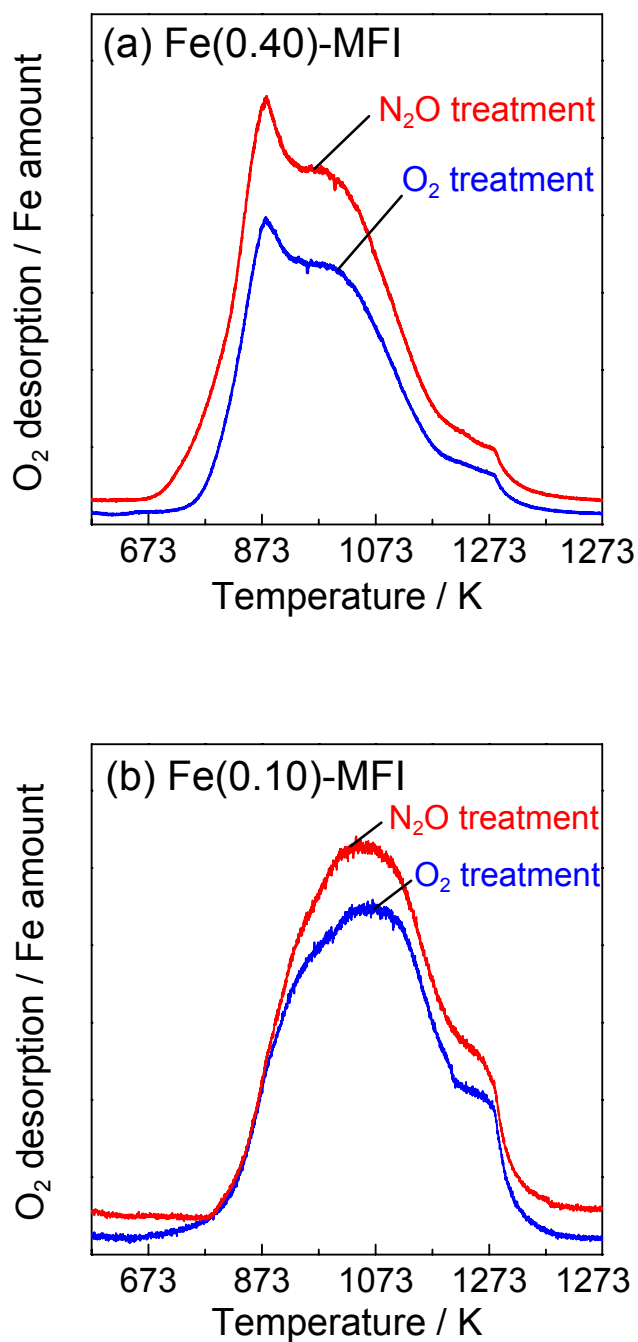
Figure 3-8. Temperature-programmed desorption of oxygen after O_2 and N_2O treatments normalized by Fe loading amount.

Reaction temperature: from room temperature to 1273 K, 10 K/min, 30 min hold.

Gas composition: He, 55 ml/min. Catalyst weight: 30 mg. Pretreatment: 100% O_2 flow, 773 K, 1 h, or 10% N_2O/He flow, 773 K, 1 h.

(a) N₂O+H₂ reaction

(b) N₂O+CO reaction
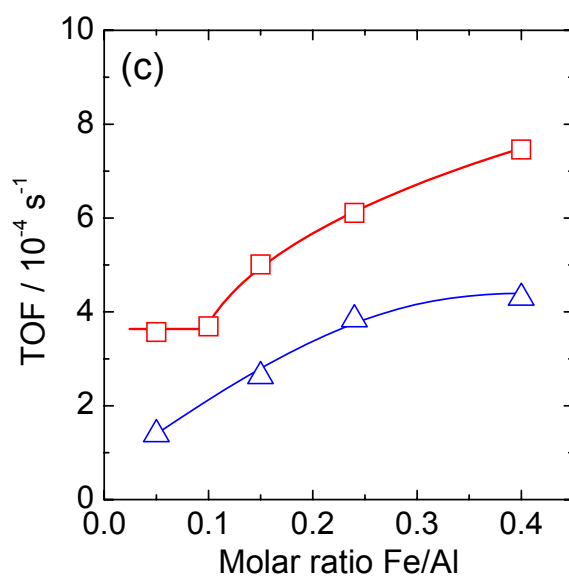
(c) TOF as a function of molar ratio of Fe/Al
calculated at 573 K (□ : CO) and 623 K (△ : H₂).

Figure 3-9. Reaction temperature dependence of N_2O conversion of Fe-MFI catalyst in N_2O reduction with H_2 and CO in the absence of O_2

● : Fe(0.40)-MFI, ▲ : Fe(0.24)-MFI, ■ : Fe(0.15)-MFI, ▼ : Fe(0.10)-MFI and ◆ : Fe(0.05)-MFI.

Gas composition: (a) 1000 ppm N_2O, 1000 ppm H_2 (He balance).

(b) 1000 ppm N_2O, 1000 ppm CO (He balance)
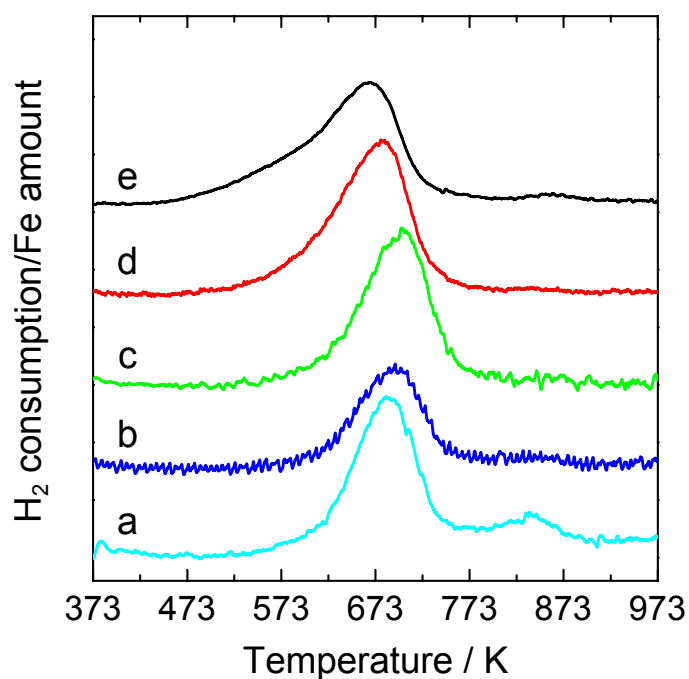
Figure 3-10. Temperature-programmed reduction in hydrogen over Fe-MFI catalysts normalized by Fe loading amount. (a) Fe(0.05)-MFI, (b) Fe(0.10)-MFI, (c) Fe(0.15)-MFI, (d) Fe(0.24)-MFI and (e) Fe(0.40)-MFI.

Reaction temperature: from room temperature to 973 K, 10 K/min.

Gas composition: 5.0% H_2/Ar, 30 ml/min. Catalyst weight: 50 mg. Pretreatment: 100% O_2 flow, 773 K, 1 h.

(a) N₂O conversion

(b) CH₄ conversion

(c) CO₂ selectivity

(d) TOF calculated at 573 K
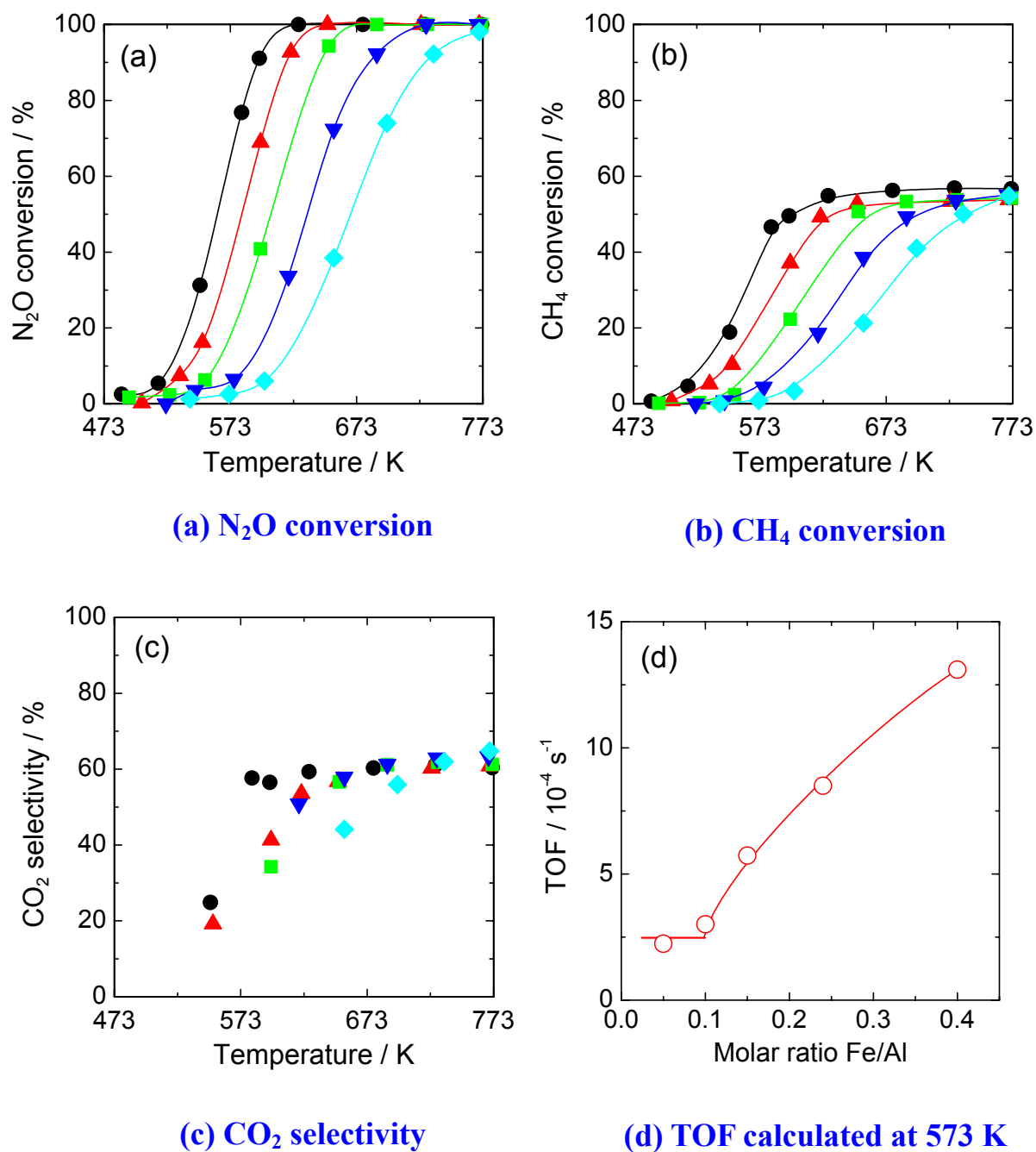
Figure 3-11. Reaction temperature dependence of catalyst performance of Fe-MFI catalyst in N_2O reduction with CH_4 in the absence of O_2.

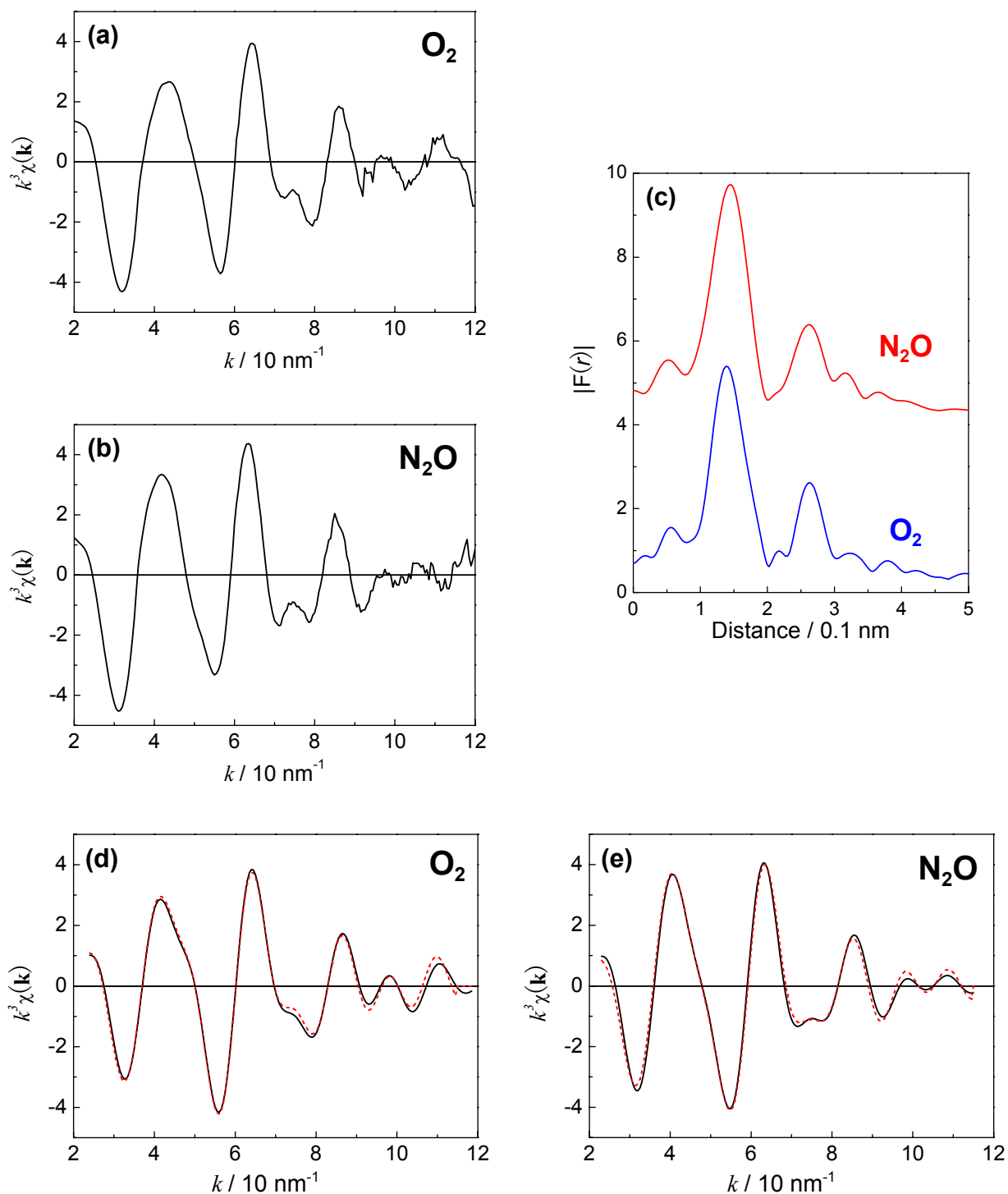● : Fe(0.40)-MFI, ▲ : Fe(0.24)-MFI, ■ : Fe(0.15)-MFI, ▼ : Fe(0.10)-MFI and ◆ : Fe(0.05)-MFI.

Gas composition: 950 ppm N_2O, 500 ppm CH_4 (He balance).
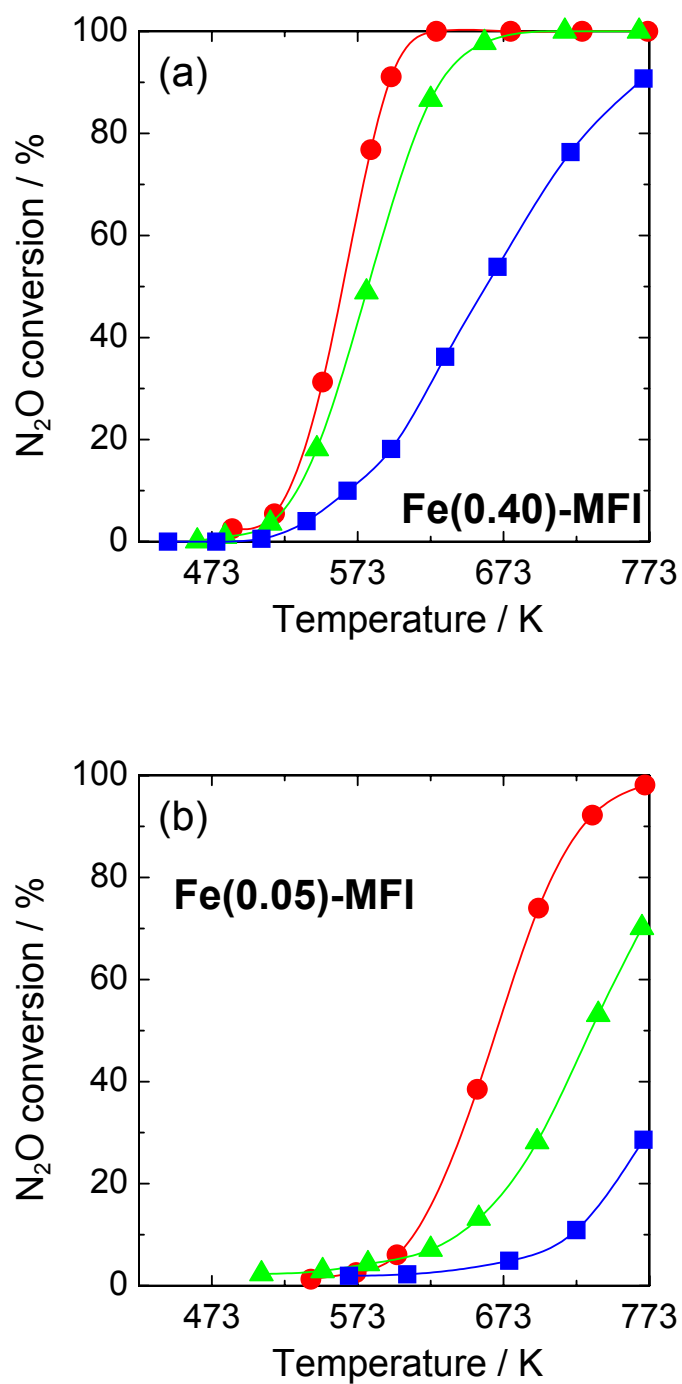
Figure 3-12. Comparison of N_2O conversion in N_2O reduction with various reductants in the absence of O_2 over Fe-MFI catalysts.

●: CH_4,　▲: CO,　■: H_2.

Reaction conditions were shown in the figure caption in Figs. 3-9 and 3-11.

Figure 3-13. (a, b): k^3-weighted Fe K-edge EXAFS for Fe(0.10)-MFI catalyst after treatment with (a) O_2 or (b) N_2O. (c): Fourier transform of k^3-weighted Fe K-edge EXAFS for Fe(0.10)-MFI catalyst after treatment with O_2 (Fourier transform range: 25-115 nm^{-1}) or N_2O (Fourier transform range: 23-115 nm^{-1}). (d)(e): Fourier filtered EXAFS data (solid line) and calculated data (dotted line) of Fe(0.10)-MFI after treatment with (d) O_2 or (e) N_2O. Fitting results are listed in Table 3-2.
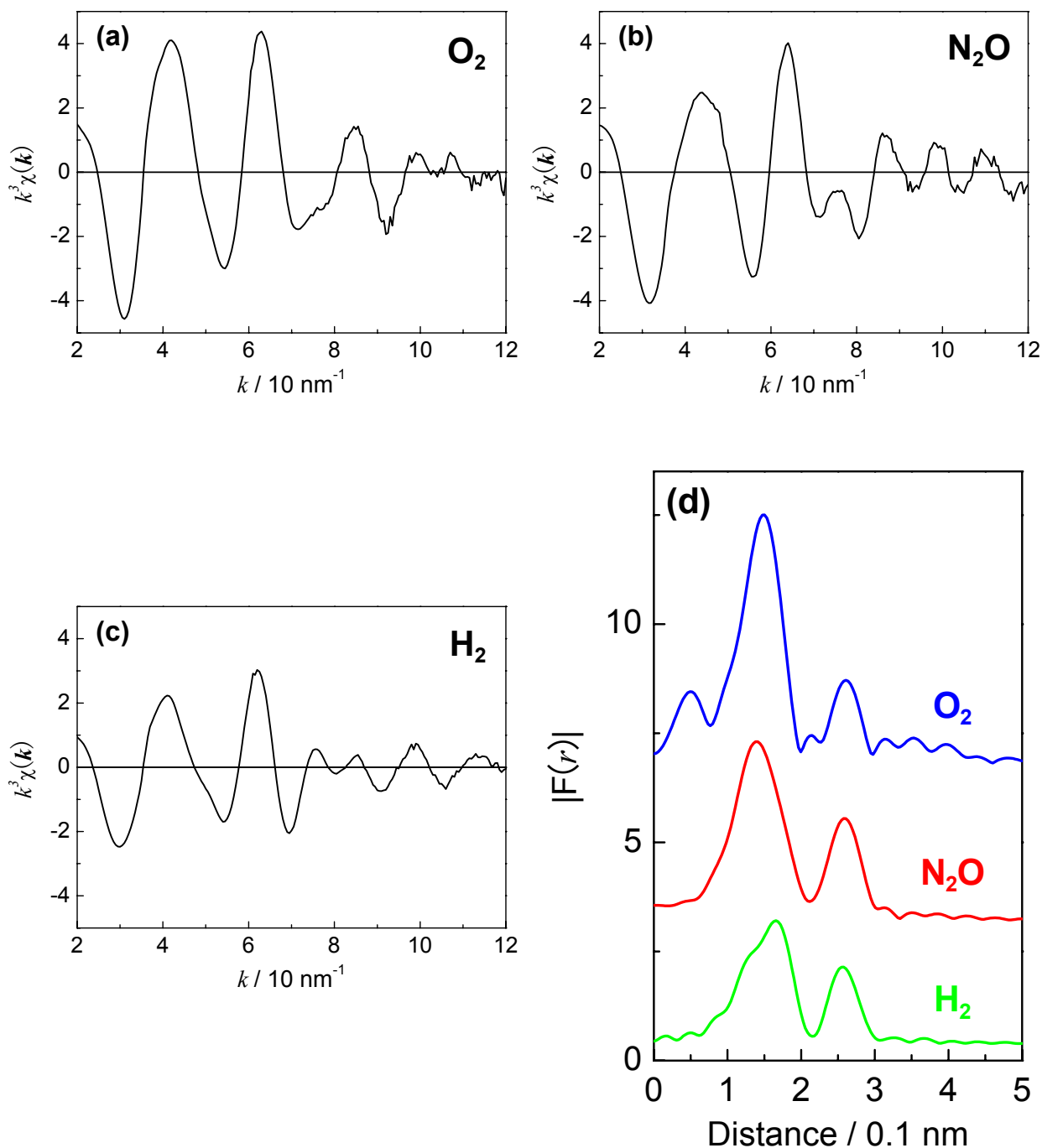
Figure 3-14. k^3-weighted Fe K-edge EXAFS for Fe(0.40)-MFI catalyst after treatments with (a) O$_2$, (b) N$_2$O, and (c) H$_2$. (d): Fourier transform of k^3-weighted Fe K-edge EXAFS for Fe(0.40)-MFI catalyst after treatments with O$_2$, N$_2$O, and H$_2$. Fourier transform range: 24-115 nm^{-1}.
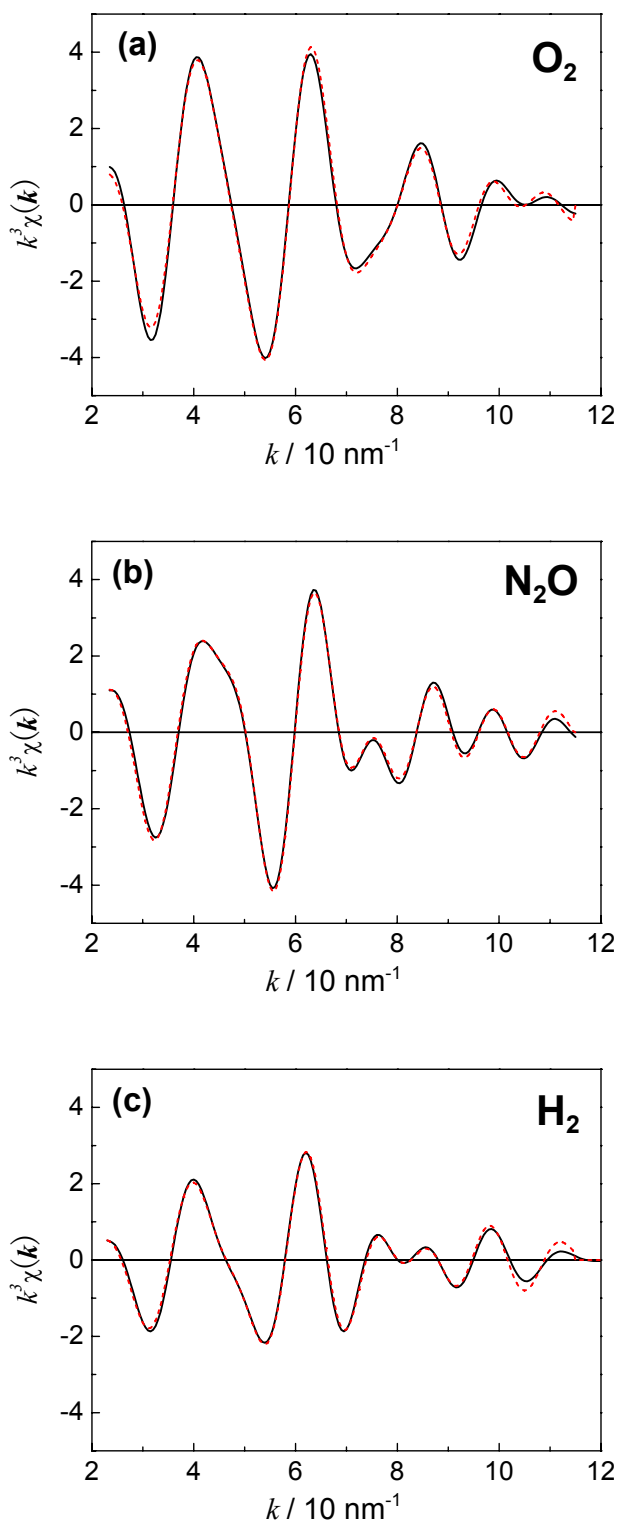
Figure 3-15. Fourier filtered EXAFS data (solid line) and calculated data (dotted line) of Fe(0.40)-MFI after treatments with (a) O_2, (b) N_2O, and (c) H_2. Fitting results are listed in Table 3-3.
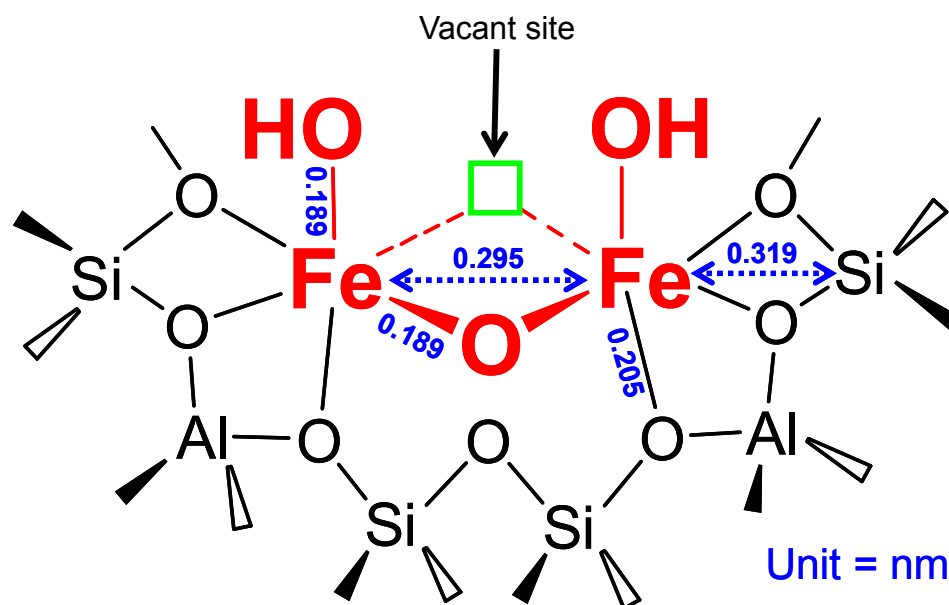
Vacant site

Figure 3-16. Proposed structure for binuclear Fe ion species in Fe-MFI catalyst.

Chapter 4

Reaction between N$_2$O and CH$_4$ over Fe-BEA catalyst: A possible role of nascent oxygen transients from N$_2$O

4.1. Introduction

Nitrous oxide (N$_2$O) has been long considered as a relatively harmless species and has suffered from a lack of interest from environmental scientists and engineers. However, during the last decade, a grown concern can be noticed since N$_2$O is a harmful gas in our environment, contributing to the greenhouse effect and the ozone layer depletion. Therefore, catalytic decomposition of N$_2$O [1, 2] and selective catalytic reduction (SCR) of N$_2$O with reductants such as hydrocarbons [3-9] have been proposed as the effective method of N$_2$O abatement. In particular, Kunimori's group has reported that Fe ion-exchanged BEA zeolite (Fe-BEA) catalysts are active at low temperatures (523 ~ 623 K) for the SCR of N$_2$O with CH$_4$ in the presence of excess O$_2$, although CH$_4$ is one of inactive molecules among hydrocarbons, and the oxidation of CH$_4$ by O$_2$ required high temperatures above 723 K over Fe-BEA catalyst [8, 9].

In general, oxygen species dissociated from N$_2$O have been considered to be reactive in some catalytic reaction systems. Lunsford and coworkers [10, 11] proposed the formation of reactive O$^-$ ions from N$_2$O in the partial oxidation of CH$_4$ by N$_2$O over supported molybdenum oxide catalysts. Panov *et al*. [12] found that active oxygen species (α-oxygen) were formed over Fe-ZSM-5 catalysts by N$_2$O treatment at 523 K. This α-oxygen, which was stable up to 573 K [13], readily reacted with benzene to produce phenol even at room temperature [14]. On the other hand, a different view of surface catalysis can be introduced because dynamic aspects are important to elucidate the reaction mechanism. In an NH$_3$ + N$_2$O reaction system, Au and Roberts [15] have addressed a role of short-lived oxygen transients (O$^{\delta-}$(s)) produced on a Mg (0001) surface. Here, the notation (s) refers to the surface transient species, *i.e.*, nascent oxygen just dissociated from N$_2$O, which has not yet been accommodated to the catalyst surface. Roberts and coworkers [16, 17] proposed that such "hot" oxygen transients may exhibit a high chemical reactivity which is district from thermally accommodated O(a) (*i.e.*, chemisorbed oxygen species). According to Roberts [17], the life time of O$^{\delta-}$(s) is the order of 10 ns, but may be

different depending on the catalytic system. For instance, Ertl [18] reported that the life time of hot O* adatoms was 0.3 ps for O_2 chemisorption on Pt(111).

In this chapter, an investigation between N_2O and CH_4 over Fe-BEA catalyst is given by using a pulse reaction technique, a temperature-programmed desorption (TPD), and an infrared (IR) spectroscopy. A possible role of nascent oxygen transients from N_2O in the reaction of N_2O with CH_4 over Fe-BEA catalyst is discussed.

4.2. Experimental

The BEA zeolite support (H-BEA; SiO_2/Al_2O_3 = 25) was supplied by Reference Catalyst committee, Catalysis Society of Japan (JRC-HB 25 (1)). Fe-BEA catalyst was prepared by ion-exchange with a dilute solution of $FeSO_4$ at 323 K for 20 h, and calcined for 3 h at 773 K [4, 7, 9]. The weight loading of Fe over BEA zeolite support was 1.6 wt%, which was determined by an ICP chemical analysis. All reactant gases were of high-purity chemical grade and were used without further purification. The pulse reaction experiments were performed in a microcatalytic pulse reactor [2]. A quartz tube reactor (ID, 4mm) was charged with 30 mg (Fe: 3.0 μmol) of the Fe-BEA catalyst, and it was treated in H_2 for 0.5 h at 723 K followed by O_2 treatment for 1 h at 773 K before measurement. Helium was used as a carrier gas at a flow rate of 55 cm³/min. A pulse of N_2O (0.26 μmol) and/or CH_4 (0.13 μmol) was injected by a switching valve. The effluent was analyzed in an on-line gas chromatograph system equipped with a TCD detector (Shimadzu GC-8A) and a differentially pumped quadrupole mass spectrometer (Balzers, QMS 200 F) [2]. TPD measurements in He flow were performed using 30 mg of the Fe-BEA catalyst. The analysis equipment used was reported previously [2]. The temperature was increased from room temperature to 1073 K at a constant heating rate of 10 K min⁻¹ and was kept at 1073 K for 20 min. In TPR experiment, the sample was heated in 5% H_2/Ar flow (30 cc min⁻¹) at a constant heating rate of 10 K min⁻¹, and H_2 consumption was monitored by TCD [20]. FT-IR spectra were recorded by a Nicolet Magna 550 spectrometer with a resolution of 4 cm⁻¹ (16 or 64 scans), using a quartz glass IR cell equipped with a sample holder, electric heater and KBr windows. The sample holder can be moved from the heater section to the window section in the IR cell. The sample for the IR measurements was prepared by pressing catalyst powder ground in an agate mortar into a wafer of *ca.* 16 mg cm⁻² (50 mg, 20 mm∅). A dehydrated sample was

prepared in the IR cell by outgassing a fresh sample at 523 K for 30 min, and then pretreated under 76 Torr of O_2 or N_2O at 773 K for 1h, followed by briefly pumping at room temperature. The IR experiments for the reaction of N_2O (10 Torr) + CH_4 (5 Torr) mixture and for the reaction of the surface species produced with N_2O (10 Torr) were performed in a static system. All IR measurements were carried out at room temperature. The base pressure of the vacuum line connecting to the IR cell was kept at lower than 10^{-5} Torr.

4.3. Results and discussions

4.3.1. Surface oxygen species in the N_2O + CH_4 reaction over Fe-BEA catalyst

Simultaneous pulsing of N_2O and CH_4 mixture and sequential pulsing of N_2O and CH_4 were performed over Fe-BEA catalyst at 473 ~ 773 K. The pulse experiment for direct N_2O decomposition was also carried out at 600 ~ 773 K. Figure 4-1 shows the conversion of N_2O or CH_4 as a function of reaction temperature. The activity in the N_2O + CH_4 system showed an extremely high N_2O conversion even at low temperatures (*e.g.*, at 573 K), whereas the activity in the direct N_2O decomposition showed a low N_2O conversion at 673 K. The result indicates that CH_4 plays an important role in the N_2O reduction. Figure 4-2 shows O_2-TPD spectra from the Fe-BEA catalyst after H_2 reduction at 723 K followed by exposure to O_2 or N_2O at 523 K for 1 h. After the O_2 treatment, O_2 starts to desorb above 793 K with a maximum occurring around 973 K. After N_2O treatment, however, new peaks appeared at lower temperatures (573 K ~ 873 K). The result suggests that extra O(a) species (O/Fe = 0.25), which are different from those by the O_2 treatment, exist over the N_2O-treated Fe-BEA catalyst. However, the CH_4 pulse experiment after the N_2O treatment (Fig. 4-1) showed that no products were detected at temperatures between 473 K and 623 K, and the CH_4 conversions were low even above 673 K. The results indicate that the O(a) species deriving from N_2O were not reactive with CH_4 at the low temperatures. Coexistence of N_2O and CH_4 in the gas phase is necessary for the high SCR activity at the low temperatures.

Panov and coworkers [13, 14] claimed that an O atom from N_2O molecule (*i.e.*, α-oxygen), which cannot be produced by O_2, readily reacted with CH_4 to produce CH_3OH over a Fe-ZSM5 catalyst even at room temperature. In our reaction system, however, the products were not CH_3OH but N_2, CO_2, and H_2O. This difference between the Fe-BEA and the Fe-ZSM-5

presumably derives from the preparation methods of the catalysts. Panov and coworkers [14] prepared the Fe-ZSM-5 zeolite by hydrothermal synthesis with the addition of iron as FeCl$_3$ to an initial gel. The Fe-ZSM-5 was transferred to the NH$_4$-form by exchange with an ammonia buffer and then calcined at 823 K in air [14]. Additional calcination at 1173 K was performed to increase the concentration of the active α-sites [14]. The calcination at the high temperature seems to be essential for the formation of the α-oxygen species [13, 14]. Therefore, state and/or structure of the Fe ion species may be quite different from those of our Fe-BEA catalyst by the ion exchange method.

4.3.2. IR measurements of OH groups over Fe-BEA zeolite catalyst

Figure 4-3 shows IR spectra in the hydroxyl stretching (v_{OH}) region of the Fe-BEA catalyst after O$_2$ or N$_2$O pretreatment. Five peaks (3781, 3745, 3683, 3664 and 3605 cm^{-1}) were observed over the catalyst. The peaks at 3781, 3745, 3664 and 3605 cm^{-1} were also observed over the H-BEA zeolite support (Fig. 4-3(a)). Therefore, these peaks at 3745, 3664 and 3605 cm^{-1} were assigned to the terminal silanols (external Si-OH), OH groups associated with extra-framework aluminum and bridging OH groups (*i.e.*, Brønsted acidic site) of BEA zeolite, respectively [21-23]. The 3781 cm^{-1} band has already been assigned to a hydroxyl group attached to a tricoordinated aluminum atom linked to the network *via* two oxygen bonds [21, 23]. The Fe-BEA catalyst shows a new band at 3683 cm^{-1}, which can be assigned to the OH group on Fe ion species. Mauvezin *et al*. [24] reported in IR study of an Fe-BEA catalyst that a band at 3670 cm^{-1} appeared after treatment in O$_2$ and N$_2$O but did not exist after H$_2$ treatment. They suggested that this band likely corresponds to OH groups on Fe^{III} species based on DFT calculations of small iron-hydroxoclusters [24]. Although the peak position is a little different from 3683 cm^{-1} of our sample, similar behavior after H$_2$ reduction was observed, as shown below.

Figure 4-4 shows the IR spectra in the v_{OH} region of Fe-BEA during the H$_2$ treatment. After O$_2$ treatment, the Fe-BEA sample was exposed to H$_2$ (40 Torr) at room temperature and heated stepwise up to 723 K. As shown in Fig. 4-4(b)-(e), the peak at 3683 cm^{-1} significantly decreased with increasing the temperature of H$_2$ treatment, while other peaks hardly changed. The reduction of the OH peak started above 523 K, and seemed to be almost complete at 723 K. At this time, the band at 1623 cm^{-1} (not shown), which derived from bending mode of H$_2$O(a),

was also observed. Therefore, the broad OH band at around 3673 cm^{-1} was perturbed by $H_2O(a)$. As shown in Fig. 4-4 (f and g), the peak at 3683 cm^{-1} hardly restored after removal of $H_2O(a)$ by the evacuation at 523 K, while the peak readily restored up to its original intensity after the O_2 treatment at 523 K. Figure 4-5 shows TPR profile of the Fe-BEA catalyst. The reduction of Fe ion species started at around 523 K, and showed a broad profile with the peak maximum at 673 K, which was assigned to the reduction of Fe^{3+} ion species to Fe^{2+} ion species [20, 24, 25]. The amount of H_2 consumed (H_2/Fe ratio) was 0.497, which is consistent with the reduction of Fe^{3+} to Fe^{2+}. The decrease in intensity of the peak at 3683 cm^{-1} correlated well with the TPR profile of Fe ion species. This result suggests that the decrease and the increase in intensity of the OH band at 3683 cm^{-1} derives from the redox of Fe ion species (*i.e.*, $Fe^{3+} \leftrightarrow Fe^{2+}$) over the Fe-BEA catalyst.

Many works have been done to elucidate the structure of Fe ion species in Fe-zeolite (MFI, BEA) catalyst system [24-28]. For Fe-MFI catalysts the formation of oxygen bridged Fe dimers was proposed and confirmed by XAFS data [26, 27]. Mauvezin *et al*. [24] claimed that Fe is mainly present as binuclear oxocations of the type $[(OH)FeOFe(OH)]^{2+}$ in an Fe-BEA catalyst system. Jia *et al*. [28] proposed a following reaction ($Fe^{3+} \rightarrow Fe^{2+}$) by H_2 treatment of an Fe-MFI catalyst:

$$[HO\text{-}Fe\text{-}O\text{-}Fe\text{-}OH]^{2+} + H_2 \rightarrow [Fe\text{-}O\text{-}Fe]^{2+} + 2H_2O. \qquad (1)$$

A reverse reaction ($Fe^{3+} \leftarrow Fe^{2+}$) would occur by O_2 or N_2O treatment, because it would be generally assumed that water is present in zeolite material system. The behaviors of the IR peak at 3683 cm^{-1} in Figs. 4-3 and 4-4 are consistent with the redox reaction of the binuclear Fe oxocations. From the result of EXAFS study, the peak at 3683 cm^{-1} have been assigned to the OH species over mononuclear and binuclear Fe ion species [29].

As shown in Fig. 4-3, the intensity of the peak at 3683 cm^{-1} is larger than the decrease in the intensities of the OH peaks at 3605 cm^{-1} and at 3664 cm^{-1} when Fe was ion-exchanged in the H-BEA support. Although a quantitative analysis of the IR bands is difficult at present, the amount of the Fe-OH site is at least comparable to those of the OH bands on the catalyst.

4.3.3. Reactivity of the Fe-OH sites in the N_2O + CH_4 mixture

In order to investigate the reactivity of the Fe-OH sites over the Fe-BEA in the reaction between N_2O and CH_4, the IR measurements were carried out under the CH_4 alone or N_2O + CH_4 mixture system. Figure 4-6 shows the IR spectra in the 4000-3500 cm^{-1} region of the Fe-BEA catalyst, which was exposed to CH_4 alone. No decrease in the intensity of the peak at 3683 cm^{-1} was observed up to 623 K, indicating that there was no reactivity of the Fe-OH sites with CH_4 only. Figure 4-7 shows the IR spectra in the 4000-2800 cm^{-1} region of the Fe-BEA catalyst, which was exposed to the N_2O + CH_4 mixture at room temperature and heated stepwise up to 523 K. As shown in Fig. 4-7(A) and (B), raising the temperature to 473 K led to a decrease of the Fe-OH site (3683 cm^{-1}) and simultaneously to the appearance of new bands at 2969, 2919, and 2826 cm^{-1}, while other IR bands of OH groups over the Fe-BEA were hardly affected by this reaction. These new bands at 2969, 2920, 2853, and 2825 cm^{-1} could be assigned to the ν_{CH} of produced adsorbed species such as $CH_xO_y(a)$ resulting from the partial oxidation of CH_4 [30-35]. Jung and Bell [32] reported in an IR study of a ZrO_2 catalyst that the bands due to methoxide group were observed at 2923 and 2817 cm^{-1}. Jung and Bell [33] also reported in the study of a Cu/ZrO_2 catalyst that the bands at 2927 and 2821 cm^{-1} were assigned to methoxide species, while Wu *et al*. [34] reported that a stronger band at 2970 cm^{-1} was assigned to formate species. In fact, I have studied adsorption of methanol on the catalyst (shown in chapter 5, §5.3.3), and confirmed that the new peaks at 2920 and 2825 cm^{-1} are assigned to adsorbed methoxy species on Fe ions (Fe-OCH$_3$) and that the 2969 and 2853 cm^{-1} peaks are assigned to formate species (Fe-OOCH). In the reaction temperature at 523 K (Fig. 4-7(A), e), the OH groups exhibited broad bands at around 3673 and 3569 cm^{-1}, which were perturbed by adsorbed water as products in the N_2O + CH_4 reaction. It should be noted that no peaks were observed in the CH stretching band region when CH_4 only was exposed to the catalyst (Fig. 4-6, not shown).

Figure 4-8 shows the IR spectra in the 4000-2800 cm^{-1} region of Fe-BEA after the N_2O + CH_4 reaction at 523 K for 0.5 h followed by evacuation at 523 K for 15 min. The bands of the acid-bridged OH (3605 cm^{-1}) and other OH groups of BEA zeolite were restored completely to their original intensities after removal of the adsorbed water by the evacuation at 523 K, while the OH band of an Fe ion species (3683 cm^{-1}) was not restored. The bands at 2969, 2920, 2853, and 2825 cm^{-1} were hardly changed. The sample after the evacuation at 523 K was exposed to

N$_2$O at room temperature and heated stepwise up to 573 K. It should be noted that there was no difference in the IR spectra between before and after the introduction of N$_2$O to the treated sample at room temperature. As shown in Fig. 4-8, however, raising the temperature to 473 K led to decrease of ν_{CH} region peaks (2969, 2920, 2853, and 2825 cm^{-1}) and increase of the peak at 3683 cm^{-1} up to its original intensity. These results indicate that the reaction of the surface methoxy and formate species with N$_2$O leads to regeneration of the Fe-OH sites.

4.3.4. Possible reaction mechanism in the reaction between N₂O and CH₄

In this study, it was found that the oxidation of CH$_4$ by N$_2$O in the N$_2$O + CH$_4$ mixture readily proceeded over the Fe-BEA catalyst even at the low temperatures (473 K ~ 673 K). On the other hand, the oxidation of CH$_4$ by O$_2$ over the Fe-BEA catalyst required higher temperatures (above 723 K) [8, 9]. Although the extra O(a) species resulting from the N$_2$O treatment was observed at *ca.* 873 K by the O$_2$-TPD measurements, the CH$_4$-pulsed experiment after the N$_2$O treatment showed that the reactivity of the extra adsorbed O(a) species with CH$_4$ was very low even at 623 K. In accordance with the results of the pulsed experiments, the IR study showed that the Fe-OH sites did not react with CH$_4$ only, but reacted with CH$_4$ when the N$_2$O + CH$_4$ mixture was exposed to the catalyst. The methoxy and formate species, which were formed only in the N$_2$O + CH$_4$ mixture above 423 K, readily reacted with N$_2$O even at low temperatures (~473 K; Fig. 4-8), and at the same time the Fe-OH sites were restored. These results, including the redox behavior of the IR band at 3683 cm^{-1}, suggest that the Fe ion species are the active sites for the N$_2$O + CH$_4$ reaction.

In this study, I have found that the coexistence of both N$_2$O and CH$_4$ is needed for the reaction at the low temperatures. One possible explanation may be that the concentration of real high-active Fe sites is small, for example, compared with the amount (O/Fe = 0.25, 1.7 μmol as O atom) of the extra O(a) produced by N$_2$O treatment. In such a condition, a small fraction of the Fe ion sites should be utilized repeatedly during the CH$_4$ oxidation by N$_2$O, and the coexistence of N$_2$O + CH$_4$ is necessary for the supply of active O(a) species from N$_2$O in order to attain the observable CH$_4$ conversion. However, this view point can not be reconciled with the behavior of the Fe-OH sites both in the reaction of the N$_2$O + CH$_4$ mixture and in the reaction of the methoxy and formate species with N$_2$O. Most of the Fe-OH sites appeared to take part in the

reaction (Figs. 4-7 and 4-8).

As an alternative explanation, a different view of surface catalysis can be introduced because dynamics aspects are important to elucidate the reaction mechanism [15-18, 20, 36]. In an $NH_3 + N_2O$ reaction system, Au and Roberts [15] have addressed a role of short-lived oxygen transients, *e.g.*, $O^{\delta-}(s)$ species produced on a Mg(0001) surface:

$$N_2O(g) \rightarrow N_2(g) + O^{\delta-}(s) \tag{2}$$

$$NH_3(a) + O^{\delta-}(s) \rightarrow NH_2(a) + OH(a). \tag{3}$$

Here, the notation (a) refers to an adsorbed species in its final chemisorbed state, while (s) refers to the surface transient species, *i.e.*, nascent oxygen just produced from N_2O, which has not yet been accommodated to the catalyst surface [15-17]. Roberts proposed that such "hot" oxygen transients may exhibit a high chemical reactivity which is distinct from thermally accommodated O(a) , and this view has been expanded to some catalytic systems of NH_3 and dioxygen, CH_3OH and dioxygen, and so on [16, 17]. An important role of nascent oxygen has also been proposed in N_2O decomposition on Rh catalysts [2]. According to Roberts [17], the life time of $O^{\delta-}(s)$ is the order of 10 ns, but may be different depending on the catalytic system (for O_2/Pt(111), the life time of hot O* adatoms was 0.3 ps [Ref. 18]).

A similar mechanism can be adapted for the reaction between N_2O and CH_4 over this Fe-BEA catalyst system. According to this view, the extra O(a) produced by N_2O treatment (Fig. 4-2(b)) is not reactive with CH_4, because the adsorbed oxygen species are accommodated thermally. I think that nascent oxygen transients (O*(a)), which are formed from N_2O dissociation over binuclear Fe site and diffuse on the catalyst surface, may play an important role in the activation/oxidation of CH_4 at initial steps to form methoxy species. For instance, following plausible reactions are considered at initial steps:

$$N_2O \rightarrow N_2 + O^*(a) \tag{4}$$

$$\tag{5}$$
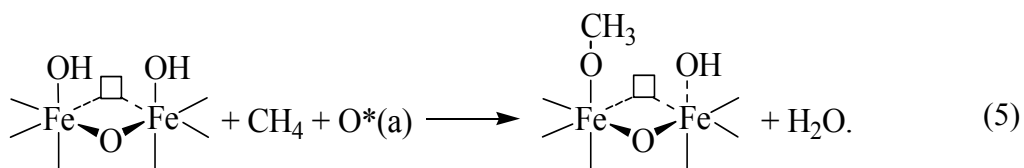
Further partial oxidation of methoxide species may lead to the formation of formate species (Fe-OOCH). Because methoxy species readily reacted with N_2O at *ca.* 473 K, accompanying with the regeneration of the Fe-OH sites, for instance, the following reaction is considered:

$$>Fe\overset{O}{\underset{O}{<}}Fe< \ + 3N_2O \longrightarrow \ >Fe\overset{O}{\underset{O}{<}}Fe< \ + CO_2 + H_2O + 3N_2 \ . \quad (6)$$
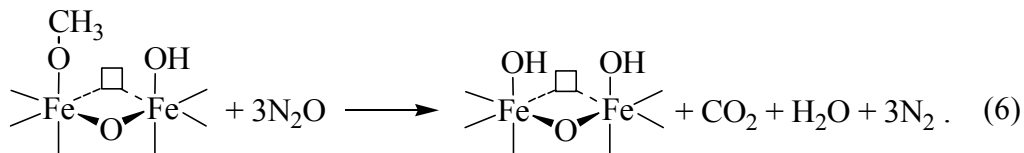
In this case, the overall reactions ((4) ~ (6)) are expressed as follows:

$$4N_2O + CH_4 \rightarrow 4N_2 + CO_2 + 2H_2O. \quad (7)$$

4.4. Conclusions

CH$_4$ reacted readily with N_2O above 473 K when the N_2O + CH$_4$ mixture was exposed to the Fe-BEA catalyst. The O_2-TPD peak was observed above 873 K after the O_2 treatment, while a new desorption peak was appeared at lower temperatures after the N_2O treatment. However, the reactivity of the extra O(a) species with CH$_4$ pulse was very low even at 623 K. The IR band at 3683 cm^{-1} was attributed to the Fe-OH sites assigned to binuclear Fe oxocations. The reduction behavior (Fe^{3+} → Fe^{2+}) of the Fe-OH peak was consistent with the H$_2$-TPR profile. The IR study showed that the Fe-OH sites did not react with CH$_4$ only, but readily reacted with CH$_4$ above 423 K when the N_2O + CH$_4$ mixture was exposed to the catalyst, accompanying with the formation of intermediate species such as Fe-OCH$_3$. The intermediate species reacted with N_2O, accompanying with the regeneration of the Fe-OH sites. A possible role of short-lived oxygen transients (O*(a)), which are formed from N_2O dissociation, was proposed for the activation of CH$_4$.

References

[1] F. Kapteijn, J. Rodriguez-Mirasol, J.A. Moulijn, *Appl. Catal. B* **9** (1996) 25.

[2] S. Tanaka, K. Yuzaki, S. Ito, S. Kameoka, K. Kunimori, *J. Catal.* **200** (2001) 203.

[3] Y. Li, J.N. Armor, *Appl. Catal. B* **3** (1993) 55.

[4] C. Pophal, T. Yogo, K. Yamada, K. Segawa, *Appl. Catal. B* **16** (1998) 177.

[5] M. Kögel, R. Mönnig, W. Schwieger, A. Tissler, T. Turek, *J. Catal.* **182** (1999) 470.

[6] G. Centi, F. Vazzana, *Catal. Today* **53** (1999) 683.

[7] S. Kameoka, K. Yuzaki, T. Takeda, S. Tanaka, S. Ito, T. Miyadera, K. Kunimori, *Phys. Chem. Chem. Phys.* **3** (2001) 256.

[8] S. Kameoka, T. Suzuki, K. Yuzaki, T. Takeda, S. Tanaka, S. Ito, T. Miyadera, K. Kunimori, *Chem. Commun.* (2000) 745.

[9] S. Kameoka, K. Kita, T. Takeda, S. Tanaka, S. Ito, K. Yuzaki, T. Miyadera, K. Kunimori, *Catal. Lett.* **69** (2000) 169.

[10] R.-S. Liu, M. Iwamoto, J.H. Lunsford, *J. Chem. Soc., Chem. Commun.* (1982) 78.

[11] H.-F. Liu, R.-S. Liu, K.Y. Liew, R.E. Johnson, J.H. Lunsford, *J. Am. Chem. Soc.* **106** (1984) 4117.

[12] G.I. Panov, V.I. Sobolev, A.S. Kharitonov *J. Mol. Catal.* **61** (1990) 85.

[13] G.I. Panov, A.K. Uriarte, M.A. Rodkin, V.I. Sobolev, *Catal. Today* **41** (1998) 365.

[14] K.A. Dubkov, V.I. Sobolev, G.I. Panov, *Kinet. Catal.* **39** (1998) 72.

[15] C.T. Au, M. W. Roberts, *Nature* **319** (1986) 206.

[16] A.F. Carley, P. R. Davies, M. W. Roberts, *Catal. Lett.* **80** (2002) 25.

[17] M.W. Roberts, *Chem. Soc. Rev.* **25** (1996) 437.

[18] G. Ertl. *Adv. Catal.* **45** (2000) 1.

[19] W.N. Delgass, R.L. Garten, M. Boudart, *J. Chem. Phys.* **50** (1969) 4603.

[20] T. Nobukawa, K. Kita, S. Tanaka, S. Ito, T. Miyadera, S. Kameoka, K. Tomishige, K. Kunimori, *Stud. Surf. Sci. Catal.* **142** (2002) 557.

[21] C. Jia, P. Massiani, D. Barthomeuf, *J. Chem. Soc., Faraday Trans.* **89** (1993) 3659.

[22] I. Kiricsi, C. Flego, G. Pazzuconi, W.O. Parker, Jr., R. Millini, C. Perego, G. Bellussi, *J. Phys. Chem.* **98** (1994) 4627.

[23] A. Vimont, F. Thibault-Starzyk, J.C. Lavalley, *J. Phys. Chem. B* **104** (2000) 286.

[24] M. Mauvezin, G. Delahay, B. Coq, S. Kieger, J.C. Jumas, J. Olivier-Fourcade, *J. Phys. Chem. B* **105** (2001) 928.

[25] H-Y. Chen, W.M.H. Sachtler, *Catal. Today* **42** (1998) 73.

[26] P. Marturano, L. Drozdová, A. Kogelbauer, R. Prins, *J. Catal.* **192** (2000) 236.

[27] A.A. Battiston, J.H. Bitter, D.C. Koningsberger, *Catal. Lett.* **66** (2000) 75.

[28] J. Jia, B. Wen, W.M.H. Sachtler, *J. Catal.* **210** (2002) 453.

[29] T. Nobukawa, M. Yoshida, K. Okumura, K. Tomishige, K. Kunimori, *J. Catal.* **229** (2005) 374.

[30] L.H. Little, *Infrared Spectra of Adsorbed Species*, Academic Press, New York/London, (1966).

[31] A.A. Davydov, *Infrared Spectroscopy of Adsorbed Species on the Surface of Transition Metal Oxides*, John Wiley & Sons, Chichester, (1990).

[32] K.T. Jung, A.T. Bell, *J. Catal.* **204** (2001) 339.

[33] K.D. Jung, A.T. Bell, *J. Catal.* **193** (2000) 207.

[34] G. Wu, X. Chen, Y. Sun, *The Proc. of 17th North American Catalysis Society Meeting (2001, Toronto, Ontario, Canada), PS1 (Natural Gas Conversion and Related Topics), No.12*.

[35] S. Kameoka, K. Kita, S. Tanaka. T. Nobukawa, S. Ito, K. Tomishige, T. Miyadera, K. Kunimori, *Catal. Lett.* **79** (2002) 63.

[36] T. Nobukawa, S. Tanaka, S. Ito, K. Tomishige, S. Kameoka, K. Kunimori, *Catal. Lett.* **83** (2002) 5.
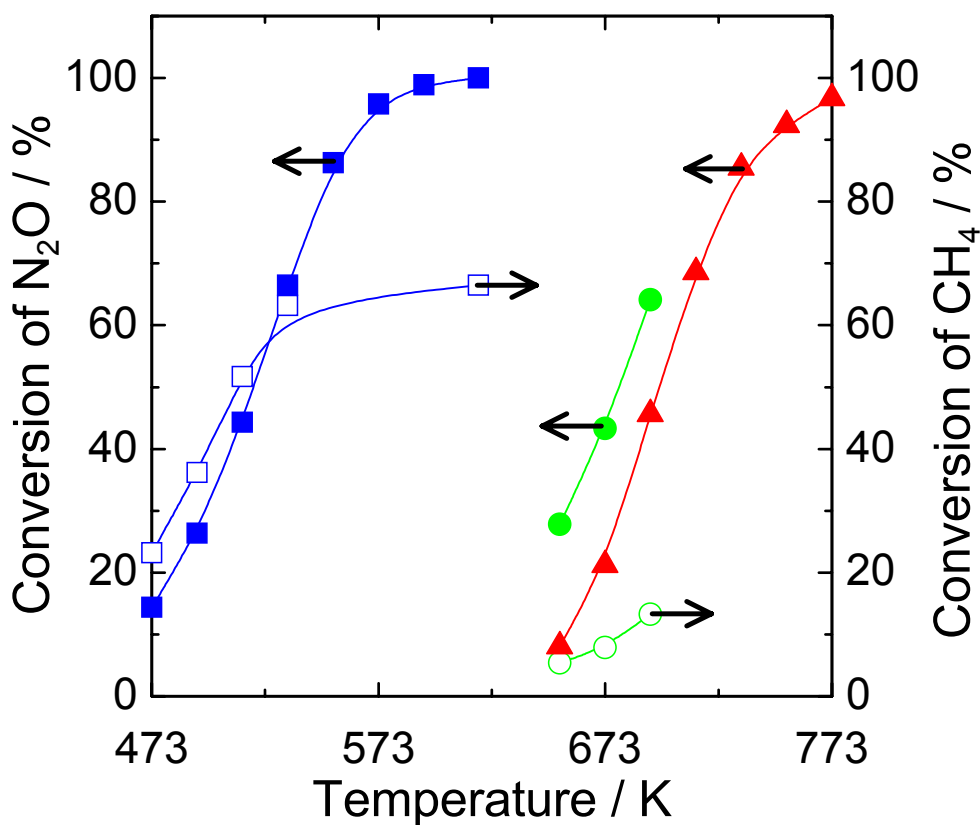
Figure 4-1. Reaction temperature dependence of N_2O and CH_4 conversion over Fe-BEA catalyst. Closed symbol: N_2O conversion, open symbol: CH_4 conversion. (▲): direct N_2O decomposition; (■, □): $N_2O + CH_4$ mixture (SCR); (○): CH_4 pulse after N_2O treatment; (●): N_2O pulse after CH_4 pulse.
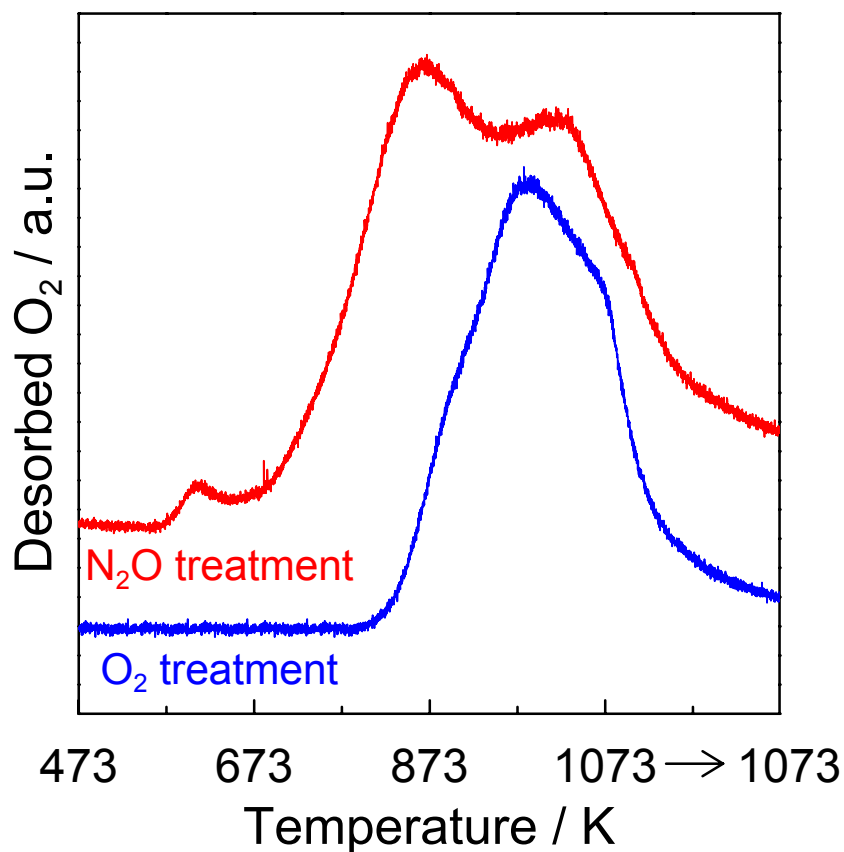
Figure 4-2. O$_2$-TPD profiles from Fe-BEA catalyst after O$_2$ or N$_2$O pretreatment.
Reaction conditions: He flow = 55 cm^3/min, temperature = 300-1073 K (10 K/min), and 0.1 MPa.
Pretreatment: 100 % O$_2$, 773 K, 1 h; 10 % N$_2$O, 523 K 1 h.
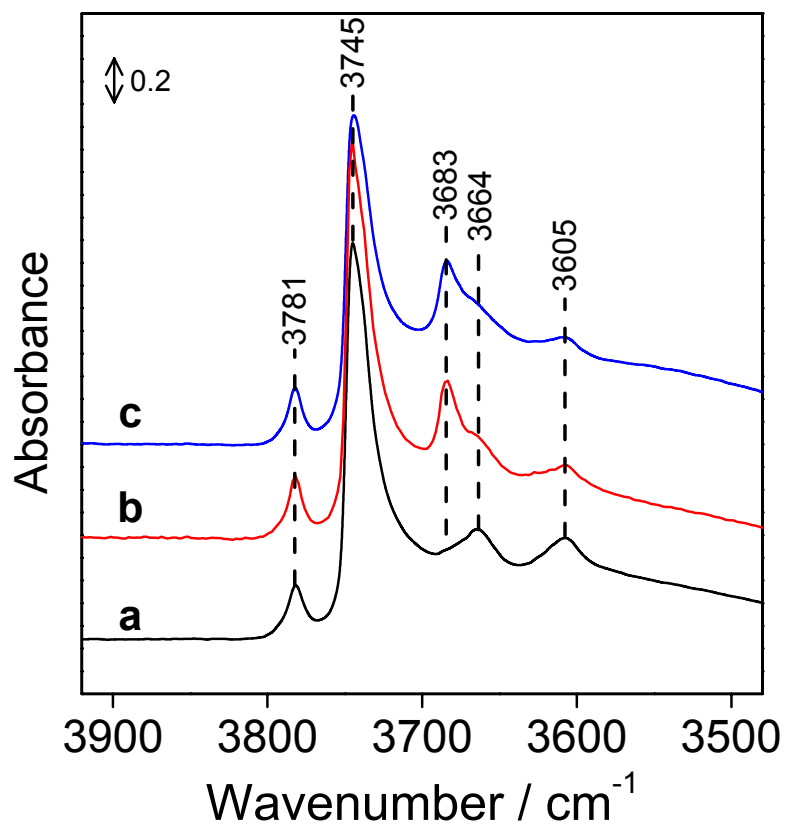
Figure 4-3. IR spectra of the OH stretching bands over Fe-BEA catalyst after different pretreatments followed by evacuation at room temperature for 15 min. (a) H-BEA (without Fe ion) after O_2 pretreatment, (b) after N_2O pretreatment and (c) after O_2 pretreatment.
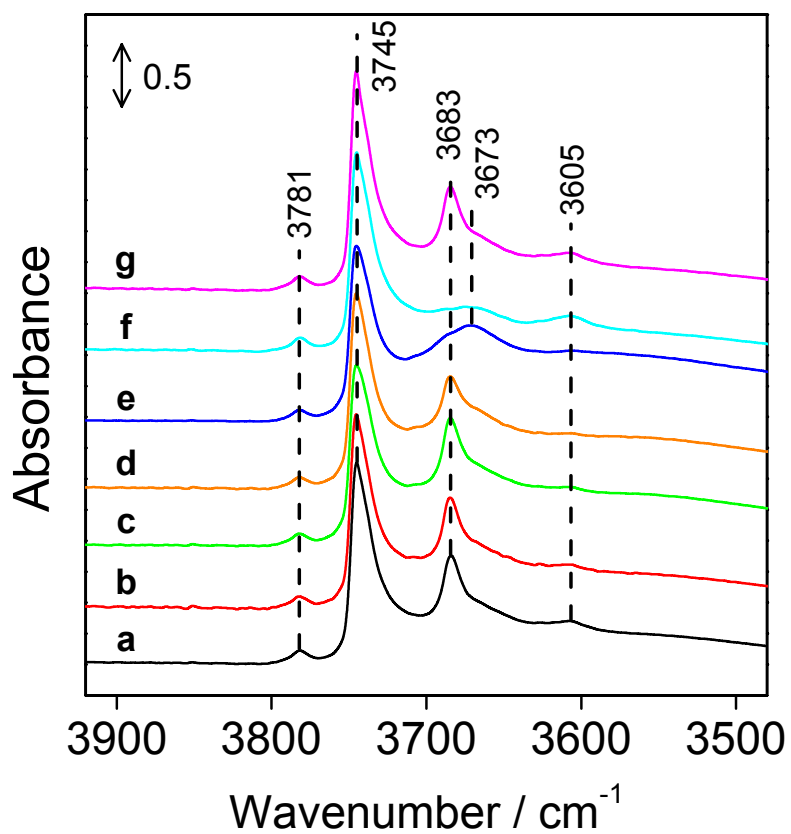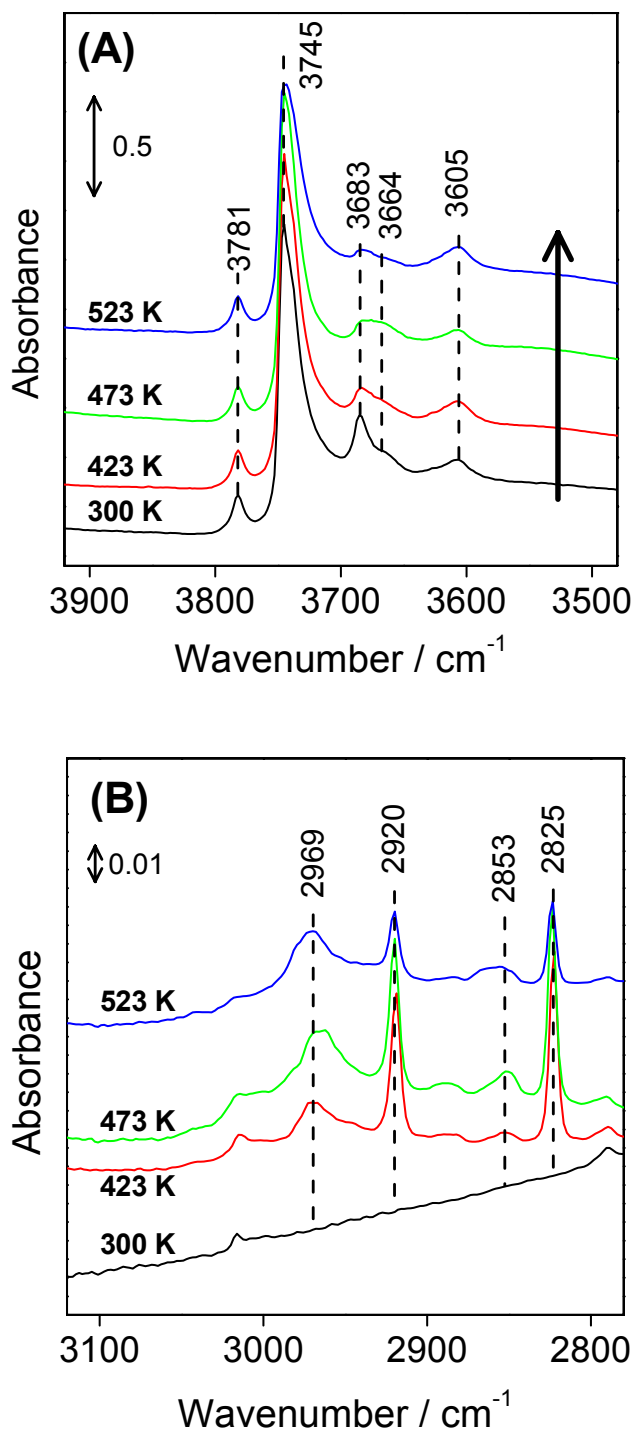
Figure 4-4. IR spectra of the OH stretching bands over Fe-BEA catalyst: (a) after O_2 treatment at 773 K; and during H_2 (40 Torr) treatment at the following temperature: (b) 300 K, (c) 523 K, (d) 623 K, (e) 723 K, followed by (f) evacuation at 523 K and (g) O_2 treatment at 523 K.
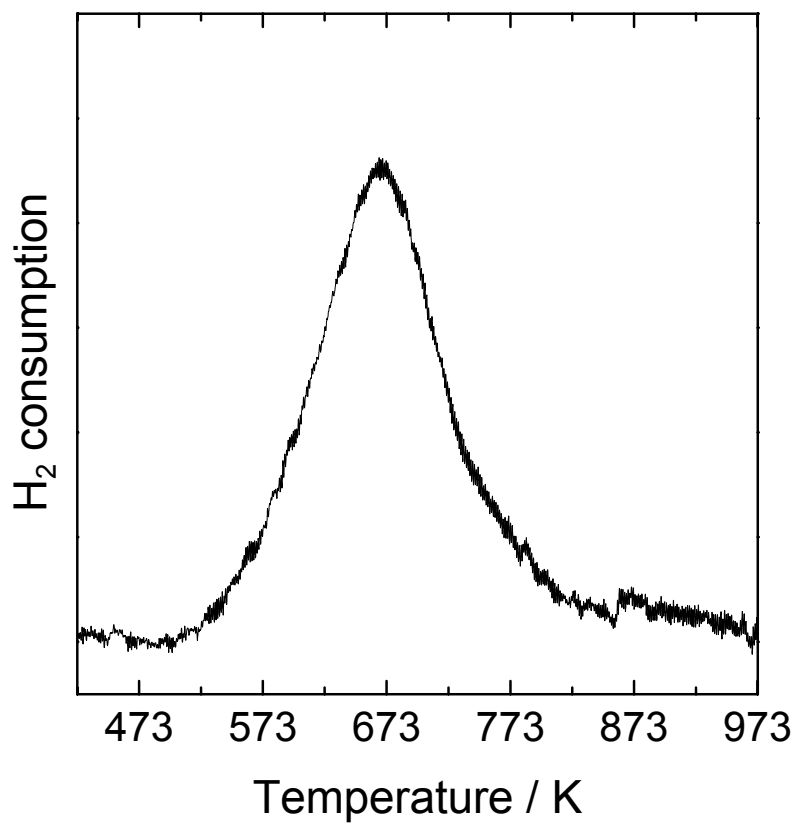
Figure 4-5. H_2 - TPR spectrum of Fe-BEA catalyst after O_2 treatment at 773 K.
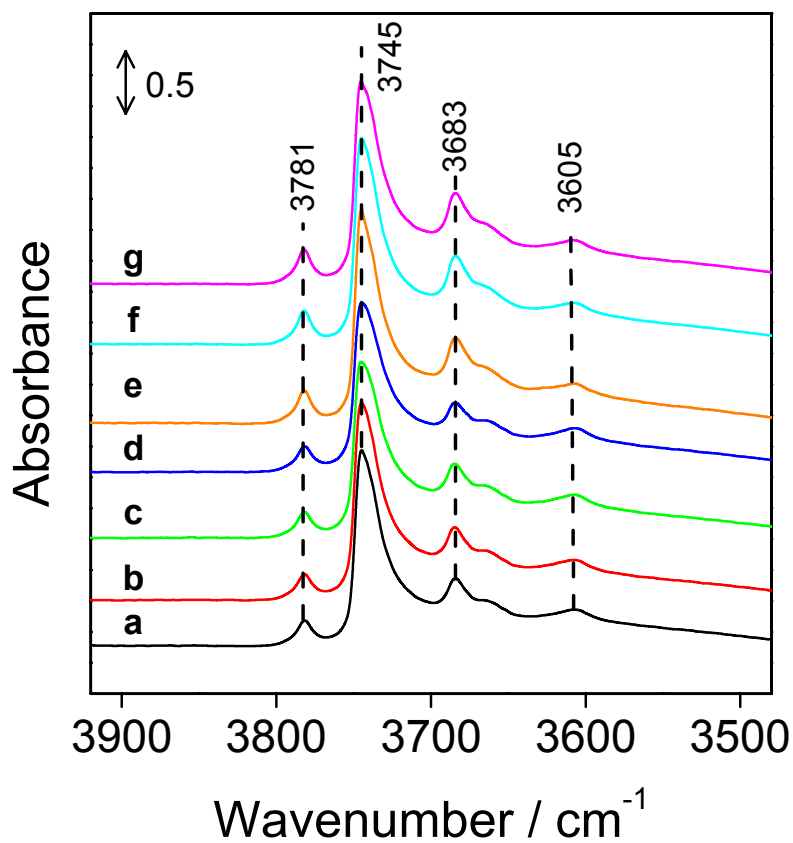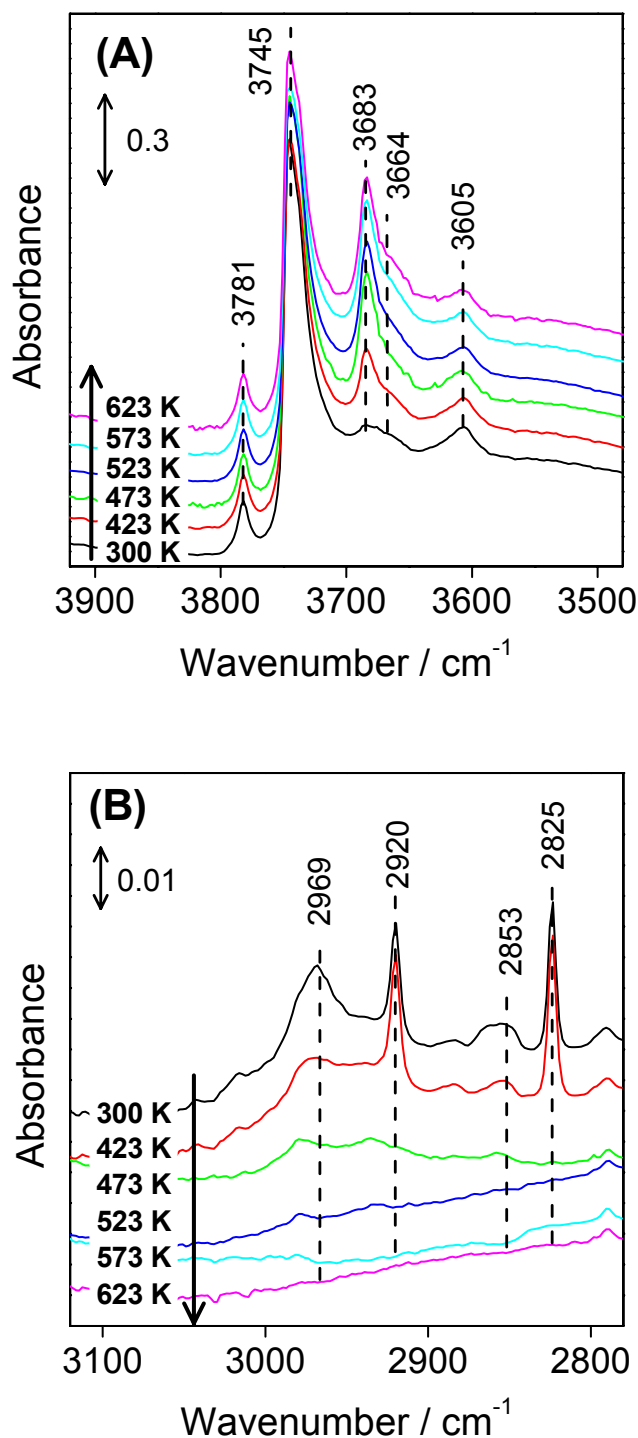
Figure 4-6. IR spectra of the OH stretching bands in CH_4 alone (5 Torr): (a) after O_2 treatment at 773 K, (b) CH_4 at 423 K, (c) CH_4 at 523 K, (d) CH_4 at 623 K; and (e) after N_2O treatment at 773 K, (f) CH_4 at 423 K, (g) CH_4 at 523 K.

Figure 4-7. FTIR spectra in the OH stretching band (A) and the CH stretching band (B) regions of the reaction of N_2O with CH_4 over Fe-BEA catalyst.

Reaction conditions: N_2O (1.3 kPa) + CH_4 (0.67 kPa), total pressure = 2.0 kPa, reaction temperature = 300-523 K. Evacuation was carried out after reaction at 523 K. Pretreatment: O_2, 10 kPa, 773 K, 1 h.

Figure 4-8. FT-IR spectra in the OH stretching band (A) and the CH stretching band (B) regions of the reaction of the intermediate species with N₂O over Fe-BEA catalyst.

Reaction conditions: $N_2O = 1.3 kPa$, reaction temperature = 300-623 K.

Pretreatment: N_2O (1.3 kPa) + CH_4 (0.67 kPa), 523 K, 1 h. Evacuation was carried out after pretreatment.

Chapter 6

Role of active oxygen transients for CH_4 activation in $CH_4 + N_2O$ reaction over Fe-MFI catalyst

6.1. Introduction

Nitrous oxide (N_2O) contributes to the greenhouse-effect, a phenomenon caused by strong absorbance of infrared radiation in the atmosphere. The global warming potential (GWP) per molecule of N_2O is about 300 times as high as that of carbon dioxide [1]. According to Intergovernmental Panel on Climate Change (IPCC) report, the atmospheric burden of N_2O continues to increase by about 0.25%/yr [2]. Furthermore, N_2O also takes part in the destruction of the stratospheric ozone layer. From an environmental point of view, therefore, the catalytic decomposition of N_2O ($N_2O \rightarrow N_2 + 1/2O_2$) and the selective catalytic reduction (SCR) of N_2O with reductant have been attracting much attention [3-26].

The SCR of N_2O with CH_4 in excess oxygen [20-26] is promising in terms of the cost, and the reaction is also interesting from the view point of the activation of methane, which has generally low reactivity compared with other reductants. I have reported that the $CH_4 + N_2O$ reaction in excess oxygen started at about 500 K over Fe-MFI and Fe-BEA catalysts, while the oxidation of CH_4 with O_2 required high temperatures above 723 K over these Fe-zeolite catalysts [20, 25, 26]. This indicates that N_2O is essential for the activation of methane, which is related to selective reaction between CH_4 and N_2O. From the view point of the selectivity, CH_4 is a more efficient reductant than C_2H_6 and C_3H_6 [26]. Furthermore, the reaction rate of N_2O reduction with CH_4 is higher than that of H_2 and CO over Fe-MFI [26].

In general, oxygen species dissociated from N_2O have been considered to be reactive in some catalytic reaction systems. Lunsford and coworkers [27] have proposed the formation of reactive O^- ions from N_2O in the partial oxidation of CH_4 by N_2O over supported molybdenum oxide catalysts. Panov *et al.* [28] have found that active oxygen species (α-oxygen) were formed over Fe-ZSM-5 catalysts by N_2O treatment at 523 K after the activation in vacuum at high temperature. The α-oxygen, which was stable up to 573 K [29], readily reacted with benzene (or CH_4) to produce phenol (or CH_3OH) even at room temperature [29, 30]. As shown in Figs. 2-5

and 4-2, Fe-zeolite (BEA and MFI) catalysts after O_2 treatment at 773 K, oxygen species can be deposited on the catalysts by N_2O treatment at 523 K. However, no reaction was observed, when CH_4 gas was exposed to the treated catalysts, as shown in Fig. 4-6 [23, 25, 31]. In contrast, simultaneous exposure of N_2O and CH_4 to Fe-zeolite after O_2 treatment at 773 K drastically promoted the reaction between CH_4 and N_2O. Therefore, I have proposed that nascent oxygen transients (O*(a)) from N_2O dissociation before accommodation on stable adsorption sites can play an important role in activation and oxidation of CH_4 [23-25]. Here, notation "(a)" refers to an adsorbed species, while "*" refers to a transient state, *i.e.*, O*(a) has not yet been thermally accommodated to the catalyst surface. The existence of short-lived oxygen (O*(a)) is also supported by the results of $C_3H_8 + N_2O$ reaction using temporal analysis of products (TAP) [32].

I have also reported that the activity of Fe-MFI catalysts in N_2O reduction with CH_4 was dependent on Fe content [25, 26]. From the results of EXAFS and pulse reaction experiments, the catalytically active sites are found to be binuclear Fe species [25, 26]. Several groups have also proposed that the binuclear Fe species are active in the NO + hydrocarbon system [33-35]. During the study, I have found that N_2O treatment of the catalyst after H_2 reduction at 773 K gave sharp O_2 and NO desorption peaks at a low temperature (around 610 K). Similar desorption peaks on the sample treated under various conditions have also been observed by other groups [35-40]. Kiwi-Minsker group has reported the formation of surface oxygen and adsorbed NO during N_2O decomposition over low Fe content after steaming and high-temperature calcinations in inert atmosphere [38-40]. Roy and Pirngruber [41] have also reported that the oxygen species, which are formed after high-temperature treatment in H_2 or He followed by N_2O treatment, increased the activity of N_2O decomposition. In the case of N_2O decomposition, such adsorbed oxygen species have been considered as active species such as promoting the oxygen desorption from active sites [38-41]. These adsorbed species might also contribute to the methane activation in the SCR of N_2O with CH_4. The aim of this study was to characterize the adsorbed species formed from various treatments by means of TPD, FTIR and EXAFS techniques. Furthermore, I have measured the activity of the surface oxygen species with CH_4, and the reaction rates have been compared with the reaction rates of a mixture of CH_4 and N_2O. On the basis of the comparison of the reaction rates, I discuss the CH_4 activation mechanism in the SCR of N_2O with CH_4.

6.2. Experimental

Fe-MFI catalysts were prepared by an ion-exchange method using an aqueous solution of $FeSO_4 \cdot 7H_2O$ (Wako Pure Chemical Industries Ltd., 98%) for 20 h at 323 K under nitrogen atmosphere to avoid the precipitation of $Fe(OH)_3$ [25]. Na-MFI (TOSOH Co., SiO_2/Al_2O_3 = 23.8) was used as the catalyst support. The catalyst was separated from the solution by the filtration after ion exchange procedure. It was washed thoroughly with distilled water and dried at 383 K overnight, followed by the calcination in air at 773 K for 3 h. The loading amount of Fe on MFI was 2.6 wt% and 0.35 wt%, respectively, determined by ICP analysis. The molar ratio of Fe/Al is 0.37 and 0.05, respectively. The catalyst is denoted as Fe(X)-MFI, where X stands for molar ratio of Fe/Al.

Temperature-programmed desorption (TPD) was carried out in a closed circulating vacuum system (Fig. 6-1) equipped with a variable leak valve, by which the gas was introduced into a differentially pumped quadrupole mass spectrometer (Balzers QMS 200F). Four kinds of pretreatments were carried out: (1) H_2 treatment (11 kPa) at 773 K for 30 min, followed by O_2 treatment (19 kPa) at 773 K for 30 min, (2) H_2 treatment (11 kPa) at 773 K for 30 min, followed by N_2O (unless otherwise stated, 19 kPa) treatment at 523 K for 1 h, (3) high-temperature treatment (HT) in vacuo at 1073 K for 1 h, followed by N_2O (19 kPa) treatment at 523 K for 1 h, (4) H_2 treatment (11 kPa) at 773 K for 30 min, followed by N_2O (19 kPa) treatment at 523 K for 1 h, and then H_2O treatment (2 kPa) at 400 K for 10 min in order to investigate the influence of H_2O for adsorbed species. These are denoted as $H_2 + O_2$, $H_2 + N_2O$, $HT + N_2O$, and $H_2 + N_2O + H_2O$ treatments, respectively. After these pretreatments, the catalyst sample was cooled down to 400 K, and then evacuated at 400 K for 10 min. The samples were heated with the rate of 10 K/min from 400 K to 1073 K (or 773 K), and kept at 1073 K (or 773 K) for 30 min.

In-situ FTIR spectra were recorded by a Magna 550 spectrometer (Nicolet) with a resolution of 4 cm^{-1} (16 scans) in a transmission mode, using a quartz glass IR cell with CaF_2 windows connected to the closed circulating vacuum system. The sample was pressed into a diameter of 20 mm and a weight of about 50 mg [23]. The samples were treated in a manner similar to TPD experiment. In order to make assignments of the adsorbed species over Fe-MFI after $H_2 + N_2O$ and $HT + N_2O$ treatments, the catalyst had been first reduced at 773 K for 30 min, and then exposed to NO (26 kPa) at 523 K for 30 min, followed by evacuation at 523K for 10

min, and then exposed to O_2 (13 kPa) at 523 K for 10 min. This treatment is denoted as H_2 + NO + O_2. The catalyst was evacuated at 400 K for 10 min after each treatment. The spectra were collected at 300 K in a vacuum, and were normalized on the basis of the intensities of the zeolite framework overtone bands at around 2000cm^{-1}.

The samples for EXAFS measurement were prepared by pressing 50 mg of catalyst powder [26]. The H_2 + O_2 and H_2 + N_2O treatments were carried out in the closed vacuum circulating reactor. After these kinds of pretreatment, I transferred the sample to the measurement cell without exposing the sample disk to air using a glove box filled with nitrogen [26]. Fe *K*-edge EXAFS was measured at the BL-12C station of the Photon Factory at the High Energy Accelerator Research Organization, with an Si(111) crystal in the monochromator (see section 3.2.4.). The EXAFS data were collected in a transmission mode at 100 K. The details of measurement conditions and the analysis method were described in chapter 3 and Refs 42 and 43. The phase shift and backscattering amplitude of Fe-Si and Fe-Fe bonds were calculated using the software FEFF8.2 [44] and the program ATOMS [45]. The theoretical Fe-Fe reference was calibrated on EXAFS data obtained from Fe_2O_3 (hematite) at 100 K by fitting in *R* space.

The reaction of CH_4 and N_2O over the treated catalysts was carried out by using the same apparatus for the TPD experiment. In this experiment, labeled methane ($^{13}CH_4$) was used to avoid mass signal overlap such as 28 (CO and N_2) and 44 (CO_2 and N_2O). After the pretreatment (O_2, H_2 + N_2O, HT + N_2O, H_2 + N_2O + H_2O), $^{13}CH_4$ (50 μmol, 0.8 kPa) was exposed to the catalyst at 523 K. The mixture of N_2O (100 μmol, 1.6 kPa) and $^{13}CH_4$ (50 μmol, 0.8 kPa) was also exposed to the catalyst at 523 K. The molar ratio of CH_4 or N_2O to Fe amount on the catalyst was calculated to be 0.3 or 0.6, respectively. Neon was also added in the reactant gases as the internal standard. The reactant and product gases were analyzed by the on-line QMS. The concentration of $^{13}CH_4$, N_2, ^{13}CO, NO, O_2, N_2O, $^{13}CO_2$, and Ne was based on the mass signal at 17, 28, 29, 30, 32, 44, 45, and 20, respectively.

6.3. Results

Figure 6-2 shows TPD profiles of Fe-MFI catalysts after different treatments. The amounts of desorbed species (O/Fe, NO/Fe) are listed in Table 6-1. In the TPD profile of Fe(0.37)-MFI after H_2 + O_2 treatment, a broad peak was observed in the range of 673 K to 1073 K (Fig. 6-2(a)).

According to the previous study [25], the O$_2$ peak at low temperature region (673 – 900 K) is assigned to the desorption from binuclear Fe species, and that at high temperature region (900 – 1073 K) is due to that from mononuclear Fe species. On the other hand, in the TPD profile of Fe(0.37)-MFI after H$_2$ + N$_2$O treatment, sharp O$_2$ and NO desorption peaks were observed at around 610 K (Fig. 6-2(b)). The desorption of O$_2$ in the temperature range of 673 – 1073 K was also observed, although the desorption amount decreased significantly. Particularly, the decrease in the desorption amount in the temperature range of 673 – 900 K (O$_2$ desorption from binuclear Fe species [25]) is more significant, compared with that after H$_2$ + O$_2$ treatment. In the case of Fe(0.05)-MFI (Fig. 6-2(c)), where it is determined that mononuclear Fe is major species [25, 26], only small NO desorption peak was observed. On the other hand, the O$_2$ desorption at the temperature range of 900 - 1073 K, which is derived from mononuclear Fe species, was observed on Fe(0.05)-MFI (Fig. 6-2(c)). El-Malki *et al.* have reported that O$_2$ and NO were released from Fe-MFI after H$_2$ + N$_2$O treatment at around 610 K in the TPD experiment [35]. They have concluded that these desorption peaks from Fe-MFI after H$_2$ + N$_2$O treatment can be assigned to the decomposition of nitro and nitrate ion species, which is formed from N$_2$O on binuclear Fe clusters [35]. On the other hand, Coq *et al.* have reported that sharp O$_2$ and NO peaks were observed on Fe-BEA catalysts after H$_2$ and N$_2$O treatment, and proposed that the oxygen species were formed on mononuclear Fe species [37]. In this case, however, the desorption of O$_2$ and NO at around 610 K was significantly suppressed over the Fe(0.05)-MFI after H$_2$ + N$_2$O treatment, compared with Fe(0.37)-MFI. The disagreement might be due to the difference of the zeolite (MFI, BEA). The results on Fe-MFI suggest that the adsorbed species are formed on binuclear Fe species by H$_2$ and N$_2$O treatment.

The TPD profile after HT + N$_2$O treatment is also shown in Fig. 6-2(d). The sharp O$_2$ and NO desorption peaks were also observed in the same temperature range. The peaks were larger than those of the Fe(0.37)-MFI after H$_2$ + N$_2$O treatment. This suggests that similar adsorbed species were formed on the catalyst after HT + N$_2$O treatment. This is due to the formation of reduced Fe ion sites (Fe^{2+}), which is caused by the reduction of Fe sites after O$_2$ desorption at the high-temperature treatment (autoreduction) [38-41]. On the other hand, the amount of desorbed oxygen in the high temperature range of 900 – 1073 K was significantly decreased. It can be thought that the structural changes of Fe species over Fe(0.37)-MFI occurred by the high

temperature treatment, such as aggregation of Fe species and/or partial dealumination of zeolite framework Al. According to Hensen *et al.* [46], severe calcination and steaming at 973 K induced the growth and ordering of the iron oxide aggregates and dealumination.

Figure 6-3 shows FTIR spectra of Fe(0.37)-MFI after different pretreatments. The bands of bridging hydroxyl groups (i.e., Brønsted acidic sites and/or binuclear Fe sites) (3611 cm^{-1}) and silanol groups (3745 cm^{-1}) as well as a weak band (3664 cm^{-1}) assigned to the hydroxyl groups connected with extraframework aluminum species are clearly distinguished (Fig. 6-3(A)) [46-48]. The band at 3672 cm^{-1} could be assigned to hydroxyl groups on Fe^{3+} species (Fe-OH) [24]. The intensity of the bands at 3672 and 3611 cm^{-1} was decreased by H$_2$ treatment. The Fe-OH band was decreased because Fe^{3+} sites were reduced to Fe^{2+} [23], and Brønsted acidic sites also decreased after H$_2$ treatment. The decrease in the band intensity of Brønsted acid sites over Fe-ZSM-5 might be due to the removal of acid protons as water followed by interaction with charge-compensating iron complexes, because the intensity was reproduced by exposure of water. As an alternative explanation, because of the reduction of binuclear Fe sites, the bridging hydroxyl groups on binuclear Fe sites might be removed. Hensen et al. have also reported more pronounced behavior in the case of Fe-MFI after steaming at 973 K [46]. After H$_2$ + N$_2$O treatment (Fig. 6-3(c)), the intensity of Brønsted acidic sites also decreased, and the intensity of Fe-OH was regenerated because Fe^{2+} species were oxidized by N$_2$O. In the lower frequency region (Fig. 6-3(B)), two peaks were observed after H$_2$ + N$_2$O treatment. The bands at 1620 – 1630 cm^{-1} could be assigned to nitro group, and the band at 1568 cm^{-1} could be assigned to nitrate ion on the Fe ion species [35]. After HT + N$_2$O treatment, similar bands at 1624 and 1568 cm^{-1} were observed (Fig. 6-3(B)). Furthermore, the intensity of these bands was stronger than that after H$_2$ + N$_2$O treatment. This result indicates that the amount of nitro and nitrate species was larger than that after H$_2$ + N$_2$O treatment, which was also supported by the result of TPD experiment (Fig. 6-2(d)). In addition, the intensity of the silanol groups after HT + N$_2$O treatment (Fig. 6-3(d)) was decreased compared with that after H$_2$ + N$_2$O treatment, which may be caused by the aggregation of Fe species. Figure 6-3(C) shows nitro and nitrate species formed by the exposure of O$_2$ after NO adsorption on Fe ion species. These results suggest that the adsorbed species formed on the Fe ion species were almost similar between H$_2$ + N$_2$O and H$_2$ + NO + O$_2$ treatments. These species were formed after H$_2$ + N$_2$O treatment only over binuclear Fe

species, and were stable until around 550 K. This behavior is in good agreement with that of the TPD peak at 610 K.

Figure 6-4 shows TPD profiles after $H_2 + N_2O$ treatment with different N_2O pressures over Fe(0.37)-MFI. It is clearly shown that the highest desorption peaks of O_2 and NO were observed when the pretreatment pressure of N_2O was 19 kPa. This indicates that the formation of nitro and nitrate species on the Fe(0.37)-MFI was dependent on the pressure of N_2O in $H_2 + N_2O$ treatment. Figure 6-5 shows the peak reproducibility of O_2 and NO profiles in TPD after the repetition of $H_2 + N_2O$ treatment. Both O_2 and NO peaks exhibit good reproducibility from the second to the fourth pretreatment. However, in the case of the first time pretreatment, the desorption peaks were not so large. This phenomenon may be related to the existence of the physically adsorbed water over the catalyst before the first run, because the amount of desorbed water in the repetition of TPD was drastically decreased after the second time TPD experiment (Fig. 6-5(C)). In fact, the nitro and nitrate species were strongly influenced by water vapor. Figure 6-6 shows TPD profiles of Fe(0.37)-MFI after $H_2 + N_2O + H_2O$ treatment. The O_2 desorption peak at around 610 K was drastically suppressed compared to $H_2 + N_2O$ treatment (Fig. 6-2(b)), and two sharp NO peaks were only observed in the temperature range of 400 – 673 K. However, the amount of NO desorption was decreased significantly after $H_2 + N_2O + H_2O$ treatment, as shown in Table 6-1. This indicates that adsorbed nitro and nitrate species were readily decomposed by water vapor at 400 K.

Figure 6-7(A) shows the Fe K-edge EXAFS oscillations for Fe(0.37)-MFI measured after $H_2 + O_2$ and $H_2 + N_2O$ treatments. The Fourier transforms (FT) of k^3-weighted EXAFS oscillations for Fe(0.37)-MFI are shown in Fig. 6-7(B), and their fitting results are shown in Fig. 6-7(C). The detailed curve fitting results are listed in Table 6-2. The assignments of each shell were based on the results of O_2-TPD, H_2-TPR, and TOF values on SCR of N_2O with CH_4. The details of this procedure were shown in Ref [26]. Two kinds of Fe-O bonds with different bond length are assigned, and these are denoted as Fe-O_1 and Fe-O_2. This is based on the TPD result (Fig. 6-2(a)), in which the profile obviously shows two different O_2 desorption peaks at lower (673 - 900 K) and higher (900 - 1073 K) temperature regions. The Fe-O_1 and Fe-O_2 bonds can be ascribed to O atoms of the OH species coordinated with Fe ion species [26, 49] and O atoms in the zeolite lattice, respectively. The peak with a longer distance of 0.2 - 0.3 nm can be assigned

to Fe-Si bond [25, 48]. However, the structure after H$_2$ + N$_2$O treatment was clearly different from that after H$_2$ + O$_2$ treatment. The intensity of the peak in the range of 0.1 – 0.2 nm decreased remarkably, in contrast, the FT peak near 0.25 nm grew clearly (Fig. 6-7(B)). According to curve fitting results, a quite shorter Fe-O bond with 0.180 nm and Fe-Fe bond can be assigned after H$_2$ + N$_2$O treatment. However, both binuclear and mononuclear Fe species were present in this sample, because the Fe-Fe coordination number was less than unity. Kummer *et al*. [50] have reported that there are a linear relation ship between Fe oxidation state and Fe-O distance. The Fe-O bond distance of 0.180 nm is longer than the value of 0.161 nm for the terminal Fe^{4+}-O$^-$ group with strong double bond character [51]. Therefore, the Fe-O bond with 0.180 nm can be ascribed to the oxygen atoms bounded to Fe$^{(3+\delta)+}$ ions. These EXAFS results and interpretations are also supported by the report by Jia *et al*. [52].

In order to elucidate the role of the surface oxygen species in the SCR of N$_2$O with CH$_4$, I investigated the reactivity of ^{13}CH$_4$ over Fe(0.37)-MFI after the different treatments. Reaction time dependence of amounts of reactants (^{13}CH$_4$) and products (^{13}CO, ^{13}CO$_2$) over Fe(0.37)-MFI is shown in Fig. 6-8. As shown in Fig. 6-8(A), the activation of ^{13}CH$_4$ did not proceed at all over Fe(0.37)-MFI after O$_2$ treatment. In contrast, ^{13}CH$_4$ can be activated over the catalyst after H$_2$ + N$_2$O treatment, as shown in Fig. 6-8(B). The product ^{13}CO$_2$ was increased with reaction time. In the case of HT + N$_2$O treatment (Fig. 6-8(C)), the initial activation rate of ^{13}CH$_4$ was very fast because the concentration of the adsorbed species was higher than that after H$_2$ + N$_2$O treatment. However, the reaction of ^{13}CH$_4$ was suddenly inhibited after 10 min. This can be interpreted that the adsorbed oxygen species were consumed completely, and additive activation of ^{13}CH$_4$ did not proceed on the catalyst surface. It means that the reaction between ^{13}CH$_4$ and the adsorbed oxygen species was not catalytic. When ^{13}CH$_4$ is oxidized to CO$_2$ by oxygen atom ([O]), the reaction proceeds as shown in eq. (1).

$$^{13}CH_4 + 4[O] \rightarrow {}^{13}CO_2 + 2H_2O \qquad\qquad (1)$$
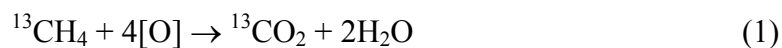
The amount of activated ^{13}CH$_4$ until 10 minutes is 9.0 μmol, and the amount of adsorbed oxygen atoms ([O]) in nitro and nitrate species is 35 μmol, which is estimated from the TPD result (O/Fe = 0.14, NO/Fe = 0.11) after HT + N$_2$O treatment (Table 6-1). The formation of N$_2$ was observed in the reaction in Fig. 6-8(C). Therefore, ^{13}CH$_4$ was consumed by the oxygen atoms [O] on the

catalyst surface stoichiometrically. I also investigated the effect of H$_2$O treatment in ^{13}CH$_4$ reaction over the activated catalyst after H$_2$ + N$_2$O treatment. As shown in Fig. 6-8(D), the reaction of ^{13}CH$_4$ did not proceed after H$_2$ + N$_2$O + H$_2$O treatment, compared to the result in Fig. 6-8(B). This phenomenon is in good agreement with the result of TPD after H$_2$ + N$_2$O + H$_2$O treatment (Fig. 6-6). It can be thought that the adsorbed surface species were completely decomposed by the water treatment. Kiwi-Minsker *et al*. [38] have also reported that the presence of water strongly inhibited the formation of NO and the reactivity of the adsorbed oxygen species. Similar result was also observed in the ^{13}CH$_4$ reaction after HT + N$_2$O + H$_2$O treatment (not shown).

The reaction of the mixture of ^{13}CH$_4$ + N$_2$O was also performed after the different treatments. Figure 6-9 shows the results of ^{13}CH$_4$ + N$_2$O reaction over Fe(0.37)-MFI after O$_2$ and H$_2$ + N$_2$O treatments. As shown in Fig. 6-9(A), ^{13}CH$_4$ and N$_2$O were converted more rapidly to produce ^{13}CO, ^{13}CO$_2$ and N$_2$ over the catalyst after O$_2$ treatment. Over the catalyst after H$_2$ + N$_2$O treatment, the reaction of ^{13}CH$_4$ with N$_2$O also proceeded (Fig. 6-9(B)), although the reaction rate was smaller than that after O$_2$ treatment. The initial rate of ^{13}CH$_4$ consumption is also shown in Fig. 6-9. As shown in Fig. 6-9(A), the consumption rate of ^{13}CH$_4$ was larger than that the rate of ^{13}CO formation over the catalyst after O$_2$ treatment. On the other hand, the reaction rate of ^{13}CH$_4$ consumption and ^{13}CO$_2$ formation was almost similar over the catalyst after H$_2$ + N$_2$O treatment (Fig. 6-9(B)). In both cases, the converted amount of N$_2$O was almost the same as the produced amount of N$_2$. This can be explained by the accumulation of adsorbed methoxy species on the catalyst surface [24], which was observed by FTIR (not shown). The important point is that the presence of N$_2$O strongly influenced r_{CH4} on the catalyst after O$_2$ treatment (Figs. 6-8(A) and 6-9(A)), and r_{CH4} in Fig. 6-9(A) was much higher than r_{CH4} in Figs. 6-8(B) and 6-9(B).

Figure 6-10 shows FTIR spectra during the reactions corresponding to the experiments in Figs. 6-9(A) and (B). As shown in Figs. 6-10(A) and (B), the peak (2823 cm^{-1}) assigned to adsorbed methoxy species [24] was observed during CH$_4$ + N$_2$O reaction over the catalyst. As shown in Fig. 6-9(B), ^{13}CH$_4$ and N$_2$O were reacted over Fe(0.37)-MFI after H$_2$+N$_2$O treatment. Regarding carbon containing products, the selectivity of CO$_2$ formation was much higher than that in Fig. 6-9(A). Because the nitro and nitrate species, which was formed after H$_2$ + N$_2$O

treatment, are highly reactive toward CO [35], it can be thought that produced CO was oxidized to CO$_2$ completely. The difference between the rate of CO$_2$ production and the rate of CH$_4$ consumption in Fig. 6-9(B) was much smaller than that in Fig. 6-9(A). This behavior is consistent with the result of Fig. 6-10. The growing rate of adsorbed methoxy species over the catalyst after O$_2$ treatment was 6 times as high as that after H$_2$ + N$_2$O treatment. This comparison suggests that the difference between production rate of carbon containing compound and the consumption rate of CH$_4$ is due to the accumulation of adsorbed methoxy species on the catalyst surface. Over the catalyst after H$_2$ + N$_2$O treatment, the presence of N$_2$O does not influence the r_{CH4} of methane consumption significantly. In contrast, the presence of N$_2$O strongly influenced the r_{CH4} on the catalyst after O$_2$ treatment, and furthermore, the r_{CH4} in Fig. 6-9(A) was about 7 times as high as that of CH$_4$ alone (Fig. 6-8(B)) after H$_2$ + N$_2$O treatment.

6.4. Discussion

6.4.1. Temperature-programmed desorption

Simultaneous desorption of O$_2$ and NO in the range of 520 - 673 K, which was derived from the decomposition of nitro and nitrate species from FTIR study, was observed after H$_2$ + N$_2$O or HT + N$_2$O treatment over binuclear Fe species. The desorption temperature range in the TPD spectra after the treatments was similar to that of α-oxygen, which has been proposed by Panov *et al.* [29] as active species for the partial oxidation of benzene to phenol and methane to methanol. However, the NO desorption was observed simultaneously in this study. Furthermore, the partial oxidation activities of benzene to phenol and methane to methanol were not observed over this catalyst under the similar reaction conditions on the basis of the previous reports [29, 30]. This means that the observed species might be different from α-oxygen. Li *et al.* [53] have reported that two factors, the introduction of extraframework Al and high-temperature treatment in He at 1173 K, contribute to increase the concentration of α-oxygen. They have also proposed that the active sites are the mixed Fe-Al oxide clusters formed between extraframework Fe and Al [54, 55] and/or some specific Fe species, *e.g.*, magnetite clusters [56]. This means that the formation of α-oxygen needs some specific conditions such as dealumination and/or aggregation of Fe species. In this study, small dealumination of zeolite framework Al and aggregation of Fe species was observed only after HT + N$_2$O treatment judging from FTIR. Therefore the

conditions of Fe species might be different from these catalysts, compared with Fe-zeolite catalysts with high α-oxygen concentration. However, it should be pointed out that almost no work using TPD technique has been performed to characterize the α-oxygen species [28-30].

The sharp O$_2$ desorption peak significantly disappeared by exposure of H$_2$O at 400 K after H$_2$ + N$_2$O treatment (Fig. 6-6). This means that the nitro and nitrate species were decomposed by water vapor. Roy and Pirngruber [41] also pointed out that a transient activity of N$_2$O decomposition over Fe-MFI catalyst after high-temperature pretreatment vanished completely after exposure to water (which is also a product of the SCR reaction). Kiwi-Minsker *et al.* [38-40] have reported that the irreversibly adsorption of water on the zeolite before N$_2$O decomposition was found to deactivate the surface oxygen in the CO oxidation and to suppress NO formation on the catalyst surface. The interaction of N$_2$O with binuclear Fe^{2+} sites was essential for the formation of the nitro and nitrate species. The adsorbed oxygen species were stable for thermal treatment until 523 K, but easily decomposed by water.

6.4.2. Reaction between the adsorbed oxygen species and CH$_4$

I have already reported that the simultaneous presence of N$_2$O with CH$_4$ is essential for the high SCR activity of N$_2$O with CH$_4$ [23, 31]. This is related to the high initial rate of CH$_4$ in N$_2$O + CH$_4$ reaction on Fe(0.37)-MFI after O$_2$ treatment (Fig. 6-9(A)). It has been proposed that the reaction mechanism of the SCR can be related to the redox of Fe^{2+} ↔ Fe^{3+} [25]. Therefore, during the SCR reaction, Fe^{2+} sites can have the opportunity to react with N$_2$O. On the basis of this study, it means that the nitro and nitrate species can be formed on the binuclear Fe^{2+} sites. However, under the SCR condition, the concentration of N$_2$O (1000 ppm) was much lower than that of O$_2$ (10 %). This means that the surface concentration of the nitro and nitrate species on the Fe sites is much lower in the SCR condition than that of the reaction in Fig. 6-8(B).

Although I observed the fast initial reaction rate of ^{13}CH$_4$ over Fe(0.37)-MFI after HT + N$_2$O treatment (Fig. 6-8(C)), this reaction can be ruled out as a major reaction step of the CH$_4$ activation in the SCR reaction, because such surface conditions after HT + N$_2$O treatment seem to be improbable in the SCR reaction. Furthermore, the nitro and nitrate species can be decomposed readily by water produced during the SCR. In fact, the activity of CH$_4$ reaction (Figs. 6-8(B) and (C)) vanished completely when the catalyst was treated with H$_2$O after H$_2$ +

N$_2$O treatment (Fig. 6-8(D)). Under the real SCR condition, therefore, it is expected that the contribution of the adsorbed species is very small. The reaction rate of CH$_4$ was much higher over the catalyst after O$_2$ treatment (Fig. 6-9(A)) than that after H$_2$ + N$_2$O treatment (Fig. 6-9(B)). The difference in the CH$_4$ activation ability becomes much larger under the real SCR condition than those shown in Figs. 6-9(A) and (B). Therefore, I can conclude that the adsorbed oxygen species, which gave the sharp TPD peaks at around 610 K, are not effective for the catalytic CH$_4$ activation in the SCR condition.

6.4.3. Activation mechanism of methane in SCR

It is suggested that the coexistence of N$_2$O in the gas phase is very important for the activation of CH$_4$, which can be caused immediately by nascent oxygen transients (O*(a)) formed by N$_2$O dissociation (N$_2$O → N$_2$ + O*(a)) [23, 31]. Thermally accommodated oxygen species (O(a)) from N$_2$O were not reactive with CH$_4$ even at 623 K [23]. Therefore, there are two types of oxygen species from N$_2$O activation: (highly reactive) nascent oxygen transients O*(a) and (non-reactive) thermally accommodated O(a). Roberts has proposed that "hot" oxygen transients, which have not yet been accommodated to the catalyst surface, may exhibit a high chemical reactivity which is distinct from thermally accommodated O(a) [57]. An important role of nascent oxygen transients (O*(a)) has also been proposed in N$_2$O decomposition on Rh catalysts [7]. In addition, a recent study of N$_2$O + C$_3$H$_8$ reaction over Fe-MFI using TAP reactor has shown that the reactivity of oxygen species from N$_2$O depends on their life time [32]. The TAP experiment has indicated that the C$_3$H$_8$ conversion decreased drastically in $\Delta t = 0.1$ s, which suggests that the life time of O*(a) is shorter than 100 ms.

In the EXAFS study [26], the active site structure of Fe-MFI is binuclear Fe complex, which has also been proposed in the literatures [33-35]. Nascent oxygen species (O*(a)) can form on binuclear Fe species and can migrate to another Fe ion sites on the catalyst surface. This can be explained by the presence of vacancy sites on binuclear Fe sites [25]. Methane can be activated by O*(a), and methoxy species are formed on Fe ion sites [24].

$$\text{Fe-OH} + \text{CH}_4 + \text{O*(a)} \rightarrow \text{Fe-OCH}_3 + \text{H}_2\text{O} \qquad (2)$$

As a result of pulse study [25], Fe^{2+} is also active for N$_2$O + CH$_4$ reaction even in the case of

mononuclear Fe sites. Since the methoxy species on Fe ion sites can promote the reduction of Fe ion sites, a large number of O*(a) can be formed on Fe ion sites. More O*(a) species can be formed on the catalyst after O$_2$ treatment (Fig. 6-9(A)) than that after H$_2$ + N$_2$O treatment (Fig. 6-9(B)), since Fe^{3+} (or Fe^{2+}) sites are oxidized to Fe$^{(3+\delta)+}$ sites by N$_2$O treatment, which are less active for N$_2$O dissociation [25].

6.5. Conclusions

Sharp O$_2$ and NO desorption peaks were observed in TPD of Fe(0.37)-MFI after H$_2$ + N$_2$O or HT + N$_2$O treatment, which were derived from the decomposition of adsorbed nitro and nitrate species. The interaction of N$_2$O with binuclear Fe^{2+} sites was essential to form the adsorbed oxygen species. The adsorbed species could be regenerated by H$_2$ + N$_2$O treatment after TPD; however, they were readily decomposed by water vapor. The EXAFS study showed that the Fe$^{(3+\delta)+}$ sites were observed after H$_2$ + N$_2$O treatment (an oxidation state higher than after O$_2$ treatment). After H$_2$ + N$_2$O or HT + N$_2$O treatment, the oxidation rate of CH$_4$ in the reaction between the adsorbed oxygen species and CH$_4$ was not so high as that in the CH$_4$ + N$_2$O reaction, which means that the adsorbed oxygen species cannot be active species for the CH$_4$ activation in the SCR reaction. The contribution of the adsorbed species is very small in the SCR condition. The simultaneous presence of CH$_4$ and N$_2$O is essential for the high SCR activity, and nascent oxygen transients (O*(a)) formed by N$_2$O dissociation can activate CH$_4$ in the SCR of N$_2$O with CH$_4$.

References

[1]   H Rodhe, *Science* **298** (1990) 1217.

[2]   J.T. Houghton, *et al*. (Eds.), *Climate Change 2001*, *The Scientific Basis*. C*ontribution of the Working Group I to the Third Assessment Report of the IPCC*, Cambridge (2001).

[3]   J. Pérez-Ramírez, F. Kapteijn, G. Mul, J.A. Moulijn, *Catal. Today* **76** (2002) 55.

[4]   J. Pérez-Ramírez, F. Kapteijn, G. Mul, J.A. Moulijn, *Appl. Catal. B* **35** (2002) 227.

[5]   J. Pérez-Ramírez, F. Kapteijn, K. Schöffel, J.A. Moulijn, *Appl. Catal. B* **44** (2003) 117.

[6]   M. Matsuoka, W.-S. Ju, M. Anpo, *Chem. Lett.* (2000) 626.

[7]   S. Tanaka, K. Yuzaki, S. Ito, S. Kameoka, K. Kunimori, *J. Catal.* **200** (2001) 203.

[8]   G. Centi, L. Dall'Olio, S. Perathoner, *J. Catal.* **192** (2000) 224.

[9]   Y. Li, J.N. Armor, *Appl. Catal. B* **1** (1992) L21.

[10] T. Turek, *Appl. Catal. B* **9** (1996) 201.

[11] J. Leglise, J.O. Petunchi, W.K. Hall, *J. Catal.* **86** (1984) 392.

[12] T. Nobukawa, S. Tanaka, S. Ito, K. Tomishige, S. Kameoka, K. Kunimori, *Catal. Lett.* **83** (2002) 5.

[13] R.W. van den Brink, S. Booneveld, J.R. pels, D.F. Bakker, M.J.F.M. Verhaak, *Appl. Catal. B* **32** (2001) 73.

[14] C. Pophal, T. Yogo, K. Tanabe, K. Segawa, *Catal. Lett.* **44** (1997) 271.

[15] A. Satsuma, H. Maeshima, K. Watanabe, K. Suzuki, T. Hattori, *Catal. Today* **63** (2000) 347.

[16] G. Delahay, M. Mauvezin, B. Coq, S. Kieger, *J. Catal.* **202** (2001) 156.

[17] S. Kameoka, K. Yuzaki, T. Takeda., S. Tanaka, S. Ito, T. Miyadera, K. Kunimori, *Phys. Chem. Chem. Phys.* **3** (2001) 256.

[18] S. Kameoka, K. Kita, S. Tanaka, T. Nobukawa, S. Ito, K. Tomishige, T. Miyadera, K. Kunimori, *Catal. Lett.* **79** (2002) 63.

[19] B.R. Wood, J.A. Reimer, A.T. Bell, M.T. Janicke, K.C. Ott, *J. Catal.* **225** (2004) 300.

[20] S. Kameoka, T. Suzuki, K. Yuzaki, T. Takeda, S. Tanaka, S. Ito, T. Miyadera, K. Kunimori, *Chem. Commun.* (2000) 745.

[21] S. Kameoka, K. Kita, T. Takeda, S. Tanaka, S. Ito, K. Yuzaki, T. Miyadera, K. Kunimori,

Catal. Lett. **69** (2000) 169.

[22] T. Nobukawa, K. Kita, S. Tanaka, S. Ito, T. Miyadera, S. Kameoka, K. Tomishige, K. Kunimori, *Stud. Surf. Sci. Catal.* **142** (2002) 557.

[23] S. Kameoka, T. Nobukawa, S. Tanaka, S. Ito, K. Tomishige, K. Kunimori, *Phys. Chem. Chem. Phys.* **5** (2003) 3328.

[24] T. Nobukawa, M. Yoshida, S. Kameoka, S. Ito, K. Tomishige, K. Kunimori, *J. Phys. Chem. B* **108** (2004) 4071.

[25] M. Yoshida, T. Nobukawa, S. Ito, K. Tomishige, K. Kunimori, *J. Catal.* **223** (2004) 454.

[26] T. Nobukawa, M. Yoshida, K. Okumura, K. Tomishige, K. Kunimori, *J. Catal.* **229** (2005) 374.

[27] R.-S. Liu, M. Iwamoto and J.H. Lunsford, *J. Chem. Soc., Chem. Commun.* (1982) 78.

[28] E.V. Starokon, K.A. Dubkov, L.V. Pirutko, G.I. Panov, *Top. Catal.* **23** (2003) 137.

[29] G.I. Panov, A.K. Uriarte, M.A. Rodkin, V.I. Sobolev, *Catal. Today* **41** (1998) 365.

[30] K.A. Dubkov, V.I. Sobolev, E.P. Talsi, M.A. Rodkin, N.H. Watkins, A.A. Shteinman, G.I. Panov, *J. Mol. Catal. A* **123** (1997) 155.

[31] T. Nobukawa, M. Yoshida, S. Kameoka, S. Ito, K. Tomishige, K. Kunimori, *Catal. Today* **93-95** (2004) 791.

[32] J. Pérez-Ramírez, E.V. Kondratenko, M.N. Debbagh, *J. Catal.* **233** (2005) 442.

[33] P. Marturano, L. Drozdová, A. Kogelbauer, R. Prins, *J. Catal.* **192** (2000) 236.

[34] A.A. Battiston, J.H. Bitter, D.C. Koningsberger, *J. Catal.* **218** (2003) 163, and references therein.

[35] El-M. El-Malki, R.A. van Santen, W.M.H. Sachtler, *J. Catal.* **196** (2000) 212.

[36] J. Nováková, M. Schwarze, Z. Tvarůžková, Z. Sobalík, *Catal. Lett.* **98** (2004) 123.

[37] G. Delahay, M. Mauvezin, B. Coq, S. Kieger, *J. Catal.* **202** (2001) 156.

[38] L. Kiwi-Minsker, D.A. Bulushev, A. Renken, *J. Catal.* **219** (2003) 273.

[39] L. Kiwi-Minsker, D.A. Bulushev, A. Renken, *Catal. Today* **91-92** (2004) 165.

[40] L. Kiwi-Minsker, D.A. Bulushev, A. Renken, *J. Catal.* **222** (2004) 389.

[41] R.K. Roy, G.D. Pirngruber, *J. Catal.* **227** (2004) 164.

[42] K. Okumura, J. Amano, N. Yasunobu, M. Niwa, *J. Phys. Chem. B* **104** (2000) 1050.

[43] K. Okumura, S. Matsumoto, N. Nishiaki, M. Niwa, *Appl. Catal. B* **40** (2003) 151.

[44] L. Ankudinov, B. Ravel, J.J. Rehr, S.D. Conradson, *Phys. Rev. B* (1998) 7565.

[45] B. Ravel, version 3.0beta8 4 March, The university of Washington, 2003.

[46] E.J.M. Hensen, Q. Zhu, M.M.R.M. Hendrix, A.R. Overweg, P.J. Kooyman, M.V. Sychev, R.A. van Santen, *J. Catal.* **221** (2004) 560.

[47] R.Q. Long, R.T. Yang, *J. Catal.* **194** (2000) 80.

[48] R. Joyner, M. Stockenhuber, *J. Phys. Chem. B* **103** (1999) 5963.

[49] A.A. Battiston, J.H. Bitter, W.M. Heijboer, F.M.F. de Groot, D.C. Koningsberger, *J. Catal.* **215** (2003) 279.

[50] K.M. Kemmer, S.D. Kelly K.A. Orlandini, A.I. Tsapin, M.G. Goldfeld, Y.D. Perfilliev, K.H. Nealson, *J. Synchrotoron Rad.* **8** (2001) 949.

[51] A.L. Yakovlev. G.M. Zhidomirov, R.A. van Santen, *J. Phys. Chem. B* **105** (2001) 12297.

[52] J. Jia, Q. Sun, B. Wen, L.X. Chen, W.M.H. Sachtler, *Catal. Lett.* **82** (2002) 7.

[53] K. Sun, H. Zhang, H. Xia, Y. Lian, Y. Li, Z. Feng, P. Ying, C. Li, *Chem. Commun.* (2004) 2480.

[54] E.J.M. Hensen, Q.Zhu, R.A. van Santen, *J. Catal.* **220** (2003) 260.

[55] K.S. Pillai, J. Jia, W.M.H. Sachtler, *Appl. Catal. B* **264** (2004) 133.

[56] P. Fejes, K. Lázár, I. Marsi, A. Rockenbauer, L. Korecz, J.B. Nagy, S. Perathoner, G. Centi, *Appl. Catal. A* **252** (2003) 75.

[57] A.F. Carley, P.R. Davies, M.W. Roberts, *Catal. Lett.* **80** (2002) 25, and references therein.

Table 6-1

Results of TPD over Fe-MFI catalysts after different treatments (Figs. 6-2 and 6-6).

Catalyst	Pretreatment	Desorption temperature range		673 - 1073 K
		520 - 673 K		
		O$_2$ desorption	NO desorption	O$_2$ desorption
		O/Fe	NO/Fe	O/Fe
Fe(0.37)-MFI ^{a}	H$_2$+O$_2$	n. d.	n. d.	0.29
Fe(0.37)-MFI ^{a}	H$_2$+N$_2$O	0.07	0.07	0.17
Fe(0.05)-MFI ^{b}	H$_2$+N$_2$O	n. d.	0.01	0.11
Fe(0.37)-MFI ^{a}	HT^c+N$_2$O	0.14	0.11	0.16
Fe(0.37)-MFI ^{a}	H$_2$+N$_2$O+H$_2$O	n. d.	0.02^d	0.14

Catalyst weight = 30 mg, ^{a} Fe = 14.0 μmol, ^{b} Fe = 1.9 μmol, ^{c} High-temperature treatment at 1073 K, ^{d} 400 – 673 K, n. d.: not detected.

Table 6-2

Results of curve fitting analysis of Fe *K*-edge EXAFS spectra after H$_2$ + O$_2$ or H$_2$ + N$_2$O treatment.

Shells	CN^{a}	R / 10^{-1} nm ^{b}	σ / 10^{-1} nm ^{c}	ΔE_0 / eV ^{d}	R_f / % ^{e}
Fe(0.37)-MFI after H$_2$ + O$_2$ treatment^{f}					
Fe-O$_1$	1.5 ± 0.1	1.90 ± 0.01	0.084 ± 0.014	0.2 ± 1.4	0.62
Fe-O$_2$	2.5 ± 0.2	2.05 ± 0.01	0.082 ± 0.010	3.8 ± 0.8	
Fe-Si	1.3 ± 0.3	3.19 ± 0.01	0.070 ± 0.026	-6.5 ± 1.8	
Fe(0.37)-MFI after H$_2$ + N$_2$O treatment^{g}					
Fe-O$_1$	0.8 ± 0.1	1.80 ± 0.01	0.080 ± 0.021	4.2 ± 2.3	0.68
Fe-O$_2$	2.6 ± 0.2	2.04 ± 0.01	0.089 ± 0.010	8.6 ± 0.9	
Fe-Si	1.0 ± 0.3	3.22 ± 0.01	0.087 ± 0.043	-2.8 ± 2.9	
Fe-Fe	0.5 ± 0.1	2.94 ± 0.01	0.058 ± 0.024	-2.8 ± 2.0	

^{a} Coordination number. ^{b} Bond distance. ^{c} Debye-Waller factor. ^{d} Difference in the origin of photoelectron energy between the reference and the sample. ^{e} Residual factor. ^{f} Fourier filtering range: 0.080 – 0.295 nm. ^{g} Fourier filtering range: 0.086 – 0.331 nm.
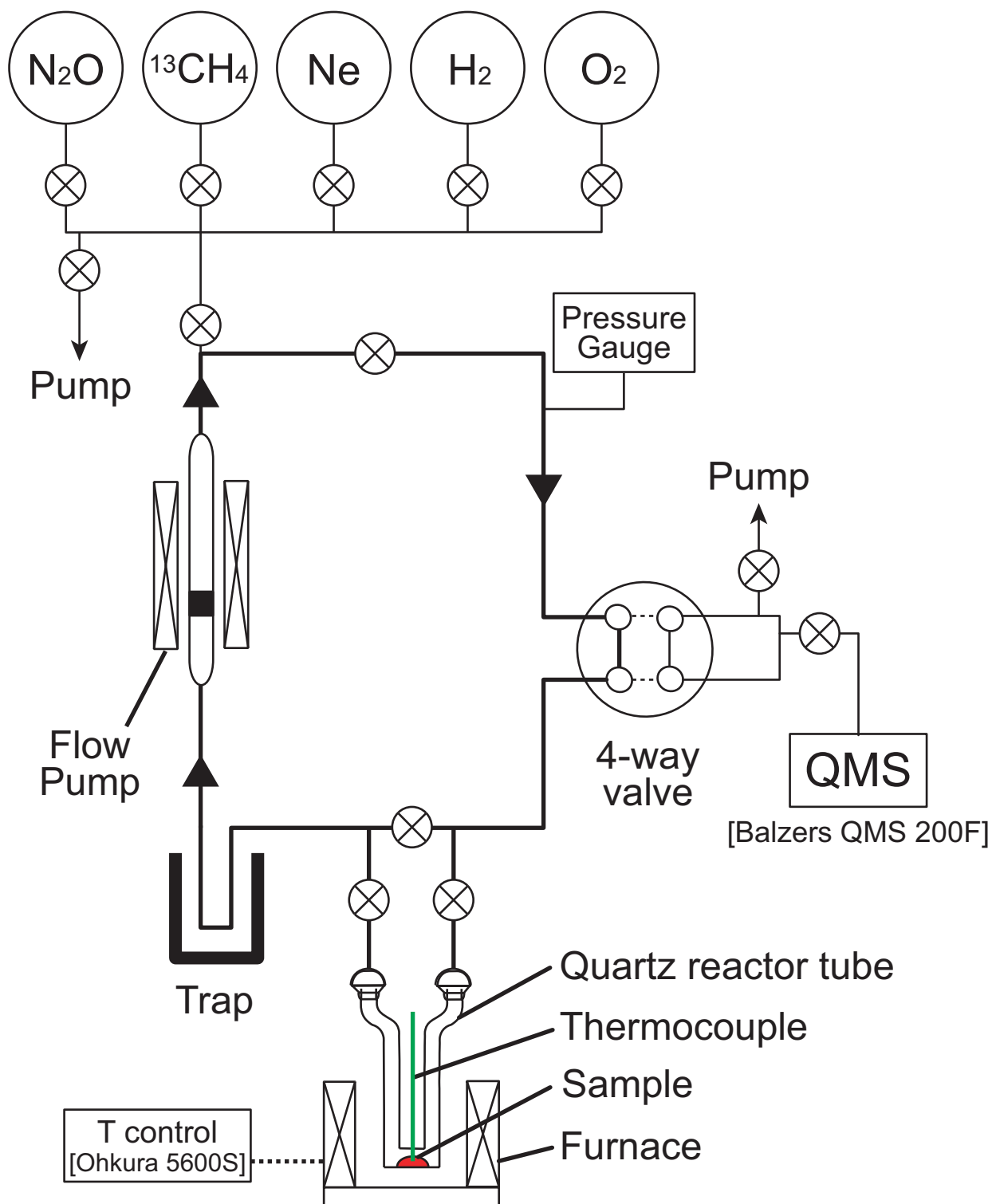
Figure 6-1. Closed circulating vacuum system equipped with a quadrupole mass spectrometer.
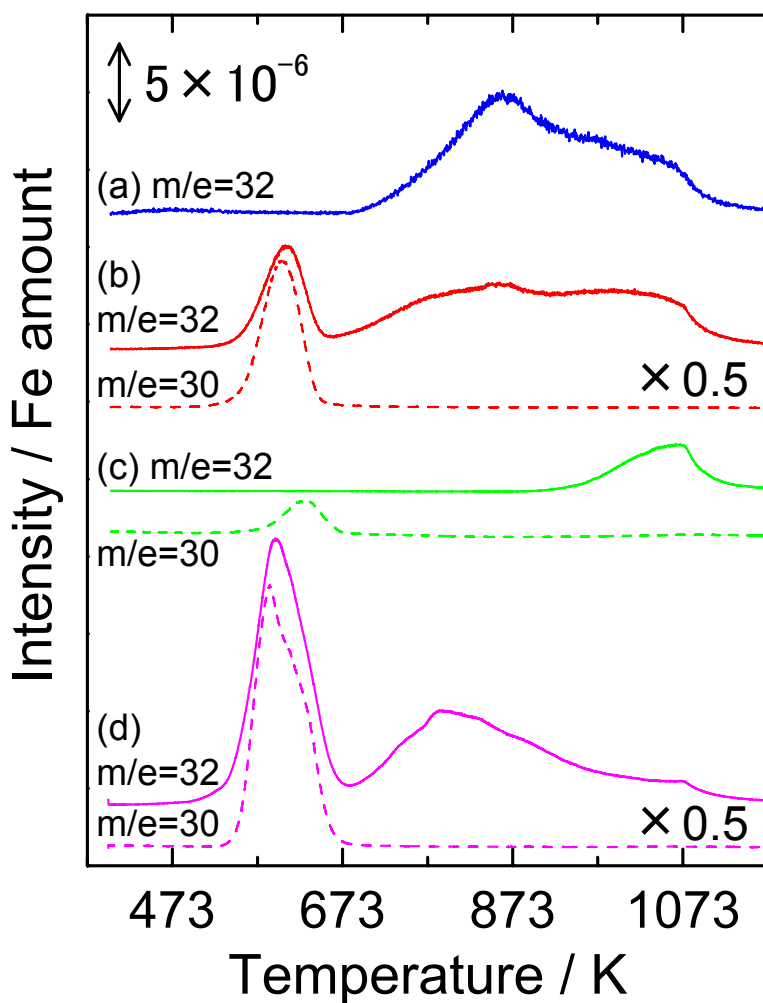
Figure 6-2. TPD profiles of Fe(0.37)-MFI (a, b, d) and Fe(0.05)-MFI (c). Pretreatment: (a) H$_2$ + O$_2$ treatment; (b), (c) H$_2$ + N$_2$O treatment; (d) HT + N$_2$O treatment.

Note that the peak intensity was normalized by the Fe amount.
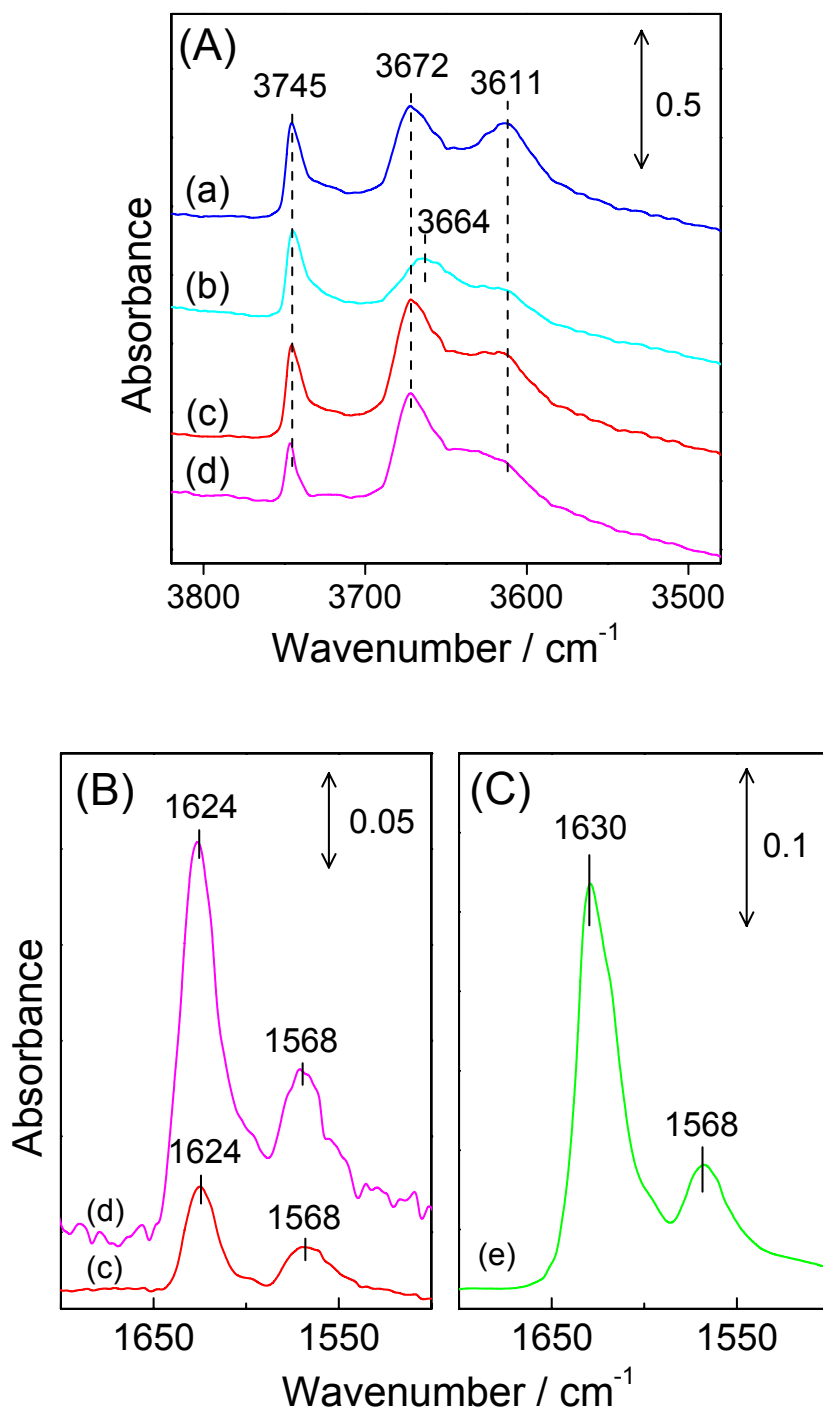
Figure 6-3. FTIR spectra of (A) OH stretching bands and (B), (C) adsorbed species over Fe(0.37)-MFI.
Pretreatment: (a) O_2 treatment, (b) H_2 treatment, (c) $H_2 + N_2O$ treatment, (d) HT + N_2O treatment, (e) $H_2 + NO + O_2$ treatment.
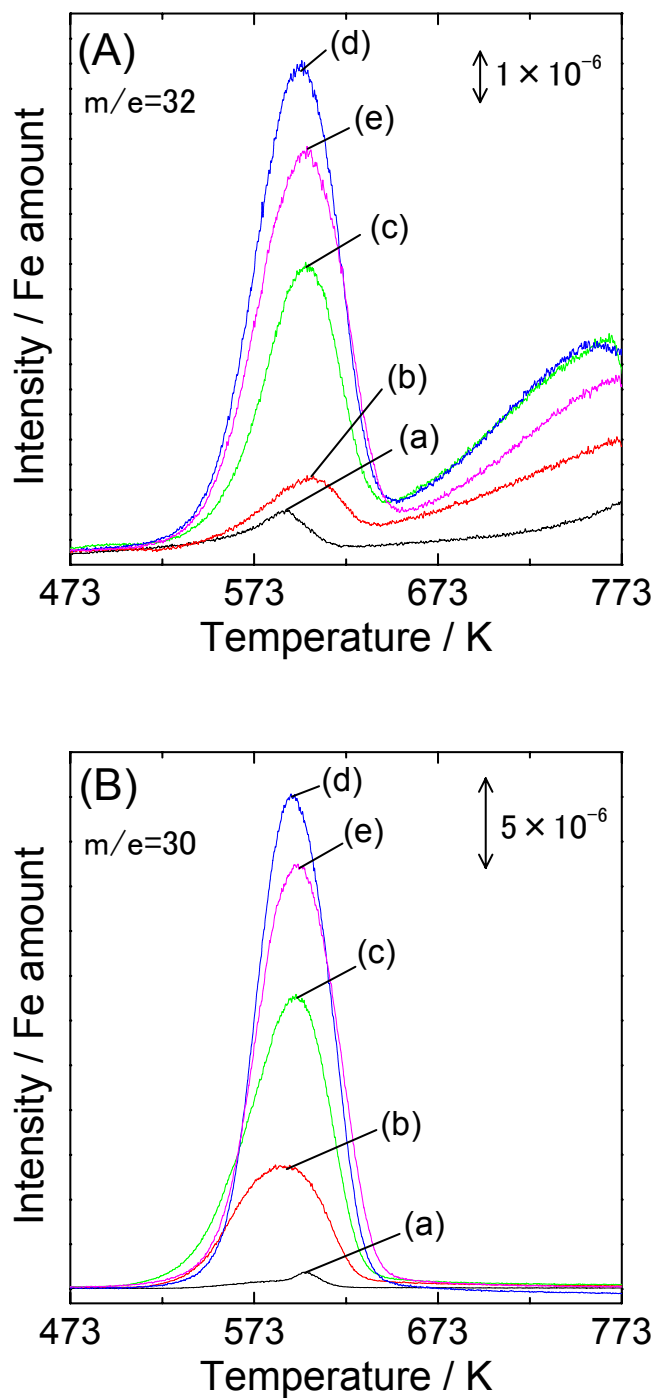
Figure 6-4. Pressure dependence of N₂O in TPD over Fe(0.37)-MFI after H₂ + N₂O treatment. (A) O₂ and (B) NO desorption profiles.

Pressure of N₂O: (a) 0.2 kPa, (b) 2.7 kPa, (c) 11 kPa, (d) 19 kPa, (e) 27 kPa.
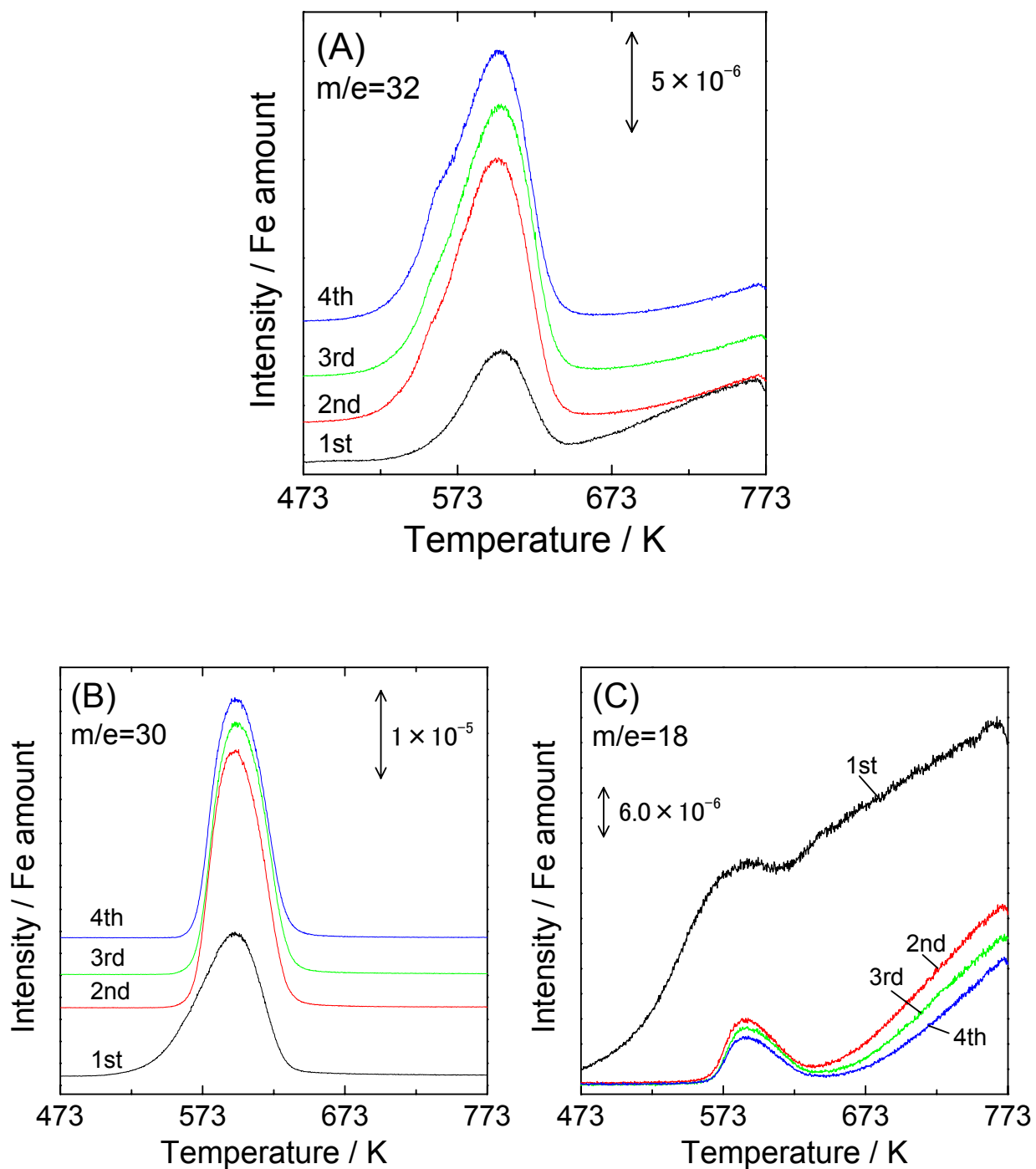
Figure 6-5. TPD profiles of (A) O$_2$, (B) NO and (C) H$_2$O desorption from Fe(0.37)-MFI after repeated H$_2$ + N$_2$O treatments.
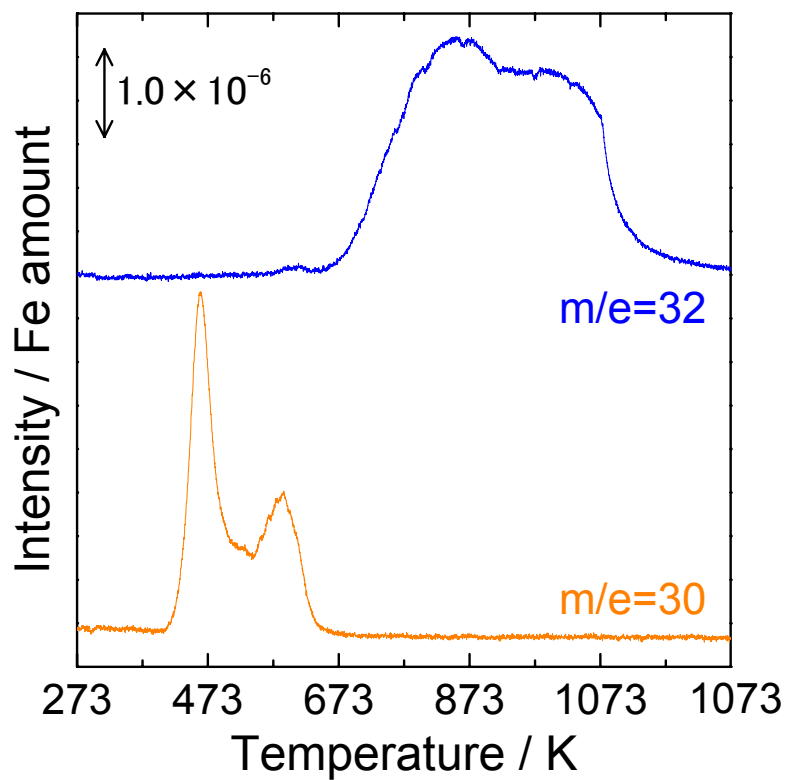
Figure 6-6. TPD profiles of Fe(0.37)-MFI after H_2 + N_2O + H_2O treatment.
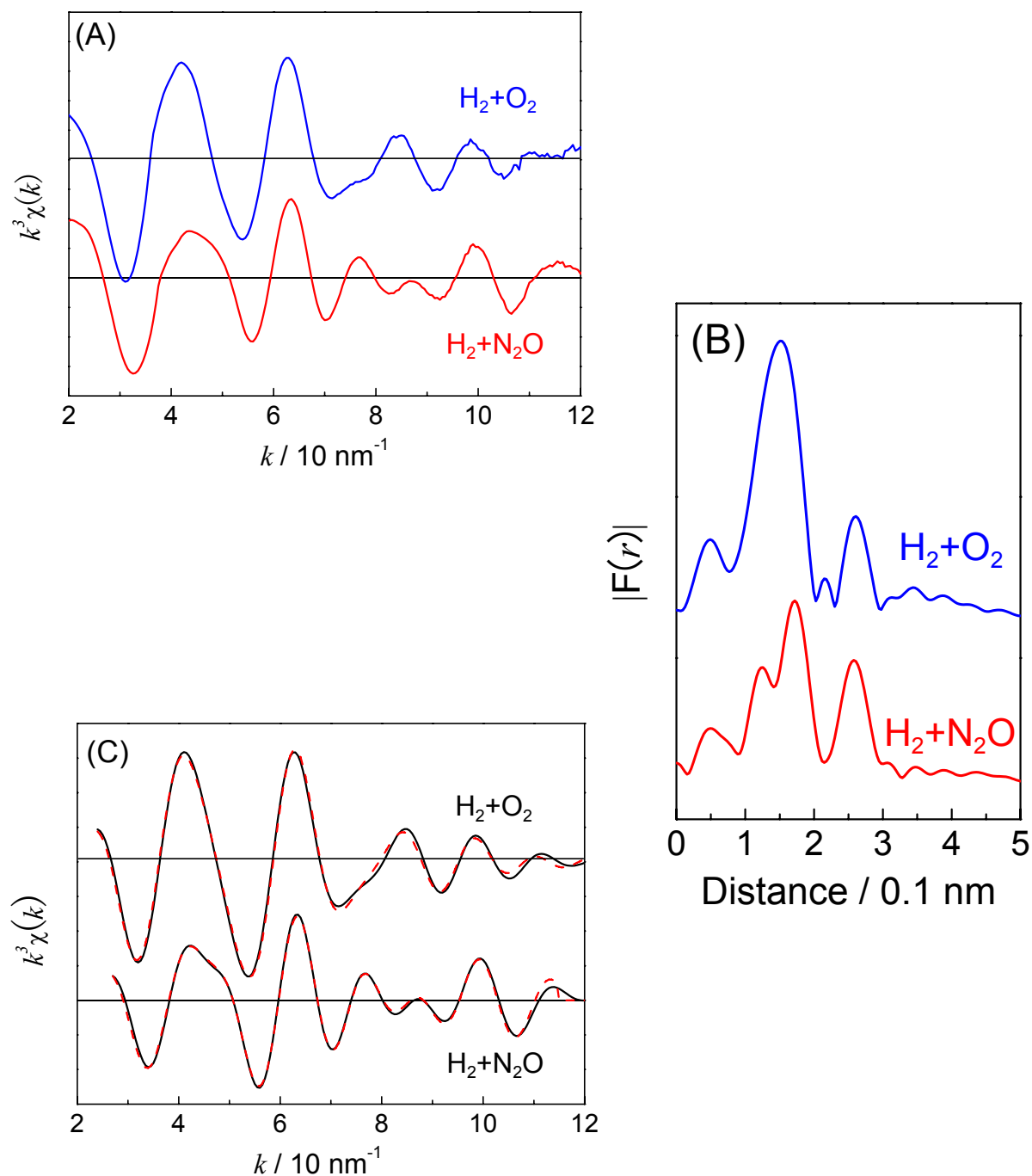
Figure 6-7. EXAFS spectra of Fe(0.37)-MFI after H_2+O_2 and H_2+N_2O treatments. (A): k^3-weighted Fe K-edge EXAFS for Fe(0.37)-MFI catalyst, (B): Fourier transform of k^3-weighted Fe K-edge EXAFS for Fe(0.37)-MFI. Fourier transform range: $24 - 120$ nm^{-1} for $H_2 + O_2$ treatment; $27 - 115$ nm^{-1} for $H_2 + N_2O$ treatment. (C): Fourier filtered EXAFS data (solid line) and calculated data (dotted line) of Fe(0.37)-MFI catalyst. Fitting results are listed in Table 2.
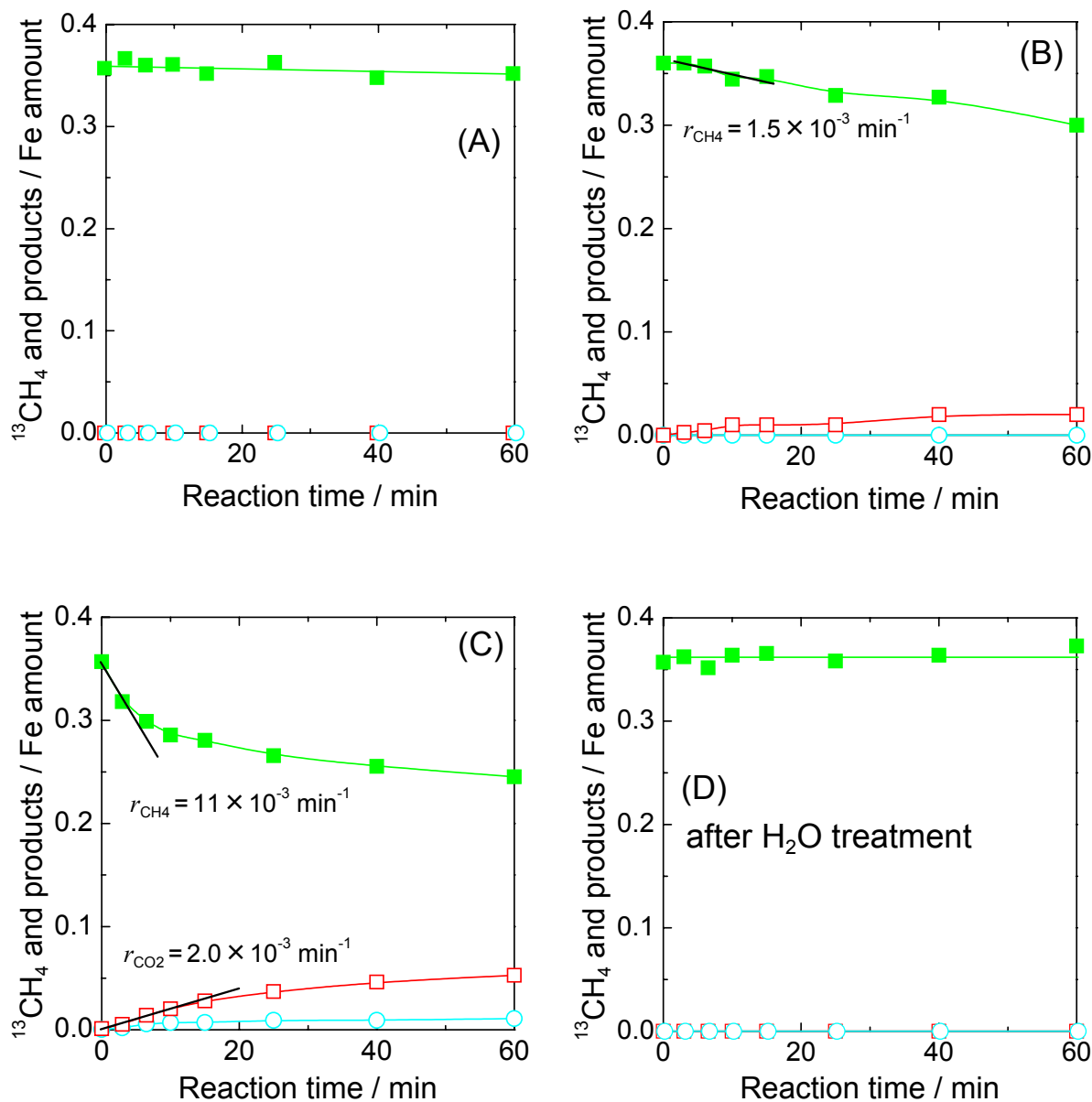
Figure 6-8. Reaction time dependence of the reaction of ^{13}CH$_4$ over Fe(0.37)-MFI after O$_2$, H$_2$ + N$_2$O and HT + N$_2$O treatments. ■: ^{13}CH$_4$, ○: ^{13}CO, □: ^{13}CO$_2$.

(A) ^{13}CH$_4$ reaction with the catalyst after O$_2$ treatment,

(B) ^{13}CH$_4$ reaction with the catalyst after H$_2$ + N$_2$O treatment,

(C) ^{13}CH$_4$ reaction with the catalyst after HT + N$_2$O treatment,

(D) ^{13}CH$_4$ reaction with the catalyst after H$_2$ + N$_2$O + H$_2$O treatment.

The catalyst was evacuated at 400 K for 5 min after each treatment. Reaction temperature = 523 K. Amount of each component was normalized by Fe amount (140 μmol in 300 mg-cat.). r_{CH4} and r_{CO2} mean the initial rate of CH$_4$ consumption and CO$_2$ formation, respectively.
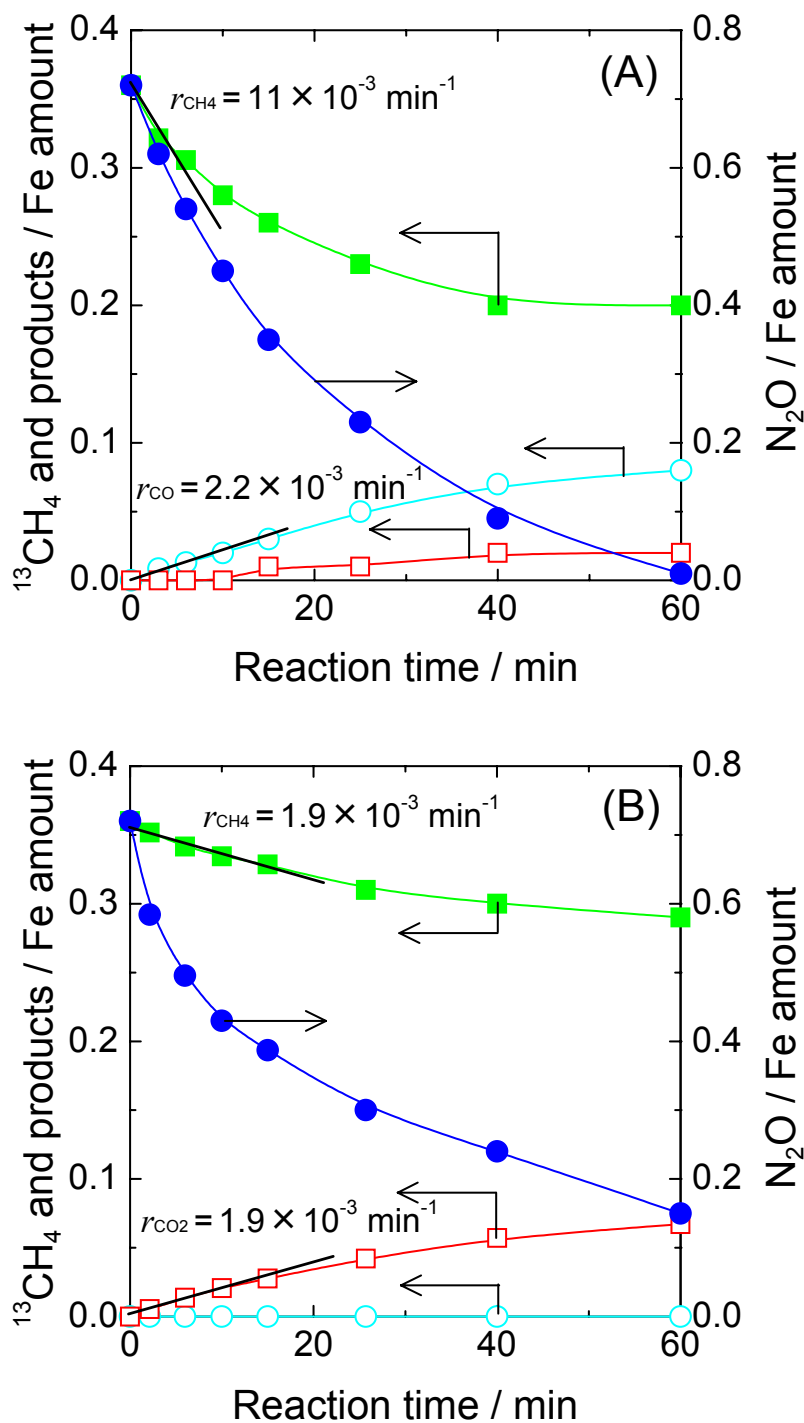
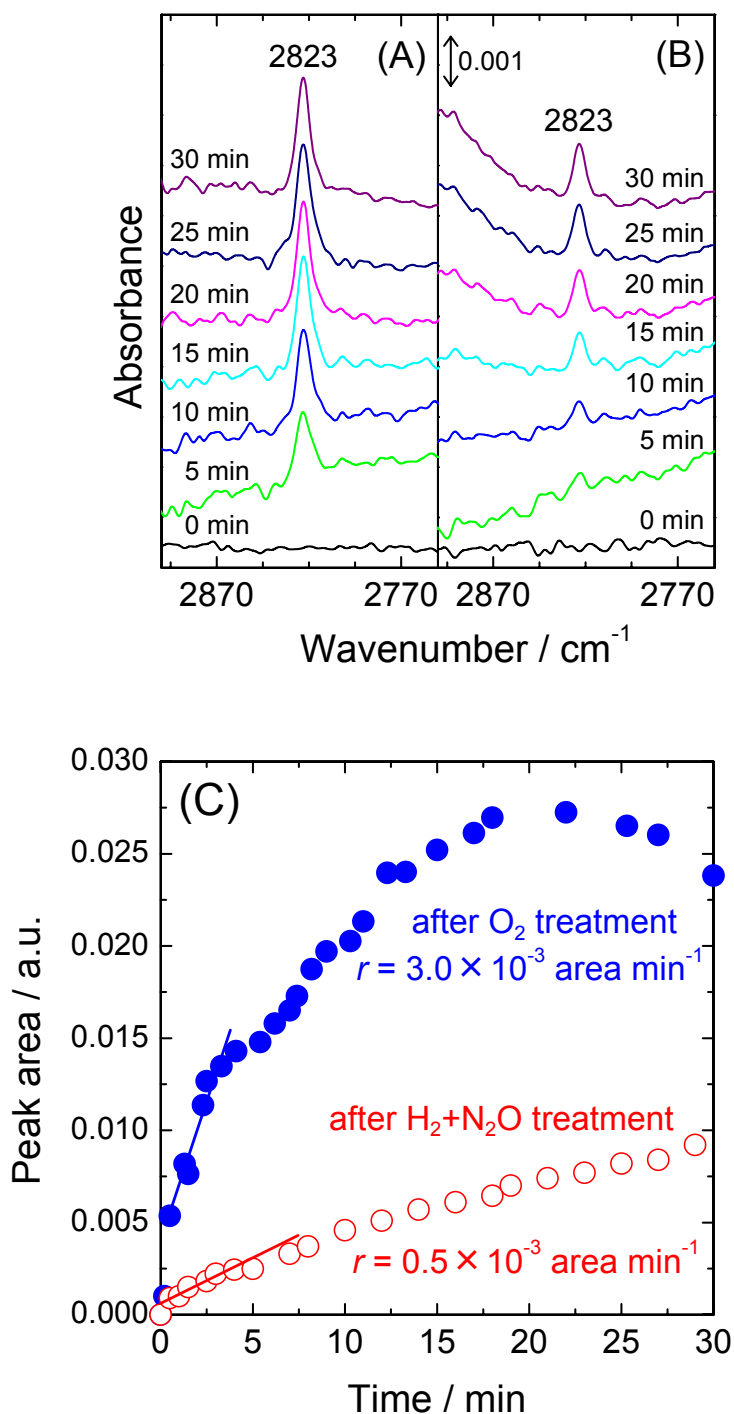**Figure 6-9.** Reaction time dependence of the reaction of $^{13}CH_4$ + N$_2$O over Fe(0.37)-MFI after O$_2$ and H$_2$ + N$_2$O treatments. ●: N$_2$O, ■: $^{13}CH_4$, ○: ^{13}CO, □: $^{13}CO_2$.

(A) $^{13}CH_4$ + N$_2$O reaction with the catalyst after O$_2$ treatment.

(B) $^{13}CH_4$ + N$_2$O reaction with the catalyst after H$_2$ + N$_2$O treatment.

Details were shown in the caption of Fig. 6-8. r_{CH4}, r_{CO} and r_{CO2} mean the initial rate of CH$_4$ consumption, CO formation and CO$_2$ formation, respectively.

Figure 6-10. In-situ FTIR spectra during the ^{12}CH$_4$ + N$_2$O reaction over Fe(0.37)-MFI after (A) O$_2$ treatment and (B) H$_2$ + N$_2$O treatment. (C) Reaction time dependence of the peak of the methoxy species (2823 cm^{-1}) in the ^{12}CH$_4$ + N$_2$O reaction (points skipped). Reaction conditions: reaction temperature = 523 K, N$_2$O = 14.4 μmol (0.2 kPa), ^{12}CH$_4$ = 7.2 μmol (0.1 kPa), diluted with He, total pressure = 11.7 kPa.

Chapter 7

Summary

In this thesis, I investigated the catalytic performance, the structure of active site species, and the reaction mechanism of the selective catalytic reduction (SCR) of N_2O with CH_4 over ion-exchanged Fe-zeolite catalysts.

The effect of the Fe content over ion-exchanged Fe-MFI catalysts was investigated in the N_2O reduction with CH_4, C_2H_6, C_3H_6, CO, and H_2 under the presence and absence of excess O_2 (Chapters 2 and 3). The Fe-MFI catalysts with different Fe content were successfully prepared by severely controlled wet ion-exchange method, and the Fe species were present as an ionic state. The catalytic activity for the N_2O reduction increased with increasing the Fe content of the Fe-MFI catalysts. In the case of N_2O reduction with hydrocarbons under excess O_2 atmosphere, the order of N_2O contribution is $CH_4 > C_2H_6 > C_3H_6$. This means that CH_4 is the most efficient reductant for the SCR of N_2O under excess O_2 atmosphere. The TOFs of N_2O reduction with CH_4 in the presence and absence of excess O_2 were drastically increased with increasing Fe/Al ratio (Fe/Al > 0.10), whereas the TOFs were lower and constant in the range of Fe/Al ≤ 0.10. The formation of more reducible Fe species, which gave a lower-temperature O_2 desorption peak, was observed over the Fe-MFI catalysts with higher Fe content (Fe/Al > 0.10). From the catalytic activity and the characterization results, it was concluded that the active sites are binuclear Fe ion species. Since the N_2O reduction with CH_4 proceeds via a redox mechanism, the reducible binuclear Fe species can exhibit higher activity (Chapters 2 and 3).

The formation of methoxy and formate species was observed during the N_2O + CH_4 reaction in the *in-situ* FTIR study (Chapters 4 and 5). From the results of kinetic study, I found that the methoxy species were oxidized with N_2O more rapidly than with O_2, on the other hand, the formate species were oxidized by both N_2O and O_2 at almost the same rate. Because the concentration of N_2O is 100 times as small as that of O_2 in the SCR condition, it can be thought that the intermediate species could be consumed by N_2O predominantly. Therefore, the N_2O + CH_4 reaction can proceed selectively even in the presence of excess O_2. Because the adsorbed intermediate species can directly reduce the Fe ion, the SCR reaction can be promoted (Chapter

5).

The role of active oxygen species for methane activation was investigated (Chapters 4 and 6). The lower-temperature O_2 desorption peak was observed over Fe-zeolite catalysts with higher Fe content (Fe/Al>0.10). The amount of lower temperature O_2 desorption was increased with N_2O treatment. This suggests that a vacant site is present over binuclear Fe species, and this vacant site can be oxidized by only N_2O. The vacant site can contribute to the N_2O dissociation even in the presence of excess O_2 atmosphere (Chapters 2 and 3), and dissociated oxygen species could accommodate on the vacant site and desorb at the lower temperatures. On the other hand, after H_2 treatment or high-temperature (HT) treatment followed by N_2O treatment, nitro and nitrite species, which gave sharp NO and O_2 desorption peaks, were formed over Fe-MFI catalyst (Chapter 6). The reaction rate of CH_4 with these adsorbed species was investigated. However, the reactivity between adsorbed oxygen species and CH_4 was very poor (Chapters 2, 4 and 6). On the other hand, high catalytic activity was observed when N_2O and CH_4 present simultaneously in the gas phase (Chapters 4 and 6). This indicates that the simultaneous presence of N_2O with CH_4 is essential for the high activity for the SCR reaction. Therefore, it can be proposed that nascent oxygen transients ($O^*(a)$) formed from N_2O dissociation can play an important role of activation/oxidation of CH_4 at initial steps (Chapters 4 and 6).

Future works

Throughout this thesis, it was found that the active site structure over Fe-zeolite catalysts and the reaction mechanism of the SCR of N_2O with CH_4 in the presence of excess O_2. The high reducibility of Fe ion sites is necessary because the $N_2O + CH_4$ reaction can be proceeded via a redox mechanism between Fe^{2+} and Fe^{3+}. However, the concentration of binuclear species was not enough; large amount of Fe ion species were present as mononuclear. This seemed to be caused by the structure of cation precursor during the ion-exchange and a feature of zeolites. The optimization of the cation precursors and support zeolites is necessary for the development of the catalyst performance in the future.

The catalytic performance of Fe-zeolite catalysts for N_2O reduction with CH_4 was almost the same as that with higher hydrocarbons (more than C_1). In order to realize a commercial catalyst for N_2O removal, the problem of the inhibitors such as H_2O, NO, and SO_2 should be overcame. The development of an effective catalyst even in the presence of these inhibitors is the most principal subject, and this is the biggest theme to achieve commercial catalyst for N_2O reduction. As the active catalysts were developed from novel catalysts and oxide catalysts to Fe-zeolite catalysts, the catalytic performance and stability for N_2O removal was improved. I hope that the breakthrough in the technology for the catalytic reduction of N_2O will be achieved in future works.

Acknowledgements

First of all, I am most grateful to my supervisor, Prof. Kimio Kunimori (Institute of Materials Science, University of Tsukuba) for guiding me to this interesting and important research field of catalytic removal of N_2O for global environmental protection. His valuable instructions, many fruitful comments, advices, and suggestions encouraged me throughout this work.

I wish to deeply appreciate Prof. Keiichi Tomishige (Institute of Materials Science, University of Tsukuba) for his much helpful discussion and his leading for achievement of Ph.D. course. His helpful discussions, suggestions and continued support were a great help to me. I would also like to express my gratitude to Prof. Yukio Nagasaki, Prof. Hiroaki Suzuki and Prof. Junji Nakamura of University of Tsukuba for their kindness to be my degree committee.

I wish to express my hearty thanks to Dr. Kazu Okumura (Tottori University) and Dr. Takeshi Kubota (Shimane University) for teaching me how to measure EXAFS and XANES spectra in the Photon Factory as well as their valuable suggestions and advice.

I wish to acknowledge my grateful thanks to Dr. Satoshi Kameoka (Tohoku University) for his many helpful suggestions, and his kind instructions and helps at the early stage of this work. I also express many thanks to Dr. Shin-ichi Ito (technical staff of University of Tsukuba) for his technical help and supports as well as fruitful discussions and comments. I wish to express my thanks to Dr. Shin-icni Tanaka (Asahi Denka), Mr. Takahiro Takeda (Tosoh) and Mr. Kenji Kita (Toyota) for their instructions and helps at the early stage of this work.

I owe my special thanks to Mr. Masanori Yoshida (Nippon Petrochemicals), Mr. Yoshio Noguchi (Tonen General), and Mr. Kou Sugawara (my colleague graduate student in University of Tsukuba) for their many helps and many discussions. I thank Mr. Tomoyasu Kagawa (a graduate student of Kyusyu University) and Mr. Yoshihiro Sato (an undergraduate student of University of Tsukuba) for their help and many discussions. This thesis could not have been completed without their kindly cooperation. I also wish to thank all the members of the Kunimori & Tomishige laboratory for giving me valuable advices, discussions, encouragement, and pleasure in my research and laboratory life.

I would like to express my hearty thanks to Dr. Junko N. Kondo (Tokyo Institute of

February 2006

Takeshi Nobukawa

List of Publications

1. S. Kameoka, S. Tanaka, K. Kita, **T. Nobukawa**, S. Ito, T. Miyadera, K. Kunimori
   "Selective catalytic reduction of N_2O with light alkanes over different Fe-zeolite catalysts"
   Studies in Surface Science and Catalysis, **135**, 321, (2001).

2. S. Kameoka, K. Kita, S. Tanaka, **T. Nobukawa**, S. Ito, K. Tomishige, T. Miyadera, K. Kunimori
   "Enhancement of C_2H_6 oxidation by O_2 in the presence of N_2O over Fe ion-exchanged BEA zeolite catalyst"
   Catalysis Letters, **79**, 63-67 (2002).

3. **T. Nobukawa**, K. Kita, S. Tanaka, S. Ito, T. Miyadera, S. Kameoka, K. Tomishige, K. Kunimori
   "Selective Catalytic Reduction of N_2O with Light Alkanes and N_2O Decomposition over Fe-BEA Zeolite Catalysts"
   Studies in Surface Science and Catalysis, **142,** 557-564 (2002).

4. **Takeshi Nobukawa**, Shin-ichi Tanaka, Shin-ichi Ito, Keiichi Tomishige, Satoshi Kameoka, Kimio Kunimori
   "Isotopic study of N_2O decomposition on an ion-exchanged Fe-zeolite catalyst: Mechanism of O_2 formation"
   Catalysis Letters, **83**, 5-8 (2002).

5. Satoshi Kameoka, **Takeshi Nobukawa**, Shin-ichi Tanaka, Shin-ichi Ito, Keiichi Tomishige, Kimio Kunimori
   "Reaction between N_2O and CH_4 over Fe ion-exchanged BEA zeolite catalyst: A possible role of nascent oxygen transients from N_2O"
   Physical Chemistry and Chemical Physics, **5,** 3328-3333 (2003).

6. **Takeshi Nobukawa**, Masanori Yoshida, Satoshi Kameoka, Shin-ichi Ito, Keiichi Tomishige, Kimio Kunimori
   "In-situ observation of reaction intermediate in the selective catalytic reduction of N_2O with CH_4 over Fe ion-exchanged BEA zeolite catalyst for elucidation of its reaction mechanism using FTIR"
   Journal of Physical Chemistry B, **108**, 4071-4079 (2004).

7. Masanori Yoshida, **Takeshi Nobukawa**, Shin-ichi Ito, Keiichi Tomishige, Kimio Kunimori
"Structure sensitivity of ion-exchanged Fe-MFI in the catalytic reduction of nitrous oxide by methane under the excess oxygen atmosphere"
Journal of Catalysis, **223**, 454-464 (2004).

8. **T. Nobukawa**, M. Yoshida, S. Kameoka, S. Ito, K. Tomishige, K. Kunimori
"The Role of Nascent Oxygen Transients in Decomposition and Selective Catalytic Reduction of N_2O"
Catalysis Today, **93-95**, 791-796 (2004).

9. **Takeshi Nobukawa**, Masanori Yoshida, Kazu Okumura, Satoshi Kameoka, Shin-ichi Ito, Keiichi Tomishige, Kimio Kunimori
"Selective Catalytic Reduction of N_2O with CH_4 over Fe-BEA Catalysts − Reaction Intermediate and Reaction Mechanism −"
Hyomenkagaku, **25**, 505-512 (2004).

10. **T. Nobukawa**, M. Yoshida, S. Kameoka, S. Ito, K. Tomishige, K. Kunimori
"Selective Catalytic Reduction of N_2O with CH_4 and N_2O Decomposition over Fe-zeolite Catalysts"
Proceedings of 14th International Zeolite Conference, 2514-2521 (2004).

11. **Takeshi Nobukawa**, Masanori Yoshida, Kazu Okumura, Keiichi Tomishige, Kimio Kunimori
"Effect of reductants in N_2O reduction over Fe-MFI catalysts"
Journal of Catalysis, **229**, 374-388 (2005).

12. Kou Sugawara, **Takeshi Nobukawa**, Yoshio Noguchi, Kazu Okumura, Shin-ichi Ito, Keiichi Tomishige, Kimio Kunimori
"Effect of Reductants in N_2O Reduction and Analysis of Active Sites Over Fe-MFI Catalysts"
Hyomenkagaku, **26**, 385-391(2005).

13. **Takeshi Nobukawa**, Kou Sugawara, Kazu Okumura, Keiichi Tomishige, Kimio Kunimori
"Role of active oxygen transients in selective catalytic reduction of N_2O with CH_4 over Fe-zeolite catalysts"
Applied Catalysis B Environmental, accepted.

14. Kou Sugawara, **<u>Takeshi Nobukawa</u>**, Masanori Yoshida, Yoshihiro Sato, Kazu Okumura, Keiichi Tomishige, Kimio Kunimori

"Dependence of Fe loading amount on N_2O reduction with NH_3 over Fe-MFI: Effect of acid site formation on Fe species"

Applied Catalysis B Environmental, submitted.

Miscellaneous

1. **<u>Takeshi Nobukawa</u>**, Masanori Yoshida, Satoshi Kameoka, Shin-ichi Ito, Keiichi Tomishige, Kimio Kunimori

"The Selective Catalytic Reduction of N_2O with CH_4 over Fe-BEA catalyst –Its Reaction Mechanism using FTIR–"

Shokubai (Catalysts & Catalysis), **45**, 419-421 (2003).

2. **<u>Takeshi NOBUKAWA</u>**, Masanori YOSHIDA, Kazu OKUMURA, Keiichi TOMISHIGE, Kimio KUNIMORI

"Structural Analysis of the Active Sites of Fe-zeolite Catalysts for Selective Catalytic Removal of Nitrous Oxide"

Photon Factory Activity Report **21**, 33 (2003).

3. **<u>Takeshi NOBUKAWA</u>**, Masanori YOSHIDA, Kou SUGAWARA, Kazu OKUMURA, Keiichi TOMISHIGE, Kimio KUNIMORI

"Structural Analysis of the Active Sites of Fe-MFI Catalysts for Selective Catalytic Removal of Nitrous Oxide"

Photon Factory Activity Report **22**, 18 (2004).

4. **<u>Takeshi Nobukawa</u>**, Kou Sugawara, Kazu Okumura, Shin-ichi Ito, Keiichi Tomishige, Kimio Kunimori

"Selective Catalytic Reduction of N_2O with CH_4 over Fe-MFI catalysts –Effect of Fe loading amount and active sites–"

Shokubai (Catalysts & Catalysis), **47**, 386-388 (2005).